Theses and Dissertations

Spring 2018

Control of swelling, electrochemical, and elongation properties of photopolymers through the modification of structure

Jacob Ryan McLaughlin
University of Iowa

Recommended Citation

McLaughlin, Jacob Ryan. "Control of swelling, electrochemical, and elongation properties of photopolymers through the modification of structure." PhD (Doctor of Philosophy) thesis, University of Iowa, 2018.
https://doi.org/10.17077/etd.1ki1ndf2

CONTROL OF SWELLING, ELECTROCHEMICAL, AND ELONGATION
PROPERTIES OF PHOTOPOLYMERS THROUGH THE MODIFICATION OF
STRUCTURE

by

Jacob Ryan McLaughlin

A thesis submitted in partial fulfillment
of the requirements for the Doctor of Philosophy
degree in Chemical and Biochemical Engineering in the
Graduate College of
The University of Iowa

May 2018

Thesis Supervisor: Professor C. Allan Guymon

Graduate College
The University of Iowa
Iowa City, Iowa

CERTIFICATE OF APPROVAL

_____

PH.D. THESIS

_____

This is to certify that the Ph.D. thesis of

Jacob Ryan McLaughlin

has been approved by the Examining Committee for
the thesis requirement for the Doctor of Philosophy degree
in Chemical and Biochemical Engineering at the May 2018 graduation.

Thesis Committee: _____
                  C. Allan Guymon, Thesis Supervisor

                  _____
                  Johna Leddy

                  _____
                  David Cwiertny

                  _____
                  Julie Jessop

                  _____
                  David Rethwisch

To my wife, Kassie

ACKNOWLEDGEMENTS

I would like to thank my family for love and support, especially my parents, who have always supported my goals and aspirations with enthusiasm. My in-laws, Joe and Dot, for their support on this journey. To my grandparents, for always encouraging me in my educational endeavors.

A special thank you to Dan and Cynthia Timmerman, for use of their cabin, my very own Walden's Pond.

To my daughter, Burke, the ultimate distraction and joy during the toughest part of writing. And last, but certainly not least, I would like to thank my wife, Kassie, for all her love and support throughout my doctoral program and for the incredible amount of assistance she has provided me during the writing process by reading and proofreading.

iv

ABSTRACT

Modifying photopolymer structure on the molecular and nanoscale level permits tailoring materials for use in a wide variety of applications. Understanding the fundamentals behind polymer structure at these levels permits the control of material properties. This work gains insight into the modification of structure on two levels, the nanoscale by use of structure templates and the molecular scale through the modification of polymer network formation.

Lyotropic liquid crystals (LLCs) are a type of self-assembling surfactant system, which in combination with photopolymerization can be used to template ordered nanostructure within polymer materials. This structure can be controlled and utilized to influence the properties of a polymer material. This research examines materials used as templating agents and the types of nanostructures that may be obtained. Additionally, their effects upon the LLC templating process and material properties is determined. Structured polymers are created using LLC templates in pursuit of materials for use in water purification processes and electrochemical devices. Through a more complete understanding of the fundamentals of the templating process, the work presented here extends the LLC templating technique to a greater variety of materials and applications in the water remediation and energy storage fields.

The second portion of this research is the use of reversible addition fragmentation chain transfer (RAFT) to modify photopolymer networks. RAFT agents are utilized to control the propagation reaction to create networks with increased homogeneity between network crosslinks. By increasing the uniformity of the polymer network, increases in polymer elongation and toughness as well as decreases in polymer modulus are observed.

The effects of RAFT agent addition on the network formation and the final properties of the photopolymer is examined. By understanding the mechanisms behind this modification technique, photopolymers can be extended into new applications where increased elongation and toughness is valued.

PUBLIC ABSTRACT

The ability to control structure on extremely small levels (nanoscale, less than 1/100,000 of a human hair) allows for unique changes to take place in material properties. These materials are created using light as an energy source to cause the polymer forming reaction to take place. Reactions that are started with light are generally very fast. This speed allows for the nanostructure to be copied from a desired pattern. Applications for these structured polymers include water purification, electronic devices, tough coatings, and thin plastic films.

By creating water-loving polymers with very small structures throughout, it is possible to greatly increase the polymer water absorption. Additionally, if structure is added to a material that responds to high temperatures by releasing water, the material will release even more water due to this internal structure. This work describes ways that these unique materials could potentially be used to purify water. Creation of small energy storage devices is another use for a structured polymer. The tiny cracks and crevices can be utilized to store electrical energy in a material.

This project also explores how a network is built within a polymer. A polymer network can be thought of as a net, or fabric. Large holes weaken the network. However, a net or fabric with equally spaced holes of the same size will result in a stronger net. The same can be said for polymer materials. A uniform network makes materials more resilient. When a polymer network is produced in a more controlled manner, materials that can stretch further without breaking are created.

Changes in material properties can be made by creating structures or better networks in a material on very small size scales. By learning how to control these

structures and networks, materials can be designed for applications in industrial, medical,

environmental, and energy storage fields.

TABLE OF CONTENTS

LIST OF TABLES

LIST OF FIGURES

xv

1: INTRODUCTION

Tailoring structure and shape of materials at the nanoscale level has been demonstrated to be a powerful method for modifying the properties of materials. The adoption of nanoscale technologies has had expansive effects on scientific fields and has even created new fields and associated applications. Semi-conductors,[1] membranes,[2–5] surface treatments,[6–8] and energy storage[9–12] are all fields that have benefitted from controlling features and structures on the nanoscale.

A great variety of strategies have been employed in the pursuit of nanoscale structure. Biotemplating uses biological structures to directly imprint features.[13–15] Lithography techniques etch a desired pattern or structure using light; advances have been made to even allow features to be created that are lower than the diffraction limit for a given wavelength.[16–18] Two photon 3D printing techniques allow the precise fabrication of 3D polymer structures on the micro and nanoscale.[19–21] Spontaneous phase separation during polymerization into nano-sized domains has been demonstrated to be a unique method of creating electronic materials and nanostructured surfaces. As polymerization takes place, thermodynamics drive components into nano-domains.[22,23] Self-assembled systems offer ease of synthesis, and a method that can be tailored for use with a wide variety of monomer systems.

The modification of polymer network structures on the nanoscale also has significant effects on properties. Changing polymer morphology at the molecular level may allow for control over thermomechanical properties of the material. The use of the step-growth reaction of thiol-ene/ynes to create low stress materials with narrow glass-transition temperature (T_g) ranges has been demonstrated.[24–26] Oligomers created with

1

reactive groups clustered on their ends create self-assembled crosslinked zones, which allow higher modulus values to be obtained compared to a random control.[27] Much research has gone into the modification of photopolymer toughness by modification of the network structure.[28] The rapid onset of gelation in photopolymer networks induces high stresses to the polymer network. Increasing the conversion at which gelation occurs by regulating network formation may allow increased toughness. Chain transfer agents have been demonstrated to reduce shrinkage stress and increase elongation by modifying network architecture.[29–31] The modification of network formation by chain transfer is a powerful tool that may permit facile control over the properties of photopolymers. This thesis will utilize ordered nanostructure systems to template polymers and will control network propagation using chain transfer agents to modify polymer properties.

1.1: Photopolymerization

Free radical photopolymerization begins with the reaction between a photoinitiator and a photon, which forms a high-energy radical. The radical goes on to react with monomers and then continues to propagate into polymer chains. Traditionally, the wavelength of these photons is in the ultra-violet (UV) range, light with wavelengths just short of visible or less than ~400nm. Visible light initiator systems are commercially available, and research of light sources and formulations for visible light are ongoing.[32,33] Initiation at higher wavelengths is desirable for the reduced energy required to generate visible light and the reduction of potential exposure to ionizing UV-light.[33,34]

Photoinitiators typically undergo either Type I or Type II initiation. Type I is a unimolecular reaction, in which the species absorbs the photon and enters an excited

2

singlet state. Through intersystem crossing to a triplet state, the initiator is cleaved and two radicals are created as shown in Equation 1.1,[35]

$$I \xrightarrow{hv} 2R^\bullet \tag{1.1}$$

where I is the initiating species and $R^\bullet$ is radical formed. The radicals formed are not necessarily of equal reactivity and both may not be capable of polymerization. Type II initiation requires two molecules. The first reacts with the photon to enter an excited state, which then abstracts a hydrogen from a second molecule, creating a single radical that goes on to react with monomer. Radicals go on to propagate as in Equation 1.2,[35]

$$R^\bullet + M \xrightarrow{k_i} M^\bullet \tag{1.2}$$

where M is the unreacted monomer, $M^\bullet$ is the new radical species, and k_i is the initiation constant. The rate of initiation is described by Equation 1.3,[35]

$$R_i = 2\Phi I_o \tag{1.3}$$

where R_i is the rate of initiation, Φ is the initiator quantum yield, and I_o is the intensity of the absorbed radiation.

After reaction with a monomer, the radical will transfer across the reacting bond. This transfer creates a propagating radical, which will continue reacting with monomers until termination, chain transfer, or monomer is no longer available to react with the radical. The rate of polymerization is dependent on the rate constant k_p, which generally governs the overall rate of reaction of a polymerization (Equation 1.4).[35]

$$M_n^\bullet + M \xrightarrow{k_p} M_{n+1}^\bullet \tag{1.4}$$

3

The constant, k_p, is assumed to be constant regardless of polymer chain length. The rate of polymerization is thus described by Equation 1.5.[35]

$$R_p = k_p[M][M^\bullet] \tag{1.5}$$

Eventually as a reaction propagates, there will be sufficient active monomers that two active center radicals will react to form inactive species, also known as termination. Termination occurs in two ways: combination and disproportionation. Combination results in the two polymer chains reacting to form one longer chain (Equation 1.6).[35]

$$M_m^\bullet + M_n^\bullet \xrightarrow{k_{tc}} M_{m+n} \tag{1.6}$$

Disproportionation results in two 'dead' polymer chains. The two radicals abstract onto one another, thus terminating both chains (Equation 1.7).[35]

$$M_m^\bullet + M_n^\bullet \xrightarrow{k_{td}} M_m + M_n \tag{1.7}$$

The rate of termination of the polymer chain is assumed to be equal to that of the initiation mechanism, which is known as the pseudo-steady state assumption. This assumption allows for the general polymerization rate equation to be derived from Equation 1.8.[35]

$$R_p = k_p[M]\left(\frac{R_i}{k_t}\right)^{1/2} \tag{1.8}$$

Substitution of Equation 1.2 for Ri gives the general rate of polymerization in Equation 1.9.[35]

4

$$R_p = k_p[M]\left(\frac{\varphi I_o}{k_t}\right)^{1/2} \tag{1.9}$$

Chain transfer is another consideration in the reaction rates of radical polymerization. Chain transfer is the abstraction of a radical from the propagating polymer chain to another molecule, usually a solvent or contaminant. However, chain transfer agents are also utilized to control molecular weight and polymer network structure. A typical chain transfer mechanism is given in Equation 1.10,[35]

$$M_n^\bullet + XA \xrightarrow{k_{tr}} M_nX + A^\bullet \tag{1.10}$$

where XA is the chain transfer agent. The subsequent reinitiation of the polymer chain that may occur afterward is shown in Equation 1.11.[35]

$$A^\bullet + M \xrightarrow{k_a} M^\bullet \tag{1.11}$$

Chain transfer often results in shorter chain lengths than would otherwise be expected if only termination by disproportionation or combination occurred. Since the chain transfer is a chain-breaking reaction, it results in shorter chain lengths, which depend on the ratio of k_p to k_{tr} and k_a to k_p. When $k_p >> k_{tr}$ and $k_a \approx k_p$, there is no effect on R_p and a decrease in chain length. This effect is the most common result of chain transfer. The rate of polymerization is sufficiently rapid and the rate of reinitiation is comparably fast, so polymerization proceeds at roughly the same rate as without the transfer. Whereas $k_p >> ktr$ and $k_a < k_p$ results in a decrease in R_p and a decrease in chain length.[35] In this case, the slower k_a results in radicals staying in the inactive state, reducing the number of active centers, which slows the rate of polymerization. In general,

chain transfer is assumed to have only small effects on polymer materials. However, special cases exist where chain transfer is also exploited to create highly controlled polymer networks, chains, particles, and branches.[36–39]

Reversible addition fragmentation chain transfer (RAFT) is a chain transfer method often employed when control over the chain length is desired. Equation 1.12 outlines the mechanism by which RAFT controls the propagation of polymerization.[40]

$$M_n^\bullet + R_1 M_m \overset{k_1}{\leftrightarrow} M_n R_1^\bullet M_M \overset{k_{-1}}{\leftrightarrow} R_1 M_n + M_n^\bullet \qquad (1.12)$$
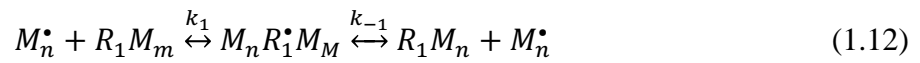
The radical is reversibly 'captured' by the RAFT agent, thus controlling the reaction.[40,41] Usually R_1 is a trithiocarbonate, dithiocarbonate, or xanthate moiety. The repeated capture and release of the radical allows for numerous chains of polymer to proceed at equal rates, thus reducing the polydispersity of the chains. The control of chain and network formation is highly desirable for some applications. Uses for RAFT include the creation of star polymers where multiple branches of roughly equal length are desired, the creation of nanoparticles with uniform size, and the controlled functionalization of surfaces or particles.[38,42–44] The use of RAFT polymerization has also been utilized for the modification of polymer properties, including the reduction of shrinkage stress and the changing of surface properties.[29–31]

The advantages offered by photopolymerization over other types of polymerization are evidenced by its widespread use in industry and academia. The most notable advantage is the rapid rate of initiation. The rate of initiation for a given photoinitiator is governed solely by the intensity of light at a given wavelength (Equation 1.3). Thus, increasing the intensity of the radiation will result in high concentrations of

radicals present in the reaction volume (Equation 1.9). Additionally, spatial and temporal control of initiating radiation is permitted by photopolymerization; polymerization can be controlled by where and how long an area is exposed. This allows for patterning to take place in areas such as photolithography, which provides the foundation for stereolithographic 3D printing.[45–47]

A significant limitation to photopolymerization includes O_2 inhibition. Initiating and propagation radicals are susceptible to reaction with oxygen forming an unreactive peroxy radical, resulting in inactive products (Equation 1.13).[35,48]

$$M_n^\bullet + O_2 \rightarrow M_nOO^\bullet \tag{1.13}$$

Steps are often taken to minimize O_2 by polymerizing in an inert atmosphere or sparging solutions to remove dissolved oxygen. Many strategies have been examined to overcome and understand oxygen inhibition.[49–51] Continuous liquid interface printing (CLIP) is a notable example that takes advantage of oxygen inhibition in radical photopolymerization. CLIP is an additive (3D) printing method which carries out the photopolymerization on the surface of an oxygen permeable membrane. Oxygen quickly inhibits the radical propagation outside of the irradiated area, thus allowing the object to be formed while the irradiated printing area is changed. This process allows continuous printing of 3D shapes.[52]

Another limitation of photopolymerization is that the thickness of sample that can be polymerized is limited by Beer's Law (Equation 1.14),

$$A=\varepsilon Lc \tag{1.14}$$

7

where A is the absorbance, ε is the molar extinction coefficient, L is the path length, and c is the concentration of the absorbing species.[35] Initiators can only interact with photons as deep as the light can penetrate the uncured monomer. For this reason, many photopolymer precursors are transparent or only lightly pigmented, permitting sufficient exposure to and transmittance of light.[53]

The lack of tough polymers available is one of the most significant limitations to the expanded use of photopolymers. Toughness is defined as the area under a stress-strain curve and is a measurement of the amount of energy a material can absorb.[28,54] Most photopolymer resins result in materials that are high modulus with low elongation or low modulus with high elongation, both of which result in materials of low toughness. Modifying the network structures is a strategy for increasing the toughness of photopolymers. Generally, the goal of the modification is to create networks with fewer imperfections and points where stress can be generated, which can weaken the network. Thiol-ene/yne polymerization accomplishes this by creating networks in which 1:1 thiol-ene/yne ratios react in a step-growth mechanism, creating a 'perfect' network with few inhomogeneities and low shrinkage stress.[25,55] Another method that was explored used controlled oligomer structures with concentrated reactive groups on the end of the molecule to induce self-assembled crosslinked zones, thus increasing modulus.[27] Modifying toughness of photopolymers using chain transfer strategies is another promising avenue and is discussed in a later section.

1.2: Lyotropic Liquid Crystals

Lyotropic liquid crystals (LLC) are a class of material that exhibit soft crystalline mesophases. The materials are considered a separate phase of matter residing between

solids and liquids since they share features with both.[56] They can be considered a defective crystal or as a melt with some orientation. The atoms in a liquid crystal have both long and short range order, corresponding to the solid or melt. The ease of which complex structures in LLCs self-assemble and the relative simplicity of their formulation when compared to thermotropic liquid crystals have made them an attractive material for sensors or templates.[4,57–60] LLCs also offer an additional degree of freedom when compared to their thermotropic counterparts. The specific mesophase formed can be governed not only by temperature and pressure, but by surfactant concentration.[61] Micelles form at lower concentrations. More complex mesophases (hexagonal, bicontinuous, and lamellar) occur at higher concentrations (Figure 1.1).[56]

      LLC surfactants allow for a variety mesophases to be templated, and the various types of surfactants can permit compatibilization with different monomer types. The variety of structures and relative ease of control make LLC systems an attractive tool for
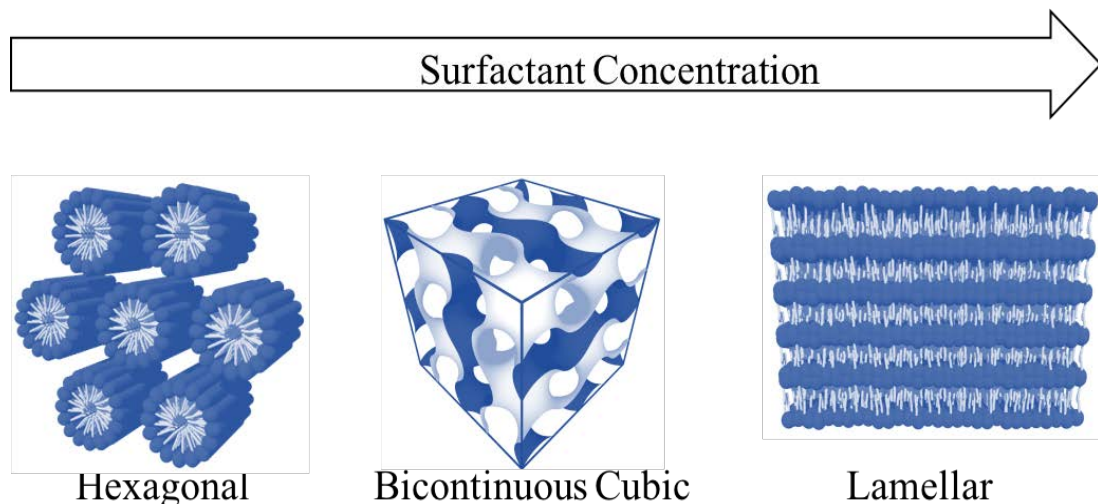
Figure 1.1. Schematic showing the progression of LLC mesophases as concentration is increased.

the nanostructuring of polymer materials.[62–65] This section will discuss surfactants used in LLC templating and the utilization of LLCs as structure directors.

1.2.1: LLC Surfactants

LLC systems are all formed by a surfactant mesogen. Surface active agents, or surfactants, are chemicals that consist of both a polar and non-polar segment. The dual nature of the molecule allows one end to act independently from the other end.[61] In an appropriate solvent, surfactants may self-assemble into LLC mesophases. The mesophase in which the surfactants self-assemble is related to the concentration and the critical packing parameter (CPP). This dimensionless number parameterizes the ratio of surfactant head group surface area to the length of the hydrophobic tail.[66] Surfactants can be classed per their chemical components, with different chemical structures allowing for a variety of different mesophases to form over different ranges. Examples of different families of surfactants are shown in Figure 1.2.

Amphiphilic or amphoteric surfactants are uncharged, consisting of a polar (hydrophilic) head and a nonpolar (hydrophobic) tail. Amphiphilic surfactants are commonly used as detergents since they do not form salts with mineral deposits in water during

washing, unlike ionic surfactants. Simple amphiphilic surfactants see a wide range of uses in cosmetics, petroleum refinery and drilling, and biological studies.[67–69] Numerous studies have examined the types and ranges of mesophases available in amphiphilic polyoxyethylene alkyl ether surfactants.[70–74] Efforts have also been carried

out to attempt to model the thermodynamics of mesophases and self-assembly in these surfactants.[75,76]
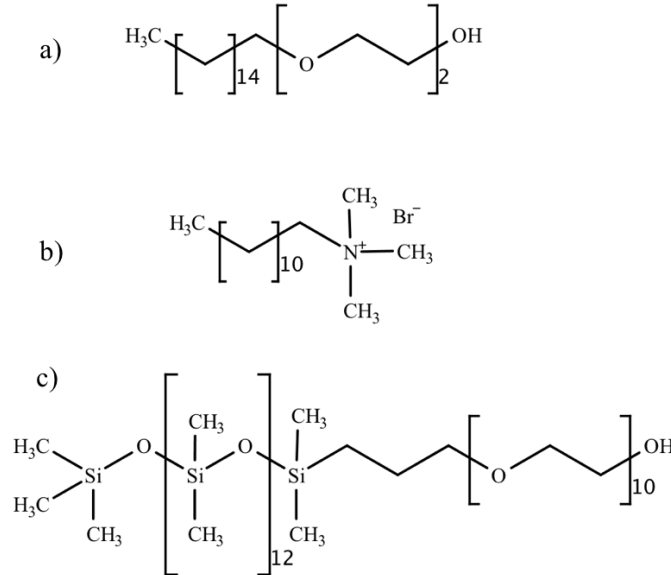
Figure 1.2. Examples of different linear surfactant types: a) amphiphilic (polyoxyethylene alkyl ether), b) ionic (lauryl based), and c) silicone (polydimethylsiloxane).

Ionic surfactants contain an ionic group, either cationic (positive charge) or anionic (negative charge). These surfactants are commonly found in soaps and detergents. Ionic surfactants containing ammonium ions are used as antibacterial agents. The ions induce super-oxidative stress in bacteria, killing them.[77,78] LLC behavior has been observed in cetyltrimethylammonium bromide (CTAB), dodecyltrimethylammonium bromide (DTAB), and sodium dodecyl sulfate (SDS).[58,79–82]

Other surfactants which exhibit LLC mesophases include linear polydimethylsiloxiane-poly(ethylene oxide) surfactants, where the hydrophobic silicone tail groups consist of a MeSi and the hydrophilic head groups of polyethylene oxides.[83–85]

11

Phase diagrams were generated with a variety of silicone oils and water, with hexagonal and lamellar mesophases observed.

A limitation of polyoxyethylene alkyl ether surfactants is that they become solids at comparatively low concentrations (Krafft point), due to their rigid hydrocarbon moieties. Krafft point, or temperature, refers to the concentration at which a surfactant mixture becomes solid. A mixture containing a high Krafft point surfactant will remain liquid even in high concentrations.[84] Due to increased flexibility of the silicone backbone chain as compared to an alkyl group, silicone surfactants permit the use of much higher concentrations without the processing issues of working with a solid precursor.

The hydrophilic-lipophilic balance (HLB) of a surfactant is one method of quantifying the nature of surfactant compatibility with a mixture. HLB compares hydrophilic and hydrophobic chain portions. The HLB is a ratio of hydrophilic to lipophilic portions of a surfactant multiplied by 20. HLB is used to easily determine surfactant compatibility and to predict the type of emulsion it tends to form with various solvents. Emulsions are categorized broadly as oil in water (O/W) and water in oil (W/O).[56] The HLB calculated for the surfactant allows easy selection of a surfactant based on the desired final formulation properties. A higher HLB indicates the surfactant is more hydrophilic and will tend to form O/W emulsions. A lower HLB is lipophilic and more suitable for use in an oily system in which an aqueous phase is to be dispersed, W/O emulsion. The HLB can be used for LLC templating to determine surfactant suitability for a monomer by comparing the relative hydrophilicity of the polymer to the HLB.[67] An HLB between three and eight will result in a W/O emulsion and would be suitable for a hydrophobic monomer. An HLB between 8 and 18 forms an O/W, preferring a hydrophilic monomer.[67,68]

12

1.2.3: Lyotropic Liquid Crystals as Structure Directors

LLCs are useful as templates for polymer systems and have been used to modify the properties of the polymer.[64,86–88] Monomer, initiator, additives, and comonomers are added to an LLC mixture and self-assemble within the mesophase per hydrophobic or hydrophilic character. After the mixture has self-assembled, it is exposed to UV radiation. During photopolymerization, the rapid initiation rate permits the structure to be approximately templated in the resulting polymer. After polymerization is complete, the LLC surfactant template is rinsed away, leaving an ordered nanostructured polymer material behind. Figure 1.3 shows a schematic for the templating processes used to create nanostructured polymers utilizing photopolymerization and LLCs. The addition of ordered nanostructure to hydrogels increases the compressive modulus of swollen gels and the swelling ratio due to structure.[89]

LLC Mesophase   LLC Mesophase + Monomer   Templated Polymer
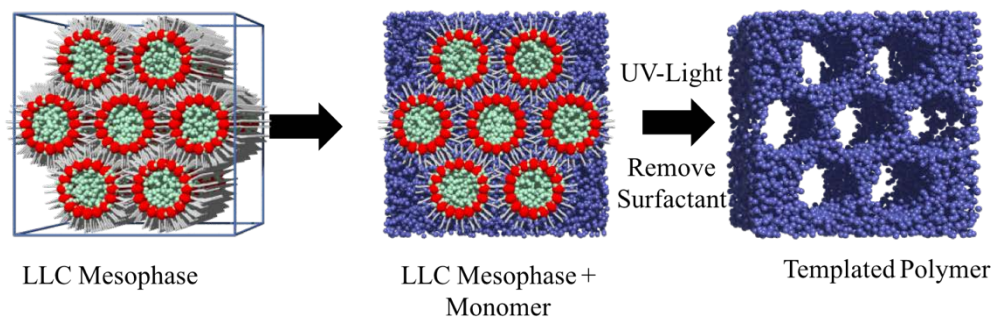
Figure 1.3. Schematic describing the process used for LLC templating with photopolymerization. The LLC mesophase shown is an inverse hexagonal mesophase.

The ionic surfactants DTAB and CTAB have been utilized as templates for polymers, though the range and type of mesophases available are somewhat limited.[69,70] Polyoxyethylene alkyl ether surfactants used as templates have been limited to the cetyl-

alcohol based agents: Brij C2, C10, and C20.[65,90,91] These surfactants display a wide range of mesophases, including the bicontinuous mesophase, which is sought after due to its high transport characteristics.[3,92]

The relationship between solvent, surfactant, and monomer is an important consideration for LLC templating. If a surfactant and monomer system does not form a homogeneous LLC mixture spontaneously, then templating will be difficult and require special consideration, such as additional surfactants, additives, or special mixing techniques. To expand the variety of monomers available for templating, it is desirable to have a wide variety of surfactants with a large range of solvent and monomer compatibilities.

1.3: Stimuli-responsive Polymers

Polymers exhibiting a response to an external stimulus are known as stimuli-responsive. Due to the novel applications they may be applied to, the materials have received much research attention. Materials that respond to temperature, pH, light, ions, and pressure have been studied.[93–95] Stimuli-responsive materials may find applications as gates, switches, or pumps within microfluidics; their stimuli response will allow for simple actuation of the microfluidic device and for facile incorporation into the microfluidic channels.[96,97] Another use for stimuli responsive materials is as potential forward osmosis draw agents, which are discussed in detail later.

N-isopropyl acrylamide (NIPAM) is a thermoresponsive polymer that has received significant interest. Following application of heat, poly(n-isopropylacrylamide) (PNIPAM) undergoes a reversible volume transition at 32 ˚C when hydrated with water. The volume transition is a consequence of a coil-to-globule transition of the polymer

14

chains. The chains transition from being hydrated with water molecules to preferring the partially dehydrated state of globules of polymer chains. Due to the hydrophilic domain of the monomer chain disassociating from water, this transition in a hydrated PNIPAM hydrogel results in the expulsion of water from the bulk hydrogel.[98] PNIPAM is often studied due to its transition temperature or lower critical solution temperature (LCST) of roughly 32 ˚C, which is near that of human biology.[99] As such, the polymer has been studied for drug delivery applications as well as biomaterial actuators.[100,101] The LCST and water absorption can be modified by copolymerization or combining hydrophilic or hydrophobic monomers with the PNIPAM.[102,103] Adding hydrophilic monomers will increase the LCST and increase swelling: adding hydrophobic monomers results in the opposite.

The addition of LLC templated structure to stimuli-responsive PNIPAM has been shown to increase the swelling ratio, the dynamic range, the water released during the deswelling event at the LCST, and the rate at which the stimuli response occurs.[86,104] The volume response to temperature is increased dramatically by the addition of LLC templated structure to the material.[86] The increased swelling combines with the internal pore structure to allow rapid and complete deswelling of the material. Additionally, the stimuli-responsive nature of materials is improved with specific nanostructure. Increases in the dynamic range of swelling are observed in materials with LLC templated structure as compared to chemically identical isotropic samples.[86,104] Using LLC templating to impart structure to a photopolymer system creates a porous nanostructure in the material, which prevents the formation of a dense deswollen 'shell' on the outside of the hydrogel. In an isotropic polymer, the formation of this shell prevents the release of water.[105] The

15

templated materials, unhindered by this densification, can continue releasing water throughout the deswelling process. This increase in transport through the material allows larger dynamic ranges of deswelling.[86]

LLC templating has also been utilized to improve the durability and stimuli-response of PNIPAM.[104] This was achieved by simultaneously polymerizing PNIPAM in the hydrophilic domain of a polyoxyethylene (2) cetyl ether hexagonal mesophase with a silicone diacrylate monomer in the hydrophobic domain to create a dual-network material. These materials exhibited increased elongation due to the addition of silicone with increased swelling and stimuli-responsive dynamic range as compared to isotropic materials.

1.4: Forward Osmosis

An application for which templated stimuli-responsive materials may be useful is forward osmosis (FO). FO is a water purification process relying on the chemical potential of a draw agent to pull water across a membrane.[106] It differs from the more commonly known reverse osmosis (RO) process in which water is forced through a membrane for purification. RO has large energy requirements due to the use of high pressure pumps, whereas FO is a low energy process, occurring via passive osmotic pressure.[107] FO utilizes the high osmotic pressure of a draw agent to draw water through a membrane. This dilution (swelling) process allows water to pass through a membrane for purification and into the draw agent.[108,109]

A major obstacle for the commercial adoption of FO is the regeneration of the draw agent, should the water need to be recovered for use or if it is desirable that the draw agent be reused. This second step required of forward osmosis draw agents adds

16

considerable complexity to their use as a water remediation method. Since regeneration of the agent and recovering the purified water is highly desirable, many methods and materials have been explored.[110–114]

Commercial methods of FO have utilized ammonia-carbon dioxide solution as a draw agent.[115] The ammonia solution forms various ammonium salts which draw water across a membrane leaving behind a concentrated brine. The ammonium salt solution is then distilled, driving off the ammonium salts as ammonia and carbon dioxide to be collected and reused. The resulting water stream may contain as little as 1 ppm ammonia.[107,115]

Another method of purifying water using FO is shown in patent literature. Trevi-systems, Inc. has developed a method using a linear poly(glycol) based polymer. This polymer system forms aggregates upon application of elevated temperatures (40-90 ˚C). The polymer aggregates are gravimetrically separated from the purified water and are of high enough molecular weight to be easily separated by a filtration process, ensuring very high purity.[116] This method is in commercial use currently in several locations around the world.

Crosslinked hydrogels are another promising polymeric material for FO applications. PNIPAM is often studied as a potential driver for FO processes due to its low stimuli-response temperature.[117] PNIPAM has been combined with superabsorbent materials such as sodium acrylate (SA) and acrylic acid in both copolymers and dual network materials.[118,119] Results of using these materials have shown promise for use as FO draw agents. The addition of SA results in higher swelling ratios when swollen in DI water, however the stimuli-response is reduced. An additional study examined the effect

particle size has on the swelling and deswelling properties of these copolymer materials.[120] It found that the diffusional mode changed from Fickian to non-Fickian as particle size increased. Further work has examined the use of polyurethane-hydrogel interpenetrating networks.[121] These materials were created by soaking a commercial polyurethane sponge in a PNIPAM and SA solution. After curing, a dense sponge is formed, which exhibited high rates of water flux. However, deswelling of the material was not examined.

Polymer swelling is best understood as the solvation of the polymer chains. A linear polymer can dissolve into an appropriate solvent, but a crosslinked polymer is incapable of dissolving, due to the chemical bonds crosslinking it into a cohesive network.[54] Therefore, when a crosslinked polymer is exposed to a solvent in which it would normally be soluble the material will swell, or absorb, the solvent. Depending on the polymer and its desired application, this can have several effects. In the case of a structural polymer such as nylon, the absorption of water can reduce the material modulus.[122,123] For a hydrogel, the swelling is desirable and being able to tailor and predict the swelling for applications may be useful, particularly for FO processes described above.

Many equations have sought to predict the amount of swelling a polymer will undergo in various solvents, temperatures, and crosslink densities. In Equation 1.15, the Flory-Rehner model describes the equilibrium swelling of a lightly crosslinked polymer network,[124]

$$-[\ln(1 - v_2) + v_2 + \chi_1 v_2^2] = \frac{V_1}{\bar{v} M_c}\left(1 - \frac{2M_c}{M}\right)\left(v_2^{\frac{1}{3}} - \frac{v_2}{2}\right) \qquad (1.15)$$

18

where v_2 is the volume fraction of polymer in the swollen mass, v_1 is the molar volume of the solvent, χ_1 is the Flory solvent-polymer interaction term, $\bar{v}$ is the specific volume of the polymer, M is the molecular mass, and M_c is the molecular mass between crosslinks.

Another property that useful for judging material suitability for FO application is osmotic pressure. Osmotic pressure is the pressure that would have to be applied to a solution to prevent it from passing into a pure solvent. Osmotic pressure measurements are typically carried out in a U-tube device (Figure 1.4). In a U-tube device, the two solutions equilibrate across the membrane, due to differences in chemical potential. The height difference between the two liquids can then be used to calculate the osmotic pressure of the substances using Equation 1.16,

$$\Pi = \rho g h \tag{1.16}$$

where $\prod$ is the osmotic pressure, ρ is the density of solution, g is the gravimetric constant, and h is the difference in heights between the two solution levels. However, a U-tube type device is not appropriate for measuring the osmotic pressure of a solid such as a hydrogel.[125] In a hydrogel, the crosslinked nature does not allow a gravimetric/density determination of pressure to occur since liquid levels cannot be measured and compared. Therefore, unique apparatuses and methods are required to quantify the osmotic pressure of hydrogel materials.[126,127]

1.5: Capacitors

A capacitor is an electrical storage device that stores energy in the form of an electrical field. Capacitors in their simplest form consist of an insulating dielectric layer sandwiched between two conductive plates.[128] When a voltage is applied to the device,

19
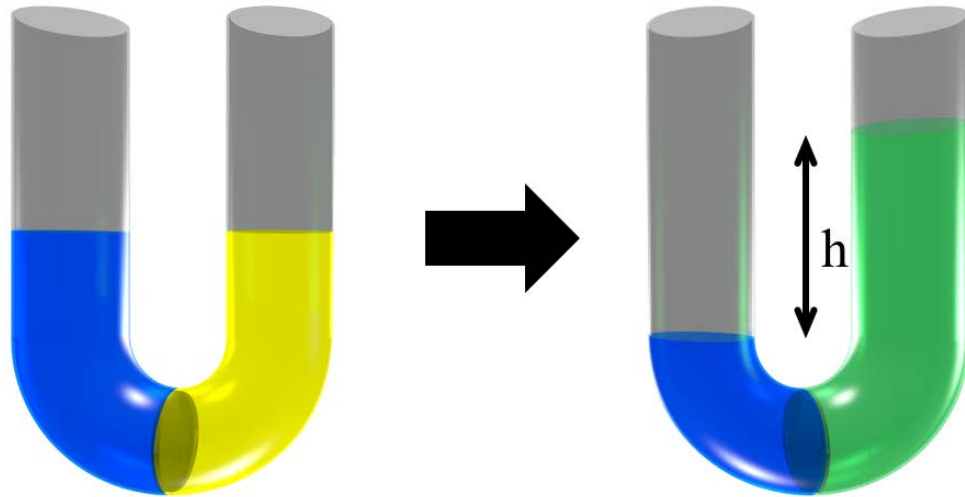
Figure 1.4. Schematic of a U-tube device used to calculate the osmotic pressure of a solution. The blue represents pure water, which is drawn across a semi-permeable membrane into the higher osmotic pressure solution (yellow). Equilibrium will be reached when the potential energy from the diluted liquid (green) surface level is equal to the osmotic pressure of the solution, (Equation 1.16).

the surfaces between the two plates collect charge between. When a load is applied, the charge will be released. A typical electric double-layer capacitor (EDLC) may consist of two conductors around a dielectric. The Capacitance (C) can be described by Equation 1.17,[10]

$$C = \frac{\varepsilon A}{D} \tag{1.17}$$

where ε is the electrolyte dielectric constant, A is the accessible surface area, and D is the distance between the ion and the plate. Commercial capacitors are designed to maximize surface area per volume and minimize D. By doing so, a material with the most energy per volume can be created. Materials for the insulating layer in an EDLC can consist of paper, polyethylene, mylar, or other polymer films, which are often coiled together to

20

maximize area per volume in a device. The conducting layer typically consists of a metal foil. These simple devices are known as film capacitors.[128] A higher performance capacitor type is an electrolytic capacitor, which consists of a passivated oxide layer on a metal film. This oxide layer acts as the dielectric. A liquid, gel, or solid electrolyte forms the negative, and the metal film the positive. Electrolytic capacitors offer higher capacitance per volume than film or ceramic types.[128]

When optimizing Equation 1.17 for maximum capacitance by increasing surface area and decreasing the distance ion travels, it stands to reason that nanomaterials could be valuable for the creation of capacitors. Nanomaterials exhibit high surface area for a given volume and since size scales are small, it can be assumed that distances between features will be small. For these reasons, carbon nanomaterials with controlled pore size are often used. Templating methods utilizing inorganic templates result in pore sizes <10 nm.[10] The ideal pore size is largely a function of the size of the electrolyte ion, with large effects being observed due to ion diffusion limitation. Increases in capacitance of carbon structures will likely come from the integration of nanoporous carbon with materials that exhibit pseudocapacitance or faradaic surface charging.

1.6: Controlling Polymer Network Morphology

Recent work has sought to apply chain transfer agents as a method for controlling network formation and crosslinking inhomogeneity.[24,30] Previously, most chain transfer agents have been used to control chain length of linear polymers and allow for the creation of grafted, star, branch, or block polymers. Liska outlines several strategies, including the use of RAFT agents, for increasing the toughness of photopolymer materials using chain transfer.[28]

21

RAFT agents have been used to direct the structure of linear and branched polymers.[27] The controlled propagation of the polymerizing radical has also been used as a method of controlling the chain formation in crosslinked materials. Leung and Bowman have explored the use of RAFT agents as a method for reducing the shrinkage stress in methacrylate dental materials. They showed that the addition of the RAFT agent allowed significant reduction in the shrinkage stress in the material. The reduction in stress was attributed to more uniform network formation by controlling radical propagation.[29] Vana and Henkel observed changes in polymer surface and elongation properties when RAFT was added to butyl acrylate (BA) prepolymer mixtures. The addition of RAFT increased the surface tack of the adhesive BA polymer and increased the elongation. However, the RAFT reduced modulus in the materials and slowed the polymerization rate significantly.[31,129]

1.7: Summary

The goal of this work is to demonstrate the relationship between polymer structure and properties and how controlling structure can be used to tailor the properties of photopolymer materials. Structure will be examined and modified on two different size scales, the nanoscale by porous templating with LLC-templates and the molecular scale by modifying radical polymerization reaction through use of RAFT agents.

Chapter 4 will describe LLC templating a copolymer of a superabsorbent and a thermoresponsive monomer to create nanostructured hydrogel materials. The effect polymer structure has on the swelling properties, deswelling properties, and reversibility of the stimuli-response will be examined. This chapter will examine how increased load levels of superabsorbent affect the fidelity of the templated structure. It will also discuss

22

the implications that reducing polymer structure has on the swelling and stimuli-responsive properties. Chapter 5 continues to examine the same templated copolymer materials, but will focus on their suitability for use as FO draw agents. To this end, the amount of flux the materials can generate through an FO membrane is tested, and the osmotic pressure of the materials is examined. Finally, the materials are placed in a proof-of-concept device as a draw agent for purifying river water.

Chapter 6 screens a wide variety of amphiphilic polyoxyethylene alkyl ether surfactants for LLC mesophase behavior. The surfactants are then used as templates for PNIPAM. The importance of templating mesophase is demonstrated by templating in the inverse and normal phases as well as with a non-LLC surfactant. The work expands the knowledge of LLC surfactants, which may allow additional monomers to be templated in this manner.

In Chapter 7, LLC templates and photopolymerization are used to create capacitive silicone films. Electrochemical properties can be modified by the simple templating of structure to a non-conducting polymer. Films are examined using cyclic-voltammetry to observe capacitive behaviors. In summary, this work will demonstrate a wide variety of applications and properties that can be modified and controlled utilizing changes in structure of polymer networks and materials.

Chapter 8 demonstrates the impact of polymer network formation by examining the thermomechanical properties of urethane diacrylate films modified during polymerization by a RAFT agent. The films are examined for changes in modulus, T_g, elongation, and toughness. Additionally, the effects of generating large amounts of radicals using high intensity light on the network formation and properties is examined

23

1.8: References

(1)   Hu, X.; Li, G.; Yu, J. C. Design, Fabrication, and Modification of Nanostructured Semiconductor Materials for Environmental and Energy Applications. *Langmuir* **2010**, *26* (5), 3031–3039.

(2)   Liu, J.; Teo, W. K.; Chew, C. H.; Gan, L. M. Nanofiltration Membranes Prepared by Direct Microemulsion Copolymerization Using Poly(ethylene Oxide) Macromonomer as a Polymerizable Surfactant. *J. Appl. Polym. Sci.* **2000**, *77* (12), 2785–2794.

(3)   Carter, B. M.; Wiesenauer, B. R.; Noble, R. D.; Gin, D. L. Thin-Film Composite Bicontinuous Cubic Lyotropic Liquid Crystal Polymer Membranes: Effects of Anion-Exchange on Water Filtration Performance. *J. Memb. Sci.* **2014**, *455*, 143–151.

(4)   Zhou, M.; Kidd, T. J. J.; Noble, R. D. D.; Gin, D. L. D. L. Supported Lyotropic Liquid-Crystal Polymer Membranes: Promising Materials for Molecular-Size-Selective Aqueous Nanofiltration. *Adv. Mater.* **2005**, *17* (15), 1850–1853.

(5)   Gin, D. L.; Bara, J. E.; Noble, R. D.; Elliott, B. J. Polymerized Lyotropic Liquid Crystal Assemblies for Membrane Applications. *Macromol. Rapid Commun.* **2008**, *29* (5), 367–389.

(6)   Ijeri, V. S.; Nair, J. R.; Gerbaldi, C.; Gonnelli, R. S.; Bodoardo, S.; Bongiovanni, R. M. An Elegant and Facile Single-Step UV-Curing Approach to Surface Nano-Silvering of Polymer Composites. *Soft Matter* **2010**, *6* (19), 4666.

(7)   Telitel, S.; Telitel, S.; Bosson, J.; Lalevée, J.; Clément, J.-L.; Godfroy, M.; Fillaut, J.-L.; Akdas-Kilig, H.; Guillaneuf, Y.; Gigmes, D.; et al. UV-Induced Micropatterning of Complex Functional Surfaces by Photopolymerization Controlled by Alkoxyamines. *Langmuir* **2015**, *31* (36), 10026–10036.

(8)   Manna, U.; Broderick, A. H.; Lynn, D. M. Chemical Patterning and Physical Refinement of Reactive Superhydrophobic Surfaces. *Adv. Mater.* **2012**, *24* (31), 4291–4295.

(9)   Zhang, H.; Wang, K.; Zhang, X.; Lin, H.; Sun, X.; Li, C.; Ma, Y. Self-Generating Graphene and Porous Nanocarbon Composites for Capacitive Energy Storage. *J. Mater. Chem. A* **2015**, *3*, 11277–11286.

(10)   Simon, P.; Burke, A. Nanostructured Carbons: Double-Layer Capacitance and More. *Electrochem. Soc. Interface* **2008**, *17* (1), 38–43.

(11)   Zhou, Y.; Wang, B.; Liu, C.; Han, N.; Xu, X.; Zhao, F.; Fan, J.; Li, Y. Polyanthraquinone-Based Nanostructured Electrode Material Capable of High-Performance Pseudocapacitive Energy Storage in Aprotic Electrolyte. *Nano Energy* **2015**, *15*, 654–661.

(12)   Yan, J.; Wang, Q.; Wei, T.; Fan, Z. Recent Advances in Design and Fabrication of Electrochemical Supercapacitors with High Energy Densities. *Adv. Energy Mater.* **2014**, *4* (4).

(13)   Yang, H.; Liang, F.; Chen, Y.; Wang, Q.; Qu, X.; Yang, Z. Lotus Leaf Inspired Robust Superhydrophobic Coating from Strawberry-like Janus Particles. *NPG Asia Mater.* **2015**, *7* (4), 176-6.

(14)   Calvert, P. Biomimetic Ceramics and Composites. *Mater. Res. Soc. Bull.* **1992**, No. October, 37–40.

(15)   Sotiropoulou, S.; Sierra-Sastre, Y.; Mark, S. S.; Batt, C. A. Biotemplated Nanostructured Materials †. *Chem. Mater.* **2008**, *20* (3), 821–834.

(16)   Buck, M. E.; Lynn, D. M. Azlactone-Functionalized Polymers as Reactive Platforms for the Design of Advanced Materials: Progress in the Last Ten Years. *Polym. Chem.* **2012**, *3* (1), 66.

(17)   Seisyan, R. P. Nanolithography in Microelectronics: A Review. *Tech. Phys.* **2011**, *56* (8), 1061–1073.

(18)   Xie, Z.; Yu, W.; Wang, T.; Zhang, H.; Fu, Y.; Liu, H.; Li, F.; Lu, Z.; Sun, Q. Plasmonic Nanolithography: A Review. *Plasmonics* **2011**, *6* (3), 565–580.

(19)   Williams, G.; Hunt, M.; Boehm, B.; May, A.; Taverne, M.; Ho, D.; Giblin, S.; Read, D.; Rarity, J.; Allenspach, R.; et al. Two-Photon Lithography for 3D Magnetic Nanostructure Fabrication. *Nano Res.* **2017**, *11* (2), 1–10.

(20)   Worthington, K. S.; Wiley, L. A.; Kaalberg, E. E.; Collins, M. M.; Mullins, R. F.; Stone, E. M.; Tucker, B. A. Two-Photon Polymerization for Production of Human iPSC-Derived Retinal Cell Grafts. *Acta Biomater.* **2017**, *55*, 385–395.

(21)   Brigo, L.; Urciuolo, A.; Giulitti, S.; Della Giustina, G.; Tromayer, M.; Liska, R.; Elvassore, N.; Brusatin, G. 3D High-Resolution Two-Photon Crosslinked Hydrogel Structures for Biological Studies. *Acta Biomater.* **2017**, *55*, 373–384.

(22)   Schulze, M. W.; McIntosh, L. D.; Hillmyer, M. A.; Lodge, T. P. High-Modulus, High-Conductivity Nanostructured Polymer Electrolyte Membranes via Polymerization-Induced Phase Separation. *Nano Lett.* **2014**, *14* (1), 122–126.

(23)   Raman, V. I.; Palmese, G. R. Nanoporous Thermosetting Polymers. *Langmuir* **2005**, *21* (4), 1539–1546.

(24)   Park, H. Y.; Kloxin, C. J.; Scott, T. F.; Bowman, C. N. Stress Relaxation by Addition-Fragmentation Chain Transfer in Highly Cross-Linked Thiol-Yne Networks. *Macromolecules* **2010**, *43* (24), 10188–10190.

(25)   Hoyle, C. E.; Bowman, C. N. Thiol-Ene Click Chemistry. *Angew. Chem. Int. Ed. Engl.* **2010**, *49* (9), 1540–1573.

(26)   Nair, D. P.; Chatani, S.; Berg, G.; Bowman, C. N. Programmable Mechanically Assisted Geometric Deformations of Glassy Two-Stage Reactive Polymeric Materials. *Appl. Mater. and Interfaces.* **2014**. *6*, 6111-6115.

(27)   Scholte, J. P.; Ki Kim, S.; Lester, C. L.; Guymon, C. A. Effects of Directed Architecture in Epoxy Functionalized Prepolymers for Photocurable Thin Films. *J. Polym. Sci. Part A Polym. Chem.* **2017**, *55* (1), 144–154.

(28)   Ligon-Auer, S. C.; Schwentenwein, M.; Gorsche, C.; Stampfl, J.; Liska, R. Toughening of Photo-Curable Polymer Networks: A Review. *Polym. Chem.* **2016**, *7* (2), 257–286.

(29)   Leung, D.; Bowman, C. N. Reducing Shrinkage Stress of Dimethacrylate Networks by Reversible Addition-Fragmentation Chain Transfer. *Macromol. Chem. Phys.* **2012**, *213* (2), 198–204.

(30)   Shah, P. K.; Stasbury, J. W.; Bowman, C. N. Application of an Addition–fragmentation-Chain Transfer Monomer in Di(meth)acrylate Network Formation to Reduce Polymerization Shrinkage Stress. *Polym. Chem.* **2017**, *8* (30), 4339–4351.

(31)   Henkel, R.; Vana, P. The Influence of RAFT on the Microstructure and the Mechanical Properties of Photopolymerized Poly(butyl Acrylate) Networks. *Macromol. Chem. Phys.* **2014**, *215* (2), 182–189.

(32)   Jiangtao, X.; Sivaprakash, S.; Nathaniel Alan, C.; Cyrille, B. Catalyst-Free Visible Light-Induced RAFT Photopolymerization. *Control. Radic. Polym. Mech.* **2015**, *1187* (1187), 247–267.

(33)   Eibel, A.; Radebner, J.; Haas, M.; Fast, D. E.; Faschauner, P.; Torvisco, A.; Lamparth, I.; Moszner, N.; Stueger, H.; Gescheidt, G. From Mono- to Tetraacylgermanes: Extending the Scope of Visible Light Photoinitiators Anna. *Polym. Chem.* **2017**, *submitted*.

(34)   Fouassier, Jean-Pierre, Lalevée, J. *Photoinitiators for Polymer Synthesis*. Wiley VCH Verlag. Weinheim, Germany, 2012.

(35)   Odian, G. *Principles of Polymerization*, 4th ed.; John Wiley & Sons, Inc.: Hoboken, New Jersey, 2004.

(36)   Lu, L.; Yang, N.; Cai, Y. Well-Controlled Reversible Addition – Fragmentation Chain Transfer Radical Polymerisation under Ultraviolet Radiation at Ambient Temperature. **2005**, 5287–5288.

(37)   Wang, R.; Luo, Y.; Li, B.; Zhu, S. Modeling of Branching and Gelation in RAFT Copolymerization of Vinyl / Divinyl Systems Modeling of Branching and Gelation in RAFT Copolymerization of Vinyl / Divinyl Systems. *Macromolecules* **2009**, No. 42, 85–94.

(38)   Liu, J.; Stansbury, J. W. RAFT-Mediated Control of Nanogel Structure and Reactivity: Chemical, Physical and Mechanical Properties of Monomer-Dispersed Nanogel Compositions. *Dent. Mater.* **2014**, *30* (11), 1252–1262.

(39)   Liu, J.; Rad, I. Y.; Sun, F.; Stansbury, J. W. Photo-Reactive Nanogel as a Means to Tune Properties during Polymer Network Formation. *Polym. Chem.* **2014**, *5* (1), 227–233.

(40)   Christopher Barner-Kowollik. *Handbook of RAFT Polymerization*; WILEY-VCH Verlag, 2008.

(41)   Wood, M. R.; Duncalf, D. J.; Rannard, S. P. Selective One-Pot Synthesis of Trithiocarbonates, Xanthates, and Dithiocarbamates for Use in RAFT / MADIX Living Radical Polymerizations. *Organic Letters.* **2006**. *8*(4), 553-556.

(42)   Aoyagi, N.; Endo, T. Functional RAFT Agents for Radical-Controlled Polymerization : Quantitative Synthesis of Trithiocarbonates Containing Functional Groups as RAFT Agents Using Equivalent Amount of CS 2. *J. Polym. Sci. Part A Polym. Chem.* **2009**, *47*, 3702–3709.

(43)   Gody, G.; Barbey, R.; Danial, M.; Perrier, S. Ultrafast RAFT Polymerization: Multiblock Copolymers within Minutes. *Polym. Chem.* **2015**, *6* (9), 1502–1511.

(44)   Moad, G. RAFT Polymerization – Then and Now. *Acs Symp. Ser.* **2015**, 211–246.

(45)   Tumbleston, J. R.; Shirvanyants, D.; Ermoshkin, N.; Janusziewicz, R.; Johnson, a. R.; Kelly, D.; Chen, K.; Pinschmidt, R.; Rolland, J. P.; Ermoshkin, a.; et al. Continuous Liquid Interface Production of 3D Objects. *Science (80).* **2015**, *347* (6228), 1349–1352.

(46)   Hinton, T. J.; Hudson, A.; Pusch, K.; Lee, A.; Feinberg, A. W. 3D Printing PDMS Elastomer in a Hydrophilic Support Bath via Freeform Reversible Embedding. *ACS Biomater. Sci. Eng.* **2016**, *2* (10), 1781–1786.

(47)   Hull, C. W. Apparatus for Production of Three-Dimensional Objects by Stereolithography. 4,575,330, 1973.

(48)   Husár, B.; Ligon, S. C.; Wutzel, H.; Hoffmann, H.; Liska, R. The Formulator's Guide to Anti-Oxygen Inhibition Additives. *Prog. Org. Coatings* **2014**, *77* (11), 1789–1798.

(49)   Kim, S. K.; Guymon, C. A. Effects of Polymerizable Organoclays on Oxygen Inhibition of Acrylate and Thiol-Acrylate Photopolymerization. *Polymer (Guildf).* **2012**, *53* (8), 1640–1650.

(50)   Shanmugam, S.; Xu, J.; Boyer, C. Aqueous RAFT Photopolymerization with Oxygen Tolerance. *Macromolecules* **2016**, acs.macromol.6b02060.

(51)   Lee, T. Y.; Guymon, C. A.; Jönsson, E. S.; Hoyle, C. E. The Effect of Monomer Structure on Oxygen Inhibition of (Meth)acrylates Photopolymerization. *Polymer (Guildf).* **2004**, *45* (18), 6155–6162.

(52)   Tumbleston, J. R.; Shirvanyants, D.; Ermoshkin, N.; Johnson, A. R.; Kelly, D.; Chen, K.; Pinschmidt, R.; Rolland, J. P.; Ermoshkin, A.; Samulski, E. T.; et al. Reports (Continuous Liquid Interface Production of 3D Objects. **2015**, March, 1–7.

(53)   Lalevée, J.; Dietlin, C.; Morlet-Savary, F.; Fouassier, J. P.; Dumur, F.; Gigmes, D.; Garra, P. Photopolymerization of Thick Films and in Shadow Areas: A Review for the Access to Composites. *Polym. Chem.* **2017**.

(54)   Brazel, C. L.; Rosen, S. L. *Fundamental Principles of Polymeric Materials*; John Wiley & Sons, Inc.: Hoboken, New Jersey, 2012.

(55)   Reddy, S. K.; Cramer, N. B.; O' Brien, A. K.; Cross, T.; Raj, R.; Bowman, C. N. Rate Mechanisms of a Novel Thiol-Ene Photopolymerization Reaction. *Macromol. Symp.* **2004**, *206* (1), 361–374.

(56)   Hyde, S. T. Identification of Lyotropic Liquid Crystalline Mesophases. In *Handbook of Applied Surface and Colloid Chemistry*; Holmberg, K., Ed.; John Wiley & Sons, Inc., 2001; pp 299–332.

(57)   Shiyanovskii, S. V.; Lavrentovich, O. D.; Schneider, T.; Ishikawa, T.; Smalyukh, I. I.; Woolverton, C. J.; Niehaus, G. D.; Doane, K. J. Lyotropic Chromonic Liquid Crystals for Biological Sensing Applications. *Mol. Cryst. Liq. Cryst.* **2005**, *434*, 587–598.

(58)   Martyniak, A.; Dilger, H.; McKenzie, I.; Scheuermann, R.; Lagerwall, J.; Roduner, E. Partitioning and Reorientational Dynamics of Phenylalcohols in SDS Lyotropic Liquid Crystalline Mesophases: An ALC-μSR Study. *Colloids Surfaces A Physicochem. Eng. Asp.* **2007**, *309* (1–3), 224–230.

(59)   Friberg, S. E.; Thundathil, R.; Stoffer, J. O. Changed Lyotropic Liquid Crystalline Structure Due to Polymerization of the Amphiphilic Component. *Science (80-.).* **1979**, *205* (4406), 607–608.

(60)   Leferink op Reinink, a. B. G. M.; Pol, E.; Petukhov, a. V.; Vroege, G. J.; Lekkerkerker, H. N. W. Phase Behaviour of Lyotropic Liquid Crystals in External Fields and Confinement. *Eur. Phys. J. Spec. Top.* **2013**, *222* (11), 3053–3069.

(61)   Barón, M. Definitions of Basic Terms Relating to Low-Molar-Mass and Polymer Liquid Crystals (IUPAC Recommendations 2001). *Pure Appl. Chem.* **2001**, *73* (5), 845–895.

(62)   Baguenard, C.; Guymon, C. A. Self-Assembled Supramolecular Architectures. Lyotropic Liquid Crystals. Edited by Nissim Garti, Ponisseril Somasundaran and Raffaele Mezzenga. *Angew. Chemie Int. Ed.* **2013**, *52* (34), 8789–8789.

(63)   DePierro, M. A.; Carpenter, K. G.; Guymon, C. A. Influence of Polymerization Conditions on Nanostructure and Properties of Polyacrylamide Hydrogels Templated from Lyotropic Liquid Crystals. *Chem. Mater.* **2006**, *18* (23), 5609–5617.

(64)   Depierro, M. A.; Guymon, C. A. Polymer Structure Development in Lyotropic Liquid Crystalline Solutions. *Macromolecules* **2014**, *47*, 5728–5738.

(65)   Worthington, K. S.; Baguenard, C.; Forney, B. S.; Guymon, C. A. Photopolymerization Kinetics in and of Self-Assembling Lyotropic Liquid Crystal Templates. *J. Polym. Sci. Part B Polym. Phys.* **2017**, *55* (6), 471–489.

(66)   Lee, Y. S. 4. Molecular Self - Assembly in Solution Ii: Bilayers, Liquid Crystals, and Emulsions. *Self-Assembly Nanotechnol. A Force Balanc. Approach* **2008**, 75–101.

(67)   Griffin, W. C. Calculation of HLB Values of Non-Ionic Surfactants. *J. Soc. Cosmet. Chem.* **1954**, 249–256.

(68) Fink, J. K. F. (Ed.). (2015). *Water-Based Chemicals and Technology for Drilling, Completion, and Workover Fluids*. Boston: Gulf Professional Publishing.

(69)   Worthington, K. S.; Green, B. J.; Rethwisch, M.; Wiley, L. A.; Tucker, B. A.; Guymon, C. A.; Salem, A. K. Neuronal Di Ff Erentiation of Induced Pluripotent Stem Cells on Surfactant Templated Chitosan Hydrogels. *Biomacromolecules* **2016**, *17*, 1684–1695.

(70)   Huang, K.-L.; Sigeta, K.; Kunieda, H. Phase Behavior of Polyoxyethylene Dodecyl Ether-Water Systems. *Prog. colloid Polym. Sci.* **1998**, *110*, 171–174.

(71)   Gliveli, D. E.; Davis, S. S.; Kayes, J. B. Critical Micelle Concentration , Surface , Volumetric , and Hydrodynamic Properties of Polyoxyethylenemonohexadecyl Ethers. *J. Colloid Interface Sci.* **1983**, *91* (1), 1–11.

(72)   Chen, Z.; Greaves, T. L.; Fong, C.; Caruso, R. a; Drummond, C. J. Lyotropic Liquid Crystalline Phase Behaviour in Amphiphile-Protic Ionic Liquid Systems. *Phys. Chem. Chem. Phys.* **2012**, *14* (11), 3825–3836.

(73)   Nandy, D.; Mitra, R. K.; Paul, B. K. Phase Behavior of the Mixtures of Poly(oxyethylene) (10) Stearyl Ether (Brij-76), 1-Butanol, Isooctane, and Mixed Polar Solvents. II. Water and Ethylene Glycol (EG) or Tetraethylene Glycol (TEG). *J. Colloid Interface Sci.* **2007**, *310* (1), 229–239.

(74)   Graca, M.; Bongaerts, J. H. H.; Stokes, J. R.; Granick, S. Nanotribology, Standard Friction, and Bulk Rheology Properties Compared for a Brij Microemulsion. *J. Colloid Interface Sci.* **2009**, *333* (2), 628–634.

(75)   Rossi, G.; Fuchs, P. F. J.; Barnoud, J.; Monticelli, L. A Coarse-Grained MARTINI Model of Polyethylene Glycol and of Polyoxyethylene Alkyl Ether Surfactants. *J. Phys. Chem. B* **2012**, *116* (49), 14353–14362.

(76)   Detcheverry, A.; Kang, H.; Daoulas, K. C.; Müller, M.; Nealey, P. F.; Pablo, J. J. De. Monte Carlo Simulations of a Coarse Grain Model for Block Copolymers and Nanocomposites Franc. **2008**, 4989–5001.

(77)   Nakata, K.; Tsuchido, T.; Matsumura, Y. Antimicrobial Cationic Surfactant, Cetyltrimethylammonium Bromide, Induces Superoxide Stress in Escherichia Coli Cells. *J. Appl. Microbiol.* **2011**, *110* (2), 568–579.

(78)   Ishikawa, S.; Matsumura, Y.; Katoh-Kubo, K.; Tsuchido, T. Antibacterial Activity of Surfactants against Escherichia Coli Cells Is Influenced by Carbon Source and Anaerobiosis. *J. Appl. Microbiol.* **2002**, *93* (2), 302–309.

(79)   Forney, B. S.; Baguenard, C.; Guymon, C. A. Effects of Controlling Polymer Nanostructure Using Photopolymerization within Lyotropic Liquid Crystalline Templates. *Chem. Mater.* **2013**, *25* (15), 2950–2960.

(80)   DePierro, M. a.; Guymon, C. A. Photoinitiation and Monomer Segregation Behavior in Polymerization of Lyotropic Liquid Crystalline Systems. *Macromolecules* **2006**, *39* (2), 617–626.

(81)   Shi, L.; Wu, X.; Lu, L.; Yang, X.; Wang, X. Molecular Mechanism for Formation of Polyaniline Lamella from a Lyotropic Liquid Crystal: An NMR Study. *J. Phys. Chem. B* **2009**, *113* (9), 2725–2733.

(82)   Desai, a.; Varade, D.; Mata, J.; Aswal, V.; Bahadur, P. Structural Transitions of Cetyltrimethylammonium Bromide Micelles in Aqueous Media: Effect of Additives. *Colloids Surfaces A Physicochem. Eng. Asp.* **2005**, *259* (1–3), 111–115.

(83)   Uddin, M. H.; Morales, D.; Kunieda, H. Phase Polymorphism by Mixing of Poly(oxyethylene)-Poly(dimethylsiloxane) Copolymer and Nonionic Surfactant in Water. *J. Colloid Interface Sci.* **2005**, *285* (1), 373–381.

30

(84) Kunieda, H.; Uddin, M. H.; Horri, M.; Furukawa, H.; Harashima, A. Effect of Hydrophilic- and Hydrophobic-Chain Lengths on the Phase Behavior of A-B-Type Silicone Surfactants in Water. *J. Phys. Chem. B* **2001**, *105* (23), 5419–5426.

(85) Rodriguez, C.; Uddin, M. H.; Watanabe, K.; Furukawa, H.; Harashima, a; Kunieda, H. Self-Organization, Phase Behavior and Microstructure of Poly(oxyethylene)Poly(dimethylsiloxane) Surfactants in Non-Polar Oil. *J. Phys. Chem. B* **2002**, *106*, 22–29.

(86) Forney, B. S.; Guymon, C. A. Fast Deswelling Kinetics of Nanostructured poly(N-Isopropylacrylamide) Photopolymerized in a Lyotropic Liquid Crystal Template. *Macromol. Rapid Commun.* **2011**, *32* (9–10), 765–769.

(87) Clapper, J. D.; Iverson, S. L.; Guymon, C. A. Nanostructured Biodegradable Polymer Networks Using Lyotropic Liquid Crystalline Templates. *Biomacromolecules* **2007**, *8* (7), 2104–2111.

(88) Clapper, J. D.; Sievens-Figueroa, L.; Guymon, C. A. Photopolymerization in Polymer Templating. *Chem. Mater.* **2008**, *20* (3), 768–781.

(89) Clapper, J. D.; Guymon, C. A. Physical Behavior of Cross-Linked PEG Hydrogels Photopolymerized within Nanostructured Lyotropic Liquid Crystalline Templates. *Macromolecules* **2007**, *40* (4), 1101–1107.

(90) Thorson, T. Phase Behavior and Stimuli Response in Lyotropic Liquid Crystalline Templated Photopolymers, University of Iowa, 2013.

(91) Clapper, J. D.; Guymon, C. A. Nanostructured Biodegradable Polymer Composites Generated Using Lyotropic Liquid Crystalline Media. *Macromolecules* **2007**, *40* (22), 7951–7959.

(92) Sorenson, G. P.; Coppage, K. L.; Mahanthappa, M. K. Unusually Stable Aqueous Lyotropic Gyroid Phases from Gemini Dicarboxylate Surfactants. *J. Am. Chem. Soc.* **2011**, *133* (38), 14928–14931.

(93) Eichenbaum, G. M., Kiser, P. F., Simon, S. A., & Needham, D. pH and Ion - Triggered Volume Response of Anionic Hydrogel Microspheres *Macromolecules*, **1998**, *31*, 5084–5093.

(94) Liu, F.; Urban, M. W. Recent Advances and Challenges in Designing Stimuli-Responsive Polymers. *Prog. Polym. Sci.* **2010**, *35*, 3–23.

(95) Zabara, A.; Negrini, R.; Onaca-Fischer, O.; Mezzenga, R. Perforated Bicontinuous Cubic Phases with pH-Responsive Topological Channel Interconnectivity. *Small* **2013**, No. 21, 3602–3609.

(96)   Zhu, C. H.; Lu, Y.; Peng, J.; Chen, J. F.; Yu, S. H. Photothermally Sensitive poly(N-Isopropylacrylamide)/graphene Oxide Nanocomposite Hydrogels as Remote Light-Controlled Liquid Microvalves. *Adv. Funct. Mater.* **2012**, *22* (19), 4017–4022.

(97)   Bäcker, M.; Raue, M.; Schusser, S.; Jeitner, C.; Breuer, L.; Wagner, P.; Poghossian, A.; Förster, A.; Mang, T.; Schöning, M. J. Microfluidic Chip with Integrated Microvalves Based on Temperature- and pH-Responsive Hydrogel Thin Films. *Phys. Status Solidi Appl. Mater. Sci.* **2012**, *209* (5), 839–845.

(98)   Pelton, R. Poly(N-Isopropylacrylamide) (PNIPAM) Is Never Hydrophobic. *J. Colloid Interface Sci.* **2010**, *348* (2), 673–674.

(99)   Sasaki, S.; Okabe, S.; Miyahara, Y. Thermodynamic Properties of N-Isopropylacrylamide in Water: Solubility Transition, Phase Separation of Supersaturated Solution, and Glass Formation. *J. Phys. Chem. B* **2010**, *114*, 14995–15002.

(100)   Illeperuma, W. R. K.; Sun, J.-Y.; Suo, Z.; Vlassak, J. J. Force and Stroke of a Hydrogel Actuator. *Soft Matter* **2013**, *9* (35), 8504–8511.

(101)   Zhang, X.; Pint, C. L.; Lee, M. H.; Schubert, B. E.; Jamshidi, A.; Takei, K.; Ko, H.; Gillies, A.; Bardhan, R.; Urban, J. J.; et al. Optically- and Thermally-Responsive Programmable Materials Based on Carbon Nanotube-Hydrogel Polymer Composites. *Nano Lett.* **2011**, *11* (8), 3239–3244.

(102)   Liu, H. Y.; Zhu, X. X. Lower Critical Solution Temperatures of N -Substituted Acrylamide Copolymers in Aqueous Solutions. *Polymer* **1999**, *40*, 6985–6990.

(103)   Ni, C.; Zhu, X.-X. X. Synthesis and Swelling Behavior of Thermosensitive Hydrogels Based on N-Substituted Acrylamides and Sodium Acrylate. *Eur. Polym. J.* **2004**, *40* (6), 1075–1080.

(104)   Forney, B. S.; Baguenard, C.; Guymon, C. A. Improved Stimuli-Response and Mechanical Properties of Nanostructured poly(N-Isopropylacrylamide-Co-Dimethylsiloxane) Hydrogels Generated through Photopolymerization in Lyotropic Liquid Crystal Templates. *Soft Matter* **2013**, *9* (31), 7458–7467.

(105)   Hertle, Y.; Zeiser, M.; Hasenöhrl, C.; Busch, P.; Hellweg, T. Responsive P(NIPAM-Co-NtBAM) Microgels: Flory-Rehner Description of the Swelling Behaviour. *Colloid Polym. Sci.* **2010**, *288* (10–11), 1047–1059.

(106)   Cath, T. Y.; Childress, A. E.; Elimelech, M. Forward Osmosis : Principles , Applications , and Recent Developments. *J. Memb. Sci.* **2006**, *281*, 70–87.

(107)   McGinnis, R. L.; Elimelech, M. Energy Requirements of Ammonia–carbon Dioxide Forward Osmosis Desalination. *Desalination* **2007**, *207* (1–3), 370–382.

(108) Wang, H.; Wei, J.; Simon, G. P. Response to Osmotic Pressure versus Swelling Pressure: Comment on " Bifunctional Polymer Hydrogel Layers As Forward Osmosis Draw Agents for Continuous Production of Fresh Water Using Solar Energy ." *Environ. Sci. Technol.* **2014**, *48*, 4214–4215.

(109) Zhao, S. Osmotic Pressure versus Swelling Pressure: Comment on " Bifunctional Polymer Hydrogel Layers As Forward Osmosis Draw Agents for Continuous Production of Fresh Water Using Solar Energy ." *Environ. Sci. Technol.* **2014**, *48*, 4212–4213.

(110) Zhang, H.; Li, J.; Cui, H.; Li, H.; Yang, F. Forward Osmosis Using Electric-Responsive Polymer Hydrogels as Draw Agents: Influence of Freezing–thawing Cycles, Voltage, Feed Solutions on Process Performance. *Chem. Eng. J.* **2015**, *259*, 814–819.

(111) Cai, Y.; Shen, W.; Wang, R.; Krantz, W. B.; Fane, A. G.; Hu, X. CO2 Switchable Dual Responsive Polymers as Draw Solutes for Forward Osmosis Desalination. *Chem. Commun. (Camb).* **2013**, *49* (75), 8377–8379.

(112) Li, D.; Wang, H. Smart Draw Agents for Emerging Forward Osmosis Application. *J. Mater. Chem. A* **2013**, *1* (45), 14049–14060.

(113) Li, D.; Zhang, X.; Yao, J.; Zeng, Y.; Simon, G. P.; Wang, H. Composite Polymer Hydrogels as Draw Agents in Forward Osmosis and Solar Dewatering. *Soft Matter* **2011**, *7* (21), 10048.

(114) Thompson, N. A.; Nicoll, P. G. Forward Osmosis Desalination: A Commercial Reality. In *IDA World Congress*; 2011; pp 1–16.

(115) McCutcheon, J. R.; McGinnis, R. L.; Elimelech, M. Desalination by Ammonia–carbon Dioxide Forward Osmosis: Influence of Draw and Feed Solution Concentrations on Process Performance. *J. Memb. Sci.* **2006**, *278* (1–2), 114–123.

(116) Carmignani, G.; Sitkiewitz, S.; Webley, J. W. Recovery of Retrograde Soluble Solute for Forward Osmosis Water Treatment. US 2012/0267308A1, 2012.

(117) Cai, Y.; Hu, X. M. A Critical Review on Draw Solutes Development for Forward Osmosis. *Desalination* **2016**, *391*, 16–29.

(118) Cai, Y.; Shen, W.; Loo, S. L.; Krantz, W. B.; Wang, R.; Fane, A. G.; Hu, X. Towards Temperature Driven Forward Osmosis Desalination Using Semi-IPN Hydrogels as Reversible Draw Agents. *Water Res.* **2013**, *47* (11), 3773–3781.

(119) Razmjou, A.; Barati, M. R.; Simon, G. P.; Suzuki, K.; Wang, H. Fast Deswelling of Nanocomposite Polymer Hydrogels via Magnetic Field-Induced Heating for Emerging FO Desalination. *Environ. Sci. Technol.* **2013**, *47* (12), 6297–6305.

(120) Razmjou, A.; Simon, G. P.; Wang, H. Effect of Particle Size on the Performance of Forward Osmosis Desalination by Stimuli-Responsive Polymer Hydrogels as a Draw Agent. *Chem. Eng. J.* **2013**, *215–216*, 913–920.

(121) Wei, J.; Low, Z. X.; Ou, R.; Simon, G. P.; Wang, H. Hydrogel-Polyurethane Interpenetrating Network Material as an Advanced Draw Agent for Forward Osmosis Process. *Water Res.* **2016**, *96*, 292–298.

(122) Effects of Moisture Absorption http://www.intechpower.com/material-information/effects-of-moisture-absorption (accessed Feb 21, 2018).

(123) Inoue, K.; Hoshino, S. Swelling of Nylon 6 Film due to Water Sorption. *J. Polym. Sci.* **1976**, *14* (8), 1513–1526.

(124) Flory, P. J.; Rehner, J. Statistical Mechanics of Cross-Linked Polymer Networks II. Swelling. *J. Chem. Phys.* **1943**, *11* (11), 521–526.

(125) Horkay, F.; Tasaki, I.; Basser, P. J. Osmotic Swelling of Polyacrylate Hydrogels in Physiological Salt Solutions. *Biomacromolecules* **2000**, *1* (1), 84–90.

(126) Manek, E.; Tombácz, E.; Geissler, E.; László, K. Search for the Origin of Discrepancies in Osmotic Measurements of the PNIPAM - Water System. *Period. Polytech. Chem. Eng.* **2017**, *61* (1), 39–50.

(127) Han, I. S.; Han, M.-H. H.; Kim, J.; Lew, S.; Lee, Y. J.; Horkay, F.; Magda, J. J. Constant-Volume Hydrogel Osmometer: A New Device Concept for Miniature Biosensors. *Biomacromolecules* **2002**, *3* (6), 1271–1275.

(128) Storey, N. *Electronics a Systems Approach*, 3rd ed.; Prentice Hall, 2006.

(129) Henkel, R.; Vana, P. Increasing the Tackiness of Statistical poly(Butyl Acrylate) and poly(Ethyl Acrylate) Network Materials via RAFT Polymerization. *Macromol. Mater. Eng.* **2015**, *300* (5), 551–561.

2: OBJECTIVES

Control and modification of polymer properties through understanding structure property relationships on the molecular, nanometer, and micrometer level are powerful tools for the tailoring of materials. This work investigates the modification of properties on two size-scales: on the nanostructure level by surfactant templating and on the molecular level by utilizing reversible addition fragmentation chain transfer (RAFT) agents to tailor network morphology. Lyotropic liquid crystal (LLC) surfactants are combined with photopolymerization to reliably template a variety of monomer types. By templating nanostructure within a polymer, a network can be formed within the material that allows higher degrees of transport and improved response kinetics and transitions to thermal stimulus. RAFT agents are used to modify the propagation of radical photopolymerization, enabling the control of network formation. This control over the formation of a polymer network morphology can modify material properties, including elongation, modulus, and toughness, of a crosslinked photopolymer.

Within the material science field, the importance of understanding and controlling material properties from 'the ground up' cannot be overstated. The overall goal of this work is to show the impact that structure of different size scales has upon the material properties of photopolymers. Additionally, this work aims to analyze how control over structure can be used for material applications. These goals will be accomplished through the following objectives:

1. Create stimuli-responsive superabsorbent materials with LLC templating and photopolymerization.

2. Determine suitability of hydrogel materials as forward osmosis draw agents.

35

3. Correlate LLC surfactant mesophase templates with swelling by utilizing linear amphiphilic surfactants of various head and tail lengths.

4. Utilize LLC templating and photopolymerization as a method for creating capacitive materials from silicone diacrylates.

5. Control network morphology and elongation of urethane diacrylates with RAFT chain transfer agents

The first objective is achieved in Chapter 4 by demonstrating that the thermo-responsive volume transition is augmented by LLC templating in poly(n-isopropyl acrylamide-sodium acrylate) (PNIPAM-SA) copolymers. Non-templated, isotropic copolymers do not retain the large volume transition apparent in templated hydrogels. Furthermore, it is demonstrated that as SA concentration increases, the complexity and degree of template retention is reduced. A corresponding reduction in the range of volume transition is also observed.

Chapter 5 fulfills the second objective by testing the flux and osmotic pressure of LLC templated PNIPAM-SA copolymers through direct and indirect methods. It is determined that LLC templated materials induce higher water flux through semi-permeable membranes. At the same time, the structure created with LLC templates does not increase the osmotic pressure. This observation combined with the findings in Chapter 4 shows promise for utilizing LLC templating techniques for forward osmosis draw agents because of the large amount of stimuli-responsive volume transition resulting from the continuous pore network.

Objective 3 is accomplished in Chapter 6 through systematic evaluation of linear amphiphilic surfactants for the presence of LLC phases when mixed with water.

Surfactants at various concentrations are then used as templates for PNIPAM hydrogels. By varying the surfactant concentration, different mesophases are used as templates. The work determines the effect of templated nanostructure on the swelling of materials and separates nanostructure effects from the simple presence of surfactant during polymerization.

Finally, Objective 4 is achieved when polymer electrochemical properties are modified utilizing LLC and photopolymerization in Chapter 7. Silicone diacrylates are templated in the lamellar mesophase on a carbon cloth electrode. The capacitance of the materials is measured using cyclic voltammetry. Values are compared to isotropic samples of the same polymer. The ordered structure within the silicone material acts as a multitude of nanoscale electric double layer capacitors, allowing the nanostructured film to exhibit several orders of magnitude more specific capacitance than non-templated films.

The fifth objective is met in Chapter 8 by modifying network morphology in urethane diacrylates polymerized in the presence of RAFT agents. By exploiting the reversible nature of the chain transfer mechanism of RAFT, chain growth can be controlled to create networks with increased elongation and reduced modulus. The network property modification is hypothesized to be caused by increased homogeneity of the molecular weight between crosslinks in the polymer network.

These objectives provide understanding regarding the fundamentals of polymer structure on the nano- and microscale and how they influence bulk properties of materials. This work demonstrates that small scale changes can have large scale impacts on the properties of materials. By studying and understanding the fundamentals of

37

structure-property relationships, especially on small size scales, new applications for photocured polymer systems can be envisioned and developed.

3: MATERIALS AND EXPERIMENTAL METHODS

This chapter describes the materials and methods used to explore the effects of small scale structure on the properties of photopolymers. Surfactant selection and the basic procedure for lyotropic liquid crystal (LLC) templating is described in the first section. This is followed by a description of the preparation of films modified with reversible addition fragmentation chain transfer (RAFT) and the preparation of capacitive silicone films. Finally, characterization methods used to observe structure, polymerization reaction kinetics, thermomechanical properties, transport, and electrochemical properties are described.

3.1: Material and Sample Preparation

3.1.1: Materials

Materials used in this study consisted of the following commercially available monomers: *n*-isopropyl acrylamide (NIPAM, Sigma-Aldrich), sodium acrylate (SA, Sigma-Aldrich), a silicone diacrylate oligomer 1500 MW (Di-1508, Siltech), and a diacrylate oligomer 3500MW, (CN 9002, Sartomer). 2,2-dimethoxy-2-phenylacetophenone (DMPA, Ciba) was used as a photoinitiator and *n-n'*methylene bisacrylamide (MBA, Sigma-Aldrich) was used as a crosslinker. Deionized water, ethanol (Sigma-Aldrich), and acetone (Sigma-Aldrich) were used as solvents. Polyethylene glycol, 6000 MW (PEG6000, Sigma-Aldrich), and sucrose (table sugar) were used as solutes to create osmotic pressure solutions. Cyanomethyl dodecyl trithiocarbonate RAFT agent was prepared as described elsewhere.[1] Figure 3.1 shows the chemical structures of materials used in this study.

A variety of surfactants were used in LLC templating processes. Surfactants with hydrophilic poly(oxy ethylene) head groups and hydrophobic alkyl tails were used in all studies. Surfactants used for modeling swelling in LLC templated hydrogels were selected based on the a wide variety of head and tail lengths available. These surfactants include head groups of ~2, ~10, and ~20 ethylene oxide groups each combined with lauryl (12), cetyl (16), and a steryl (18) alkyl groups, for a total of nine surfactants (see Figure 3.1e for representative structure). The nine surfactants are as follows: polyoxyethylene (4) lauryl ether (Brij L4, Sigma-Aldrich); polyoxyethylene (2) cetyl ether (Brij C2, Sigma-Aldrich); polyoxyethylene (2) steryl ether (Brij S2, Sigma-Aldrich); polyoxyethylene (10) lauryl ether (Sigma-Aldrich); polyoxyethylene (10) cetyl ether (Brij C10, Sigma-Aldrich); polyoxyethylene (10) steryl ether (Brij S10 Sigma-Aldrich); polyoxyethylene (23) lauryl ether (Brij L23, Sigma-Aldrich); polyoxyethylene (20) cetyl ether (Brij C20, Sigma-Aldrich); polyoxyethylene (20) steryl ether (Brij S20, Sigma-Aldrich). The systematic combinations of surfactant heads and tails allows examination of the difference that head and tail length makes with respect to compatibility, swelling, and mesophase availability.
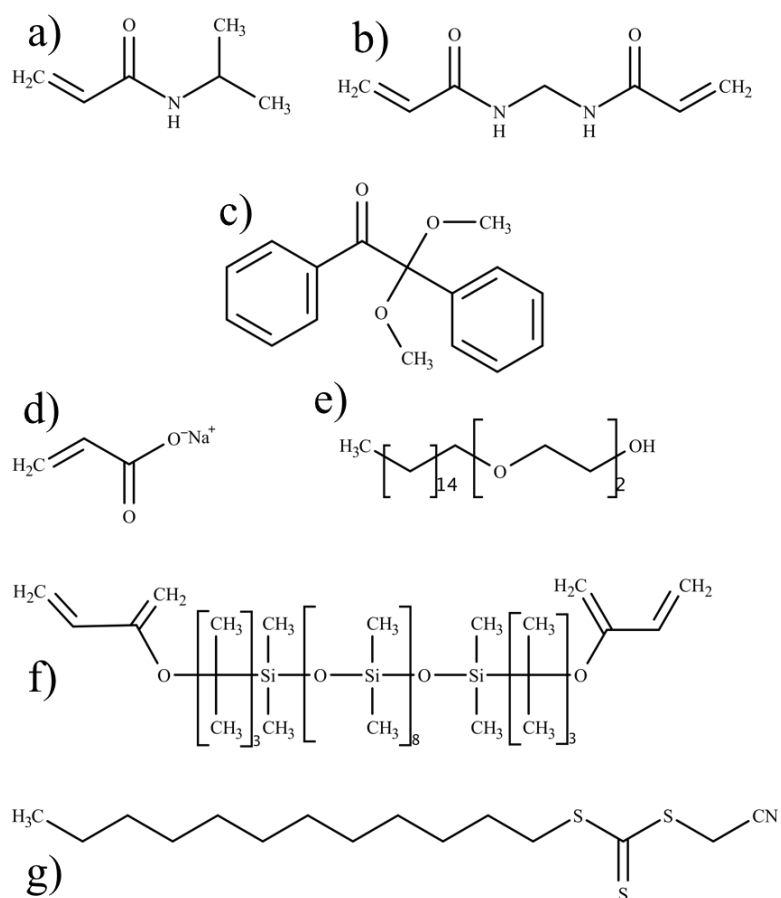
Figure 3.1. Materials used in this study include a) *n*-isopropyl acrylamide (NIPAM), b) *n-n'* methylene bisacrylamide (MBA), c) 2,2-dimethoxy-2-phenylacetophenone (DMPA), d) sodium acrylate (SA), e) polyoxyethylene alkyl ether surfactant, f) silicone diacrylate (Di-1508), and g) cyanomethyl dodecyl trithiocarbonate (CDT).

3.1.2: Polymerization

Polymerization of materials was achieved using mercury arc lamps in various form factors. The most typical was an Omnicure 1500 equipped with a collimator, allowing for a uniform hexagon-shaped beam pattern to be utilized. Occasionally, some experiments required the high intensity light from an industrial mini-belt lamp (Fusion Systems, LC-6B). Samples were passed under the belt lamp in multiple passes to achieve full conversion, with conversion analyzed between each pass.

41

3.1.3: Preparation of LLC Templated Films

LLCs were prepared by mixing surfactants with water, heating, and vortex mixing to fully incorporate and create the mesophase. Initiator and monomers were then added before additional mixing to allow self-assembly of the monomer into the liquid crystal. To ensure appropriate mixing, monomer, crosslinker, and photoinitiator were mixed together before adding surfactant and water. Achieving an LLC mesophase is often accompanied by an increase in viscosity of the mixture, occasionally resulting in extremely viscous fluids with high clearing points.

LLC templated copolymer discs for use in swelling and forward osmosis (FO) studies were prepared by heating and vortex mixing DMPA, NIPAM, and MBA. The surfactant Brij C2 was added to the mixture, heated, and vortex-mixed again before the mixture became too viscous. SA and water were then added to the mixture, heated, and vortex-mixed. The surfactant-templated mixtures were poured into 12 mm OD x 3 mm circular Teflon®-impregnated Delrin® molds while hot and allowed to cool before photocuring. The extensive mixing procedure is necessary due to the complexities of NIPAM mixing thermodynamics. NIPAM solutions exhibit many temperature dependent stable and metastable phases.[2] For example, a NIPAM solution of water will separate into a NIPAM rich phase and a water rich phase at temperatures below 25 ˚C. Following the insertion of a single NIPAM crystal, the solutions will equilibrate into a single liquid phase.

Isotropic mixtures were cooled to room temperature while being vortex mixed aggressively and then poured into Teflon®-impregnated Delrin® molds. Photopolymerization of both mixtures was performed using 10 mW/cm^2 of 365 nm light

42

from an Omnicure 1500 high-pressure mercury arc UV lamp for 20 min. The resulting discs were then rinsed in ethanol for at least 24 h to remove surfactant and unreacted monomers before being vacuum dried. This method removes over 95% of the templating surfactant.[3–5]

3.1.4: Preparation of RAFT Modified Films

Films for RAFT studies were synthesized from CN 9002, a proprietary urethane diacrylate from Sartomer of roughly 3500 g/mol. DMPA was used as the photoinitiator and samples were modified with a cyanomethyl trithiocarbonate chain transfer (RAFT) agent. Ratios from 0-5:1 RAFT: PI were created for property and polymerization kinetics analysis. Samples were heated while mixing to reduce viscosity and were then poured onto a glass slide with 300 µm spacers and then sandwiched with a second glass slide. Samples were then reheated gently with a heat gun to ensure uniformity of the films. Excessive heat may lead to bubbling and care was taken to heat minimally. Samples were polymerized under either the Omnicure 1500 as outlined above or the high intensity belt lamp at 3ft/min.

3.1.5: Preparation of Silicone Electrode Materials

Characterization of LLC templated materials for capacitance measurements requires the polymer films to be applied to an electrode. Carbon/graphite cloth was chosen due to its flexibility and ease of cutting. Polymer samples were prepared as above, then materials were placed on carbon cloth and pressed down with a silicone treated glass slide to a thickness of 300 µm as determined by spacers attached to the glass slide. The slide was then removed and the material cured under UV light for 6 min at 20 mW/cm^2 at

365 nm before being rinsed and dried as before. Electrode samples are then analyzed using cyclic voltammetry.

3.2: Characterization

3.2.1: Structure Characterization

Small-angle X-ray scattering (SAXS) was utilized to determine the mesophase of an LLC or an LLC templated system. The interaction of X-rays with electrons as the photons pass through ordered surfactant structure scatter in distinctive patterns (Figure 3.2). These patterns may be analyzed to observe the distinctive ratios for each LLC mesophase.[6] SAXS profiles are measured for templated systems to determine the structure before and after polymerization. The SAXS instrument used was a Heccus M-Braun with a Kratky-type collimator, Nonius FR590 with copper target Röntgen tube with a Ni-filtered Cu-Kα line of 0.154 nm as the radiation source and a linear PSD-50 detector. Silver stearate was used to calibrate the instrument. Care was taken that detector and beam were in optimal alignment and the beam was as narrow as is practical to obtain maximum peak resolution and minimal scattering.[7] The scattering vector, *q*, was obtained by Equation 3.1,

$$q = 4\pi \sin\frac{2\theta}{\lambda} = 2\pi/d \tag{3.1}$$

where *2θ* is the angle of scattering, *λ* is the wavelength of the X-ray (0.154 nm), and *d* is the characteristic distance between repeat structures in the LLC mesophase, also known as d-spacing. The resulting profiles were background subtracted and the resulting difference was Lorentz corrected and desmeared to correct for collimation and

wavelength effects.[7] The resulting peaks are used to index to mesophases, for examples peak ratios of √3, √4, √7, and √12 indicate the presence of a bicontinuous mesophase.[6]
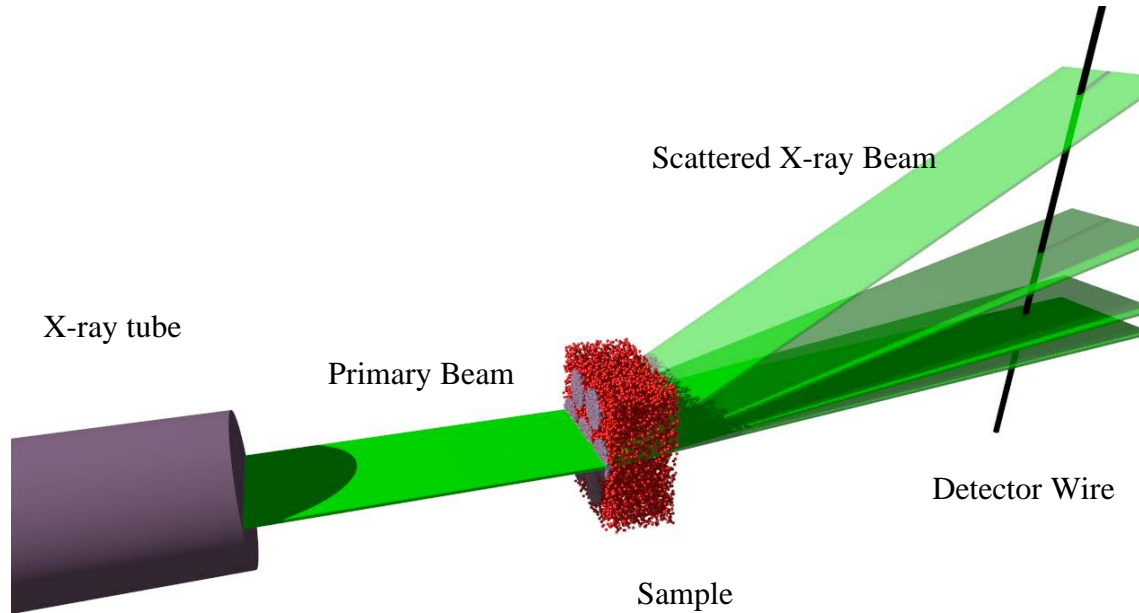
Figure 3.2. Schematic showing the means by which SAXS examines order in LLC samples.

3.2.2: Photopolymerization Kinetics

Fourier transform infrared (FTIR) spectroscopy was used to measure conversion of double bonds in RAFT modified urethane diacrylate samples. By tracking the disappearance of double bond peak from the acrylate or by comparing the peak to a non-reactive peak area or height, it is possible to determine the conversion and relative rate of polymerization for a given polymerization reaction.

3.3: Characterization of Swelling and Stimuli-responsive Properties

Testing of hydrogel materials was performed using a variety of methods to determine the effects that templating an ordered nanostructure have on the swelling and subsequent deswelling of materials. Hydrogel materials consisting of PNIPAM and its

45

copolymers were swollen in water to measure differences in swelling ratio due to LLC templated structure within the materials. Materials were weighed after rinsing and thorough drying in a vacuum chamber. Materials were then placed into water. Swelling was measured after 48 h or whenever equilibrium mass was obtained. Swelling ratio, Q, was reported as swollen mass (M_s) over dry mass (M_d), Equation 3.2.

$$Q = \frac{M_s}{M_d} \tag{3.2}$$

The stimuli-responsive characteristics of PNIPAM and its copolymers were observed in two ways. The first measured the response of the material as a function of temperature. The second measured response as a function of time in an isothermal environment. Swelling ratio at various temperatures was examined to determine the lower critical solution temperature (LCST). LCST is described as the inflection point along the curve made from the equilibrium swelling ratios of a stimuli-responsive polymer swollen at various temperatures.[8] The difference in swelling ratio at initial temperature (Q_{T_i}) and final temperature (Q_{T_f}) can be described as the dynamic range (DR) of the responsive material as shown in Equation 3.3.

$$DR = Q_{T_i} - Q_{T_f} \tag{3.3}$$

Powdered hydrogel samples of templated and isotropic samples were prepared using a standard blade coffee grinder. Samples were ground in stages and the resulting particles were sorted with a mini-sieve system (LabCo).

3.3.1: Forward Osmosis

Osmotic pressure is an important indicator of the ability of the material to function as an FO draw agent. To measure hydrogel osmotic pressure, the use of a semi-permeable membrane is required to separate the draw agent from the opposing draw solution, allowing only water to pass. FO membranes or dialysis tubing with suitably low molecular weight (MW) cutoff may be utilized to separate a solution from the hydrogel. Dialysis tubing has very high permeability to small organic molecules, therefore its resistance is considered negligible when compared to purifying membranes. The membrane serves as a barrier between the two 'solutions,' only allowing water to pass through. In this way, the U-tube allows water to move to one side of the 'U' until forces balance, preventing additional water movement. The height attained by the higher osmotic pressure liquid is used to calculate osmotic pressure with Equation 1.16. Solid materials, such as hydrogels, cannot be tested in this manner and other methods that test osmotic pressure indirectly have been designed.[9–11] By creating a calibration curve of known osmotic pressure solutions, osmotic pressure of concentrated polymer solutions and hydrogel can be approximated.[12] The hydrogel encapsulated in a semi-permeable membrane pouch is swollen in a solution to equilibrium. The swelling ratio at equilibrium can be compared to the known osmotic pressure solutions. At the osmotic pressure where the hydrogel is not able to draw significant water across the membrane, the two materials are considered to be a equilibrium. Using this information, it is possible to determine the osmotic pressure of a hydrogel by extrapolating the curve calculated by swelling at several osmotic pressures to a swelling ratio of zero.[10]

The choice of osmotic solution opposite the hydrogel is an important consideration for determining draw agent osmotic pressure. Ideally, a solution will have high water solubility and suitably high osmotic pressure at a low solution viscosity and concentration. If the solution becomes too viscous at high concentrations, difficulty maintaining a uniformly mixed solution may occur, and boundary layers may form at the membrane surface. The unmixed layer will confound the osmotic pressure measurements. If high concentrations are needed, calculating osmotic pressure using the ideal solution assumption may become inaccurate.[13]

A device based on one described by Dieng, for which the original purpose was to measure the water absorbency of clay soils, was constructed to measure mass transfer into the hydrogel polymer in real-time. A balance with real-time mass determination capabilities was modified to accept a membrane holder. A forward osmosis membrane was placed within the membrane holder. Water flowed to the back side of the membrane rejection layer. The balance was tared, and powdered hydrogel samples were then placed upon the membrane. As water was absorbed into the hydrogel, it was replaced by the reservoir. Thus, the increase in mass was recorded by the balance. The mass of water was used to calculate flux of water across the membrane in $L/m^2/h$ (LMH) by dividing the volume of water by the surface area of the exposed membrane over time.

Pouches of hydrogel materials were tested using FO membranes from Hydration Technologies, Inc. Pouches were assembled from 0.006 inch thick polyethylene film. The FO membrane was sealed around the edges using a commercial heat sealer to melt the film and membrane together, forming a watertight seal on three edges. Pouches were then weighed, filled with the desired hydrogel (powder or whole), weighed again, and sealed

completely before being placed into solution. After a given time, the pouches were removed from the solution, dabbed dry, and weighed to determine the mass of water drawn into the pouch via the osmotic pressure of the hydrogel. The flux of water into the pouch was thereby estimated.

A variation of the above pouch experiments was used to determine the osmotic pressure of a given hydrogel composition. Solutions were prepared from deionized water and PEG6000 or sucrose. Osmotic pressure was calculated by using values observed previously.[13–15] Pouches containing the hydrogel were immersed in the stirred solution and weighed as described above. The osmotic pressure calibration curve standard was used to determine the theoretical osmotic pressure of the hydrogel material.

3.3.2: Dynamic Mechanical Analysis

Methods to characterize network formation rely on derivations from thermomechanical data. Typical methods can include tensile stress-strain measurements, which allow Young's modulus to be calculated from the slope. The stress-strain curve allows the comparison of toughness and elasticity between formulations. Toughness is a measure of the amount of energy a material absorbs, and it is calculated by integrating the function of the stress-strain curve.[16] The slope of the curve gives Young's modulus, which can be used to calculate the crosslink density of a polymer network.[17] Other methods to calculate crosslink density involve swelling the network in a solvent with a known Flory solubility parameter.[18] Measuring the modulus over a wide range of temperatures is also useful for determining information about a polymer network. The tangent of loss over storage modulus versus temperature yields a peak, which corresponds to T_g. The shape and location of the T_g peak can provide information about

49

the network, including uniformity, domains, and chain behavior.[19] Tensile mode was used for quantifying the stress-strain, glass transition temperature (T_g - from Tan(δ) peaks), and toughness.[16] Samples were prepared by cutting rectangular films from prepared samples to approximately 6 x 12 mm. Temperature was increased from -100 to 50 ˚C with a strain ramp rate of 1 N/min. Dynamic mechanical analysis experiments were performed with a TA Instruments Q800 dynamic mechanical analyzer (DMA) in tensile mode. Samples of roughly 3mm by 6 mm were clamped in the tensile clamps and temperature sweeps were performed from -100 to 50 ˚C at a heating rate of 3 ˚C/min to determine the T_g of the cured urethane films by recording Tan(δ) versus temperature. Stress and strain of films were evaluated at 30 ˚C with a force rate of 1.0 N/min. From stress and strain Young's modulus was calculated from the slope of the linear portion of the curve and toughness by integrating the area under the curve.

3.3.3: Cyclic Voltammetry

The capacitance of isotropic silicone and LLC templated silicone materials was examined. Capacitance measurements were made using cyclic voltammetry. A 1 mM aqueous solution of $NaNO_3$ was prepared and sparged using N_2. A three-electrode setup was used. A platinum mesh performed as the counter electrode. The reference electrode (RE) was a saturated calomel electrode (SCE), and the working electrode (WE) consisted of the polymer samples pressed onto carbon cloth.

Cyclic voltammetry was performed (CH instruments, 760B potentiostat) at scan rates of 5, 10, 25, 50, 75, 150, and 200 mV/s, from 0.5 V to 1.3 V. Films were equilibrated in the $NaNO_3$ electrolyte solution for a minimum of 24 h before testing. The

50

envelope width from the resulting voltammogram was used to calculate the capacitance for samples at each scan rate using Equation 3.5.

$$C_d = 2i_c/v_s \qquad\qquad (3.5)$$

where C_d is the capacitance of the device, i_c is the average current observed in the envelope, and v_s is the voltage scan rate.

Analysis of capacitance was carried out using the plot of i versus v_s for low scan rates (5-20 mV/s) and i versus $\sqrt{v_s}$ for high scan rates (50-200 mV/s). The y-intercept for the linearized equation for i versus v_s was assumed to be the capacitance of the polymer film. Specific capacitance of the films was calculated by dividing the capacitance value by the mass. Volume of the polymer film was calculated from the mold dimensions.

(1)   Wood, M. R.; Duncalf, D. J.; Rannard, S. P. Selective One-Pot Synthesis of Trithiocarbonates , Xanthates , and Dithiocarbamates for Use in RAFT / MADIX Living Radical Polymerizations. *Organic Letters.* **2006**. *8*(4), 553-556.

(2)   Sasaki, S.; Okabe, S.; Miyahara, Y. Thermodynamic Properties of N-Isopropylacrylamide in Water: Solubility Transition, Phase Separation of Supersaturated Solution, and Glass Formation. *J. Phys. Chem. B* **2010**, *114*, 14995–15002.

(3)   Forney, B. S.; Guymon, C. A. Fast Deswelling Kinetics of Nanostructured poly(N-Isopropylacrylamide) Photopolymerized in a Lyotropic Liquid Crystal Template. *Macromol. Rapid Commun.* **2011**, *32* (9–10), 765–769.

(4)   Clapper, J. D.; Guymon, C. A. Physical Behavior of Cross-Linked PEG Hydrogels Photopolymerized within Nanostructured Lyotropic Liquid Crystalline Templates. *Macromolecules* **2007**, *40* (4), 1101–1107.

(5)   Forney, B. S.; Baguenard, C.; Guymon, C. A. Improved Stimuli-Response and Mechanical Properties of Nanostructured poly(N-Isopropylacrylamide-Co-Dimethylsiloxane) Hydrogels Generated through Photopolymerization in Lyotropic Liquid Crystal Templates. *Soft Matter* **2013**, *9* (31), 7458–7467.

(6)   Hyde, S. T. Identification of Lyotropic Liquid Crystalline Mesophases. In *Handbook of Applied Surface and Colloid Chemistry*; Holmberg, K., Ed.; John Wiley & Sons, Inc., 2001; pp 299–332.

(7)   Schnablegger, H.; Singh, Y. *The SAXS Guide: Getting Acquianted with the Principles*, 2nd ed.; Anton Paar GmbH.: Graz, Austria, 2011.

(8)   Bäcker, M.; Raue, M.; Schusser, S.; Jeitner, C.; Breuer, L.; Wagner, P.; Poghossian, A.; Förster, A.; Mang, T.; Schöning, M. J. Microfluidic Chip with Integrated Microvalves Based on Temperature- and pH-Responsive Hydrogel Thin Films. *Phys. Status Solidi Appl. Mater. Sci.* **2012**, *209* (5), 839–845.

(9)   Money, N. P. Osmotic Pressure of Aqueous Polyethylene Glycols ' Relationship between Molecular Weight and Vapor Pressure Deficit. *Plant Physiol.* **1989**, *91*, 766–769.

(10)   Horkay, F.; Tasaki, I.; Basser, P. J. Osmotic Swelling of Polyacrylate Hydrogels in Physiological Salt Solutions. *Biomacromolecules* **2000**, *1* (1), 84–90.

(11)   Vink, H. Precision Measurements of Osmotic Pressure in Concentrated Polymer Solutions. *Eur. Polym. J.* **1971**, *7* (2), 1411–1419.

(12)   Parsegian, V. A.; Rand, R. P.; Fuller, N. L.; Rau, D. D. Osmotic Stress for the

Direct Measurement of Intermolecular Forces. *Methods Enzymol.* **1986**, *127*, 400–416.

(13)   Granik, V. T.; Smith, B. R.; Lee, S. C.; Ferrari, M. Osmotic Pressures for Binary Solutions of Non-Electrolytes. *Biomed. Microdevices* **2002**, *4* (4), 309–321.

(14)   Michel, B. E.; Kaufmann, M. R. The Osmotic Potential of Polyethylene Glycol 6000. *Plant Physiol.* **1973**, *51* (5), 914–916.

(15)   Lewis, G. N. The Osmotic Pressure of Concentrated Solutions, and the Laws of the Perfect Solution. *J. Am. Chem. Soc.* **1908**, *30* (5), 668–683.

(16)   Brazel, C. L.; Rosen, S. L. *Fundamental Principles of Polymeric Materials*; John Wiley & Sons, Inc.: Hoboken, New Jersey, 2012.

(17)   Flory, P. J. Molecular Theory of Rubber Elasticity. *Polym. J.* **1985**, *17* (1), 1–12.

(18)   Flory, P. J.; Rehner, J. Statistical Mechanics of Cross-Linked Polymer Networks II. Swelling. *J. Chem. Phys.* **1943**, *11* (11), 521–526.

(19)   Ye, S.; Cramer, N. B.; Bowman, C. N. Relationship between Glass Transition Temperature and Polymerization Temperature for Cross-Linked Photopolymers. *Macromolecules* **2011**, *44*, 490–494.

4: RESPONSIVE SUPERABSORBENT HYDROGELS VIA PHOTOPOLYMERIZATION IN LYOTROPIC LIQUID CRYSTAL TEMPLATES[1]

In this work, stimuli-responsive, superabsorbent materials are created by copolymerization of stimuli-responsive poly(*n*-isopropyl acrylamide) (PNIPAM) in combination with superabsorbent sodium acrylate (SA) via photopolymerization in lyotropic liquid crystal (LLC) templates. Templating PNIPAM in LLC mesophases imparts nanostructure to the polymer that significantly increases transport and swelling when compared to isotropic hydrogels. These materials exhibit twice the equilibrium swelling ratio of analogous non-templated materials and show a dynamic range between the swollen and deswollen state that is 5 times greater. To further augment this stimuli-responsive range, LLC-templated PNIPAM was combined with the superabsorbent monomer sodium acrylate (SA). As SA concentration is increased, significant structure changes are observed during polymerization that leads to less-defined nanostructure and lower stimuli response. Maximum swelling and temperature response are observed at low concentrations of SA (~2 wt%). These LLC-templated copolymers exhibit stimuli-responsive volume transitions up to 40 times and equilibrium swelling ratios of 60 times their dry mass. This 600% increase in thermal response is due to the combined high swelling capabilities of SA with the enhanced thermal-response behavior induced by the LLC-templated nanostructure. Additionally, the nanostructure induces fast deswelling

---

[1]McLaughlin, J. R., Abbott, N. L., & Guymon, C. A. *Polymer* **2018.** 148, *119-126*.

rates at temperatures above the lowest critical solution temperature of PNIPAM. The high dynamic range and quick response of this composition could allow for the development of superabsorbent, stimuli-responsive hydrogels in a variety of biomaterial, microfluidic, and water remediation applications.

4.1: Introduction

Hydrogels that respond to stimuli such as light, pH, or temperature have long been studied for applications including drug delivery, microfluidics, and use in micropumps.[1–3] Poly(*n*-isopropyl acrylamide) (PNIPAM) is one such stimuli-responsive material of significant interest. PNIPAM undergoes a reversible coil-to-globule transition upon heating to a lower critical solution temperature (LCST) of approximately 32 ˚C. This transition leads to a decrease in hydrophilicity resulting in reduced water solubility of linear polymer chains.[4] In a water-swollen, crosslinked hydrogel, this collapse of the chains between crosslinks manifests as a volume decrease and water release. Due the proximity of this transition to physiological temperatures, PNIPAM been examined for use as a drug-release agent as well as in actuators, sensors, and pumps.[1,5,6] To enhance performance for these applications, several methods have been used to increase water swelling capacity and release in PNIPAM systems. Promising results have been observed by creating specific polymer morphologies including interpenetrating networks (IPN) or semi-IPNs using crosslinked PNIPAM.[7–10] Another means of significant interest for enhancing swelling capacity is to incorporate superabsorbent monomers into stimuli-responsive materials.[11,12]

Superabsorbents exhibit high degrees of swelling, often well over 10 times their dry mass.[13,14] The extensively used sodium acrylate (SA) is often incorporated for

55

applications in consumer health products such as lotions, creams, powders, diapers, and soil management.[15,16] Unfortunately, superabsorbent materials, including SA, tend to lose mechanical integrity and become weak pastes or gels when swollen[17] making them unsuitable if reuse or repeated handling is required. When incorporated with PNIPAM, SA may also limit the degree of stimuli-response. The hydrophilic nature of the superabsorbent prevents complete water release from the system. Therefore, PNIPAM materials modified with SA exhibit small dynamic ranges of water release and slow response kinetics, making them less desirable for practical applications.[6] While stimuli-responsive hydrogels incorporating SA superabsorbents have shown promise in water purification as draw agents for forward osmosis,[18–21] these materials would benefit significantly from enhanced water release speed and magnitude.

One promising means to improve the stimuli-responsive kinetics and water swelling has recently been demonstrated when templating lyotropic liquid crystal (LLC) nanostructures, in PNIPAM materials via radical photopolymerization.[22] LLC are surfactant/water mixtures with structure on the nanometer scale when mixed at appropriate concentrations. Monomers can be incorporated in LLC domains, then photopolymerized to facilitate greater degrees of nanostructure formation in the polymer.[23,24] After photopolymerization, the LLC template surfactant is removed, resulting in a template directed polymer structure (Figure 4.1). Since photopolymerization reactions proceed rapidly, the nanostructure imparted to the monomer by the LLC mesophase may, to some extent, be kinetically trapped in the resulting polymer.[25] The resulting photocured network may then exhibit distinct morphologies originating from the LLC template.[23,26] Conversely, thermal

56
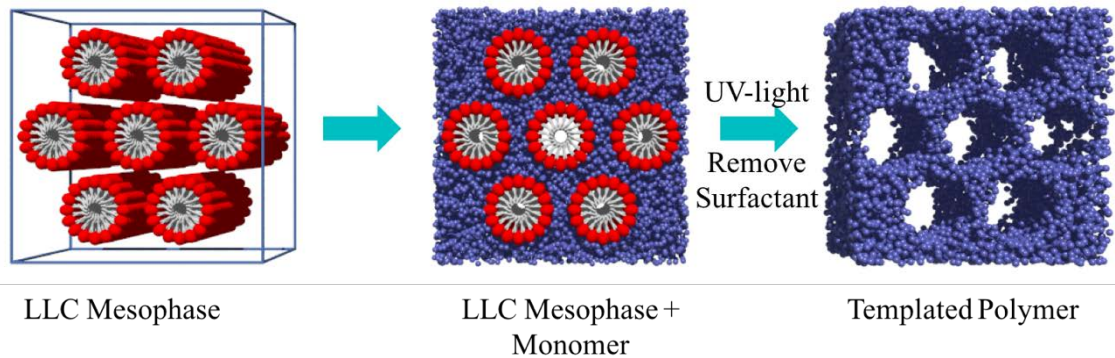
Figure 4.1. Schematic showing steps for LLC templating using photopolymerization. LLC mesophases self-assemble from water and surfactant mixtures. Monomer segregates in polar and/or non-polar domains. After photopolymerization the surfactant is removed, leaving the templated polymer.

polymerizations are relatively slow and allow for thermodynamic phase separation to occur during the polymerization, resulting in formation of significantly different structures.[27]

Through structure development and controlled porosity, LLC templating has shown great promise for controlling the swelling and mechanical properties of hydrogel materials. The structure allows enhanced transport and mechanical properties, which could be of particular utility in stimuli-responsive materials.[22,28–30] For example, recent work has shown that equilibrium swelling ratio of LLC templated PNIPAM polymer materials in water is doubled compared to non-templated equivalent materials, and have much faster deswelling of the absorbed water. The increased deswelling was attributed to the ordered structure allowing more facile transport of water to and from the hydrogel in addition to preventing the formation of a dense outer 'shell' as the material undergoes the volumetric transition and deswelling. Interestingly, even with twice the water content, the

57

nanostructured material showed little change in compressive modulus in the swollen state relative to isotropic materials.

In developing temperature-sensitive materials with high swelling capacity via copolymerization of stimuli-responsive polymers with superabsorbents, the degree of swelling of the resulting material increases. Unfortunately, this increase is accompanied by a reduction in the magnitude of the stimuli-response range.[7] We hypothesize that combining LLC templating with superabsorbent monomers will further increase swelling while also allowing increases in the stimuli-responsive range of hydrogel materials with directed structure and transport. In this work, we utilize the advantages of both LLC templating and SA copolymerization with PNIPAM to examine the impact of enhanced swelling and structure on stimuli-responsive properties.[5,7,21,31] LLC templated PNIPAM materials were copolymerized with SA to determine the effects of SA addition on structure retention, water swelling, and stimuli-response. The templated polymer structure was examined using small-angle X-ray scattering (SAXS) profile analysis and scanning electron microscopy (SEM). Material swelling and deswelling were measured as a function of temperature while deswelling kinetics were examined isothermally to elucidate thermoresponsive behavior. Finally, swelling and deswelling cycles were examined to determine the repeatability of stimuli-response. Through a combination of LLC templating and copolymerization of a superabsorbent with a stimuli-responsive monomer, novel materials that are both superabsorbent and can quickly and reversibly respond to temperature have been created.

4.2: Experimental

Monomers used to develop stimuli-responsive superabsorbent gels in this work include *n*-isopropyl acrylamide, *n,n'*-methylene bisacrylamide (MBA) crosslinker, and sodium acrylate (SA), all from Sigma-Aldrich. The photoinitiator incorporated was 2,2-dimethoxy-2-phenylacetophenone (DMPA, Ciba). Poly(oxyethylene)-2-cetyl ether (Brij 52, Sigma-Aldrich) was utilized as the templating surfactant, and ethanol as a rinse solvent to remove surfactant along with residual monomer and photoinitiator. Chemical structures of surfactants, monomers, and photoinitiator are given in Figure 4.2. All materials were used as received.

LLC-templated and isotropic hydrogels were created with copolymer compositions containing 0 to 5 wt% SA, 20 wt% NIPAM, and a 1:100 mass ratio of both MBA and DMPA to total monomer content with water comprising the remainder of each formulation. LLC-templated copolymer discs were prepared by heating and vortex mixing DMPA, NIPAM, and MBA. Surfactant (Brij 52), SA, and water were added to the mixture with heating and mixing between addition of each component. The surfactant-templated mixtures were placed into 12 mm diameter x 3 mm circular Teflon®-impregnated Delrin® molds while hot and allowed to cool before photocuring. Isotropic systems incorporating monomers, water, and photoinitiator were heated during mixing and then cooled to room temperature before being placed into the same molds. Photopolymerization of mixtures was performed using 10 mW/cm^2 of 365 nm light from an Omnicure 1500 high-pressure mercury arc UV lamp for 20 min. The resulting discs were then rinsed in ethanol for at least 24 h to remove surfactant, residual photoinitiator, and unreacted monomers before vacuum drying.[22,28,32]
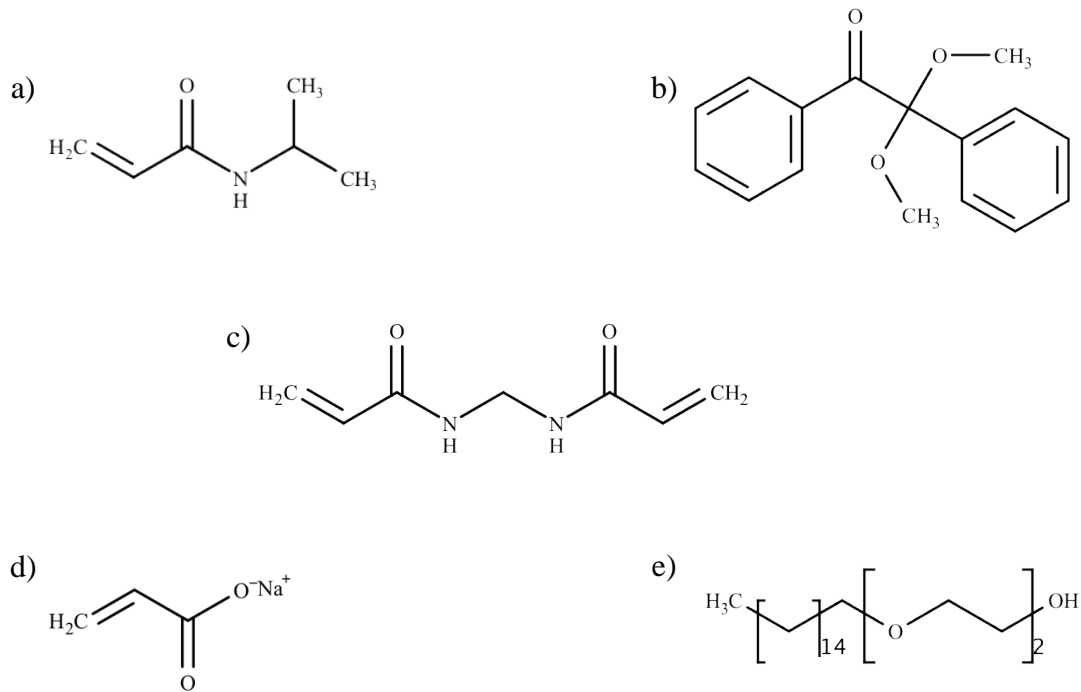
Figure 4.2. Materials used in this work including: a) *N*-isopropyl acrylamide (NIPAM),
b) 2,2-dimethoxy-2-phenylacetophenone (DMPA), c) *N-N'* methylene bisacrylamide,
d) sodium acrylate (SA), and e) polyoxyethylene (10) cetyl ether (Brij 52).

4.2.1: Small Angle X-ray Scattering (SAXS)

SAXS was used to assess LLC-structure by collecting diffraction profiles of
materials before and after polymerization. The SAXS instrument used was a Heccus M-
Braun, with a Kratky-type collimator, Nonius FR590 with copper target Röntgen tube
with a Ni-filtered Cu Kα line of 0.154 nm as the radiation source and a linear PSD-50
detector. Silver stearate was used to calibrate the instrument. Profiles are shown with
background profiles subtracted, Lorentz corrected, desmeared, and smoothed.

4.2.2: Scanning Electron Microscopy (SEM)

Samples were imaged using a Hitachi S-4800 scanning electron microscope with accelerating voltages between 1.5 kV and 2.5 kV. Prior to image collection, the samples were vacuum dried for at least 24 h, fractured, and sputter-coated with Au/Pd for three min at 10 mA. Images shown are polymer structures along the fracture plane.

4.2.3: Temperature Response of Materials

Dried discs were placed in room temperature (22 ˚C) deionized water and allowed to swell to equilibrium. Temperature response of discs was measured by allowing discs to equilibrate for 24 h at temperatures ranging from 22 ˚C to 55 ˚C. Disc mass was measured after dabbing excess water with a moistened laboratory napkin. Swelling ratio for the above experiments was calculated using Equation 3.2. All swelling and deswelling studies were performed in triplicate with error reported as standard deviation. The dynamic range (DR) of stimuli-response was defined by Equation 3.3 as the difference between equilibrium swelling ratios at two times or two temperatures. The LCST of each sample was determined by calculating the inflection point of the temperature response curve in the negative sloping region.[33,34]

4.2.4: Kinetic Swelling and Deswelling.

Discs were swollen to equilibrium mass in distilled water at 22 ˚C. To measure the rate of deswelling at elevated temperatures, the discs were placed in distilled water at 50 ˚C. The mass was then measured at different times to ascertain the degree and rate of stimuli-response. The discs were dabbed lightly with a moistened laboratory napkin to remove surface water before mass was recorded. To demonstrate the reversibility of the

stimuli-responsive behavior, the discs were immersed at 50 °C for 24 h. The samples were then re-swollen in deionized water at 22 °C for 24 h before again being immersed in water at 50 °C for 24 h. The swell/deswell cycle was repeated four times, alternating between 50 °C and 22 °C with mass recorded after each swell and deswell. The reversible dynamic range (RDR), a measure of the water that can be repeatedly absorbed and released by a sample over a 24 h swelling and deswelling cycle, was calculated by subtracting the equilibrium swelling ratios at 50 °C and 22 °C averaged for the final three cycles, (Equation 4.1).

$$RDR = Q_{22\,°C} - Q_{50\,°C} \qquad (4.1)$$

4.3: Results and Discussion

Prior work has demonstrated that LLC-templated PNIPAM hydrogels exhibit rapid and large dynamic range deswelling above the lower critical solution temperature (LCST). The network created using LLC templating also facilitates significantly increased swelling and enhanced overall stimuli-response.[22] These property enhancements are largely due to the formation of a nanostructured network directed by the LLC. Increasing the dynamic swelling and overall swelling ratio to an even greater degree could be desirable for many applications such as water remediation. This work demonstrates the generation of materials with high swelling and stimuli-response by photopolymerizing superabsorbent and stimuli-responsive monomers in LLC templates. We believe that increased swelling in combination with induced nanostructure will allow greater increases in the magnitude of the stimuli-response.

62

PNIPAM retains its nanostructure well during LLC templating,[22,28] but adding an ionic species such as SA may affect structure both before and after polymerization. To determine the influence of SA on LLC phase structure, SAXS was used to observe the LLC mesophase of templated NIPAM-SA copolymer hydrogels pre- and post-polymerization as a function of SA concentration up to 4 wt% (Figure 4.3).

In the SAXS profiles before polymerization without SA, a strong primary peak with several higher-order reflections is observed, consistent with a bicontinuous LLC mesophase.[35] Upon addition of 2 wt% SA before polymerization, similar profiles to the 0 wt% control are observed. After polymerization, the 2 wt% SA sample peaks are not as well defined compared to the pre-polymerization profile, but still indicate bicontinuous structure. These changes imply that SA disrupts the LLC structure particularly as polymerization progresses. Retention of structure is even more difficult at higher concentrations of SA. The templated 4 wt% SA profile before polymerization still indexes strongly to a bicontinuous mesophase. During polymerization, the peaks appear to shift to positions indicative of a hexagonal mesophase. The observed shift indicates mesophases are becoming less stable during polymerization with increasing SA, and that the final structure may exhibit lower degrees of or even different order indicating some degree of phase separation.

Prior work has shown that changes in ordering on the microscopic level are also observed for LLC-templated systems that mirror that found at the nanoscale. Templated hydrogels exhibit textures at micron size scales directly related to the internal nanostructures present in the material.[36] SEM was thus utilized to observe the differences in internal surface features of the isotropic and LLC-templated materials with increasing
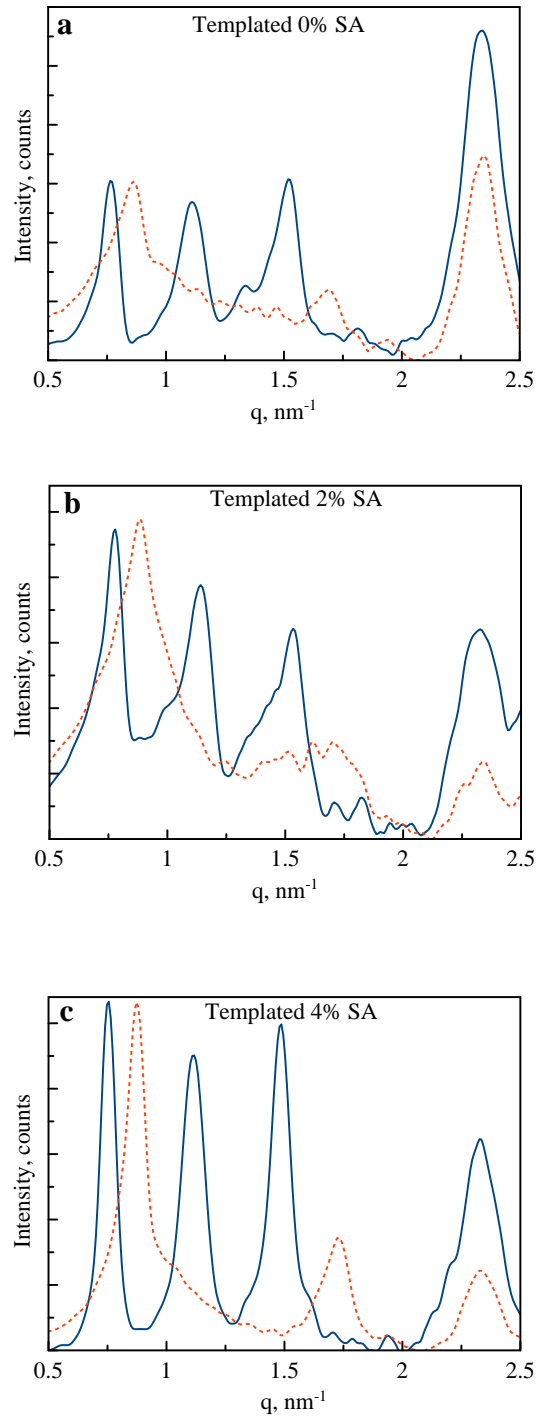
Figure 4.3. SAXS profiles of PNIPAM 20%/SA mixtures containing a) 0, b) 2, and c) 4 wt% SA templated with 40 wt% Brij 52 in water before (—) and after (---) photopolymerization.

SA loading (Figure 4.4). Isotropic material morphologies at all SA concentrations appear to be relatively uniform, with little porosity or structure definition indicative of internal structure.

On the other hand, the LLC templated materials appear to have much greater definition. In the templated 0 wt% SA sample, the internal surface appears to exhibit a well-defined porous texture, indicating that significant internal porosity is present in the responsive hydrogel. When the SA loading is increased to 2 wt%, the sample still shows defined texture, but the porosity appears to be slightly decreased. A decrease in structure definition is consistent with observations in the SAXS profiles discussed earlier. As SA is further increased to 4 wt%, the structure is much less defined, with even less evidence of porous structure. These results imply that the presence of SA disrupts LLC phase stability during polymerization and may allow less retention of the templated LLC structure. These less defined polymer morphologies may also lead to significant changes in water absorption and stimuli-response properties.

Other research has shown that water absorption of stimuli-responsive PNIPAM is increased by incorporating SA. However, the increased swelling came at the expense of stimuli-response with the additional hydrophilic moieties limiting water release. Stimuli response and swelling are both enhanced in PNIPAM hydrogels by LLC templating hydrogels in LLC mesophases.[22,28] It is therefore reasonable to believe that combining superabsorbents with LLC structure will allow even greater degrees of swelling and subsequent release of water. To determine the effect of adding SA to swelling and stimuli-response for both templated and untemplated NIPAM hydrogels, the swelling ratio was examined with increasing concentration of SA as a function of temperature

65
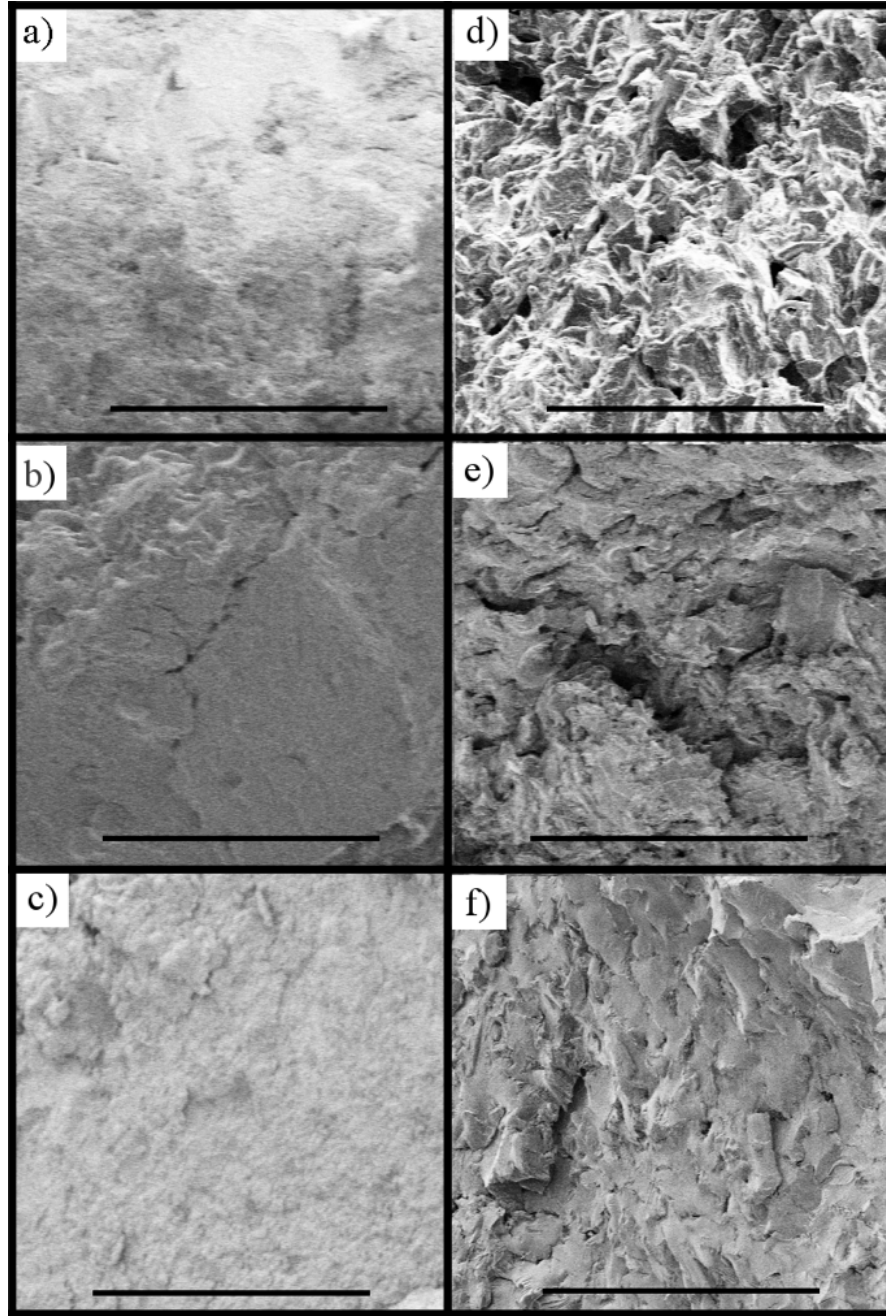
Figure 4.4. SEM micrographs comparing isotropic PNIPAM hydrogels with a) 0, b) 2, and c) 4 wt% SA and templated PNIPAM hydrogel samples with d) 0, e) 2, and f) 4 wt% SA in LLC templated materials. The scale bar represents 500 μm.

(Figure 4.5). The characteristic temperature at which the deswelling event occurs, i.e., the lower critical solution temperature (LCST) was also determined from the inflection point of each curve. LCST and swelling data for the formulations are summarized in Table 4.1. The addition of SA to isotropic PNIPAM systems causes equilibrium swelling ratios both above and below the LCST to increase significantly at temperatures with added SA (Figure 4.5a).

Untemplated control samples without SA swell to a ratio below the LCST at 22 ˚C ($Q_{22\ ˚C}$) of over 10 and subsequently deswell at higher temperatures by more than 50% above the LCST ($Q_{55\ ˚C}$). This transition results in water release approximately 5 times the dry mass resulting in a dynamic range (DR) of about 7. Upon addition of 2 and 4 wt% SA, the swelling ratio of the material increases dramatically to over 30 and 40 below the LCST respectively. Even with this greater swelling, the DR remains similar with values of approximately 8 and 10. Interestingly, the LCST at which the volume transition occurs for the SA isotropic materials increases slightly to 35 ˚C, whereas the isotropic control transitions at the lower temperature of 32 ˚C (Table 4.1). Similar shifts in LCST have been observed upon the addition of hydrophilic monomers to other stimuli-responsive systems based on increased hydrophilic nature of the hydrogel.[34,37]

Adding SA does increase swelling for PNIPAM systems, but does not result in large increases in overall water release. It is reasonable to believe that the higher porosity imparted by LLC templating may allow stimuli-responsive characteristics of PNIPAM to improve and allow greater water release at the higher swelling ratios realized due to the addition of SA. The LLC-templated control without SA deswells from about 18 to 2 times the dry mass when heated above the LCST (Figure 4.5b and Table 4.1). This

67
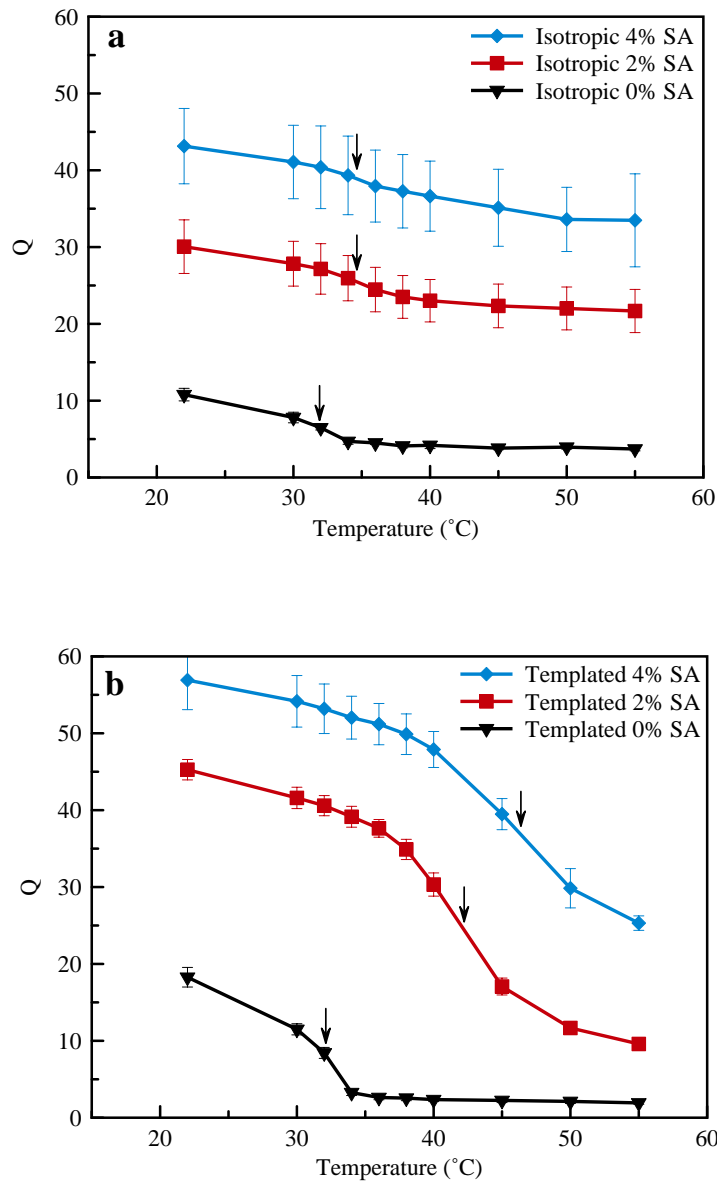
Figure 4.5. Equilibrium swelling ratios (Q) at various temperatures for a) isotropic and b) templated materials with increasing concentrations of SA. Dynamic range (DR) is the difference between $Q_{22\,°C}$ and $Q_{55\,°C}$. The LCST is found from the inflection point of each curve (as indicated by the arrow).

response represents an almost 3-fold increase from the overall dynamic range (DR) of the isotropic sample, likely due to the enhanced transport within the templated structure. As SA loading is increased to 2 wt%, the Q value equilibrium swelling ratio

Table 4.1. Swelling degree, LCST, dynamic range, post-polymerization mesophase for templated and isotropic samples at equilibrium.

Sample	$Q_{22°C}$	$Q_{55°C}$	LCST, °C	Dynamic Range	Post-polymerization mesophase
Templated 0% SA	18 ± 1	1.9 ± 0.2	32.3	16	Bicontinuous Cubic
Templated 2% SA	45 ± 1	9.6 ± 0.5	42.1	36	Bicontinuous Cubic
Templated 4% SA	57 ± 4	25.3 ± 0.9	46.3	32	Hexagonal
Isotropic 0% SA	10.8 ± 0.8	3.7 ± 0.2	32.1	7.1	N/A
Isotropic 2% SA	30 ± 4	22 ± 3	34.6	8	N/A
Isotropic 4% SA	43 ± 5	34 ± 6	34.7	10	N/A

below the LCST is significant, increased to over 45, while the equilibrium swelling ratio above the LCST is approximately 10 resulting in a DR of more than 35 times the dry mass (a full 4 and a half times increase in stimuli-response compared to the isotropic sample). The large increase in overall stimuli-response shows the synergistic effect of incorporating SA in a LLC templated material. Further increase in SA loading to 4 wt% in a templated hydrogel also brings $Q_{22 °C}$ to almost 60 with the deswollen value at 55 °C to over 30, again representing a significant increase in DR as compared to the analogous isotropic samples. Interestingly, the enhancing effect from LLC templated structure is not as large as in the 2 wt% SA sample, a trend supported by the change in morphology and decrease in observed porosity discussed previously. The reduction in defined structure in

69

the 4 wt% SA templated sample and the corresponding decrease in stimuli-response illustrates the importance of structure and pore morphology on material properties. As pore definition is decreased in templated materials with increasing SA concentration, stimuli-responsive properties move closer to those of isotropic systems.

For templated materials, SA addition affects LCST to a much larger degree than in isotropic materials. As SA loading increases in isotropic samples, the LCST increases only about 3 ˚C from 32 ˚C. On the other hand, the 2 wt% and 4 wt% templated SA samples exhibit LCSTs at the much higher temperatures of 42.1 and 46.3 ˚C, respectively. The marked increase is not likely due to changes in chemistry as the compositions are virtually identical. Instead, the large increases in LCST appear to be a consequence of the nanostructure allowing significantly more water into the system that changes the inherent behavior of the gel to act as a more hydrophilic material. With the additional water, higher energy would be required for the deswelling transition to occur, thereby driving the LCST to occur at higher temperatures. The larger magnitude of swelling and stimuli-response also appears to be directly due to the ordered structure and continuous pore network templated within the material. The structure allows additional water to be absorbed within the material and subsequently allows the hydrogel to collapse to a greater degree, expelling more water during stimuli-response events due to additional void space from the porous network.

Another possible advantage of the LLC-templated structure is faster deswelling of water from the hydrogel system.[22] To elucidate the deswelling kinetics of the copolymers as a function of SA concentration, the stimuli response of PNIPAM/SA copolymer materials was examined by immersing samples in 50 ˚C water. Mass change from water

70

expulsion was then examined as a function of time (Figure 4.6). Isotropic samples at both load levels of SA deswell slowly over 20 min, each releasing roughly an equal amount of water despite the much greater swelling at higher concentrations of SA (Figure 4.6a). The isotropic 0 wt% SA control deswells rapidly, similar to results in prior work.[22] These three isotropic samples lose roughly 6-7 times their dry mass in water after 20 min.

On the other hand, templated samples with superabsorbent SA exhibit much more rapid deswelling from equilibrium even upon incorporation of SA (Figure 4.6b). The LLC-templated 0 wt% SA sample deswells rapidly and virtually to completion in 90 s, with over double the water expelled as compared to the isotropic material. Upon addition of 2 wt% SA in templated samples, greater initial swelling is observed while the rate at water expelled is reduced. By 20 min, 90% of the release response is observed, representing a mass approximately 35 times that of the dried polymer. Interestingly, nearly 6 times more water is released by the templated 2 wt% SA sample than its isotropic analogue. Increasing SA content to 4 wt% further raises the equilibrium swelling ratio as discussed previously, however the response rate is decreased even further, due to differences in the templated structure. At 20 min, only 65% of the water that is released at equilibrium has been expelled. Even so, the templated material exhibits a much larger stimuli-response than the analogous isotropic material with about 3.5 times more water being released after 20 min.

The increase in deswelling rate in, templated samples is again likely due to the nanostructure preventing the formation of a dense deswollen outer layer of material which often occurs in non-templated materials.[38] Typically, when a PNIPAM hydrogel is deswollen, the outside surface will respond to the stimulus by expelling water. In

71
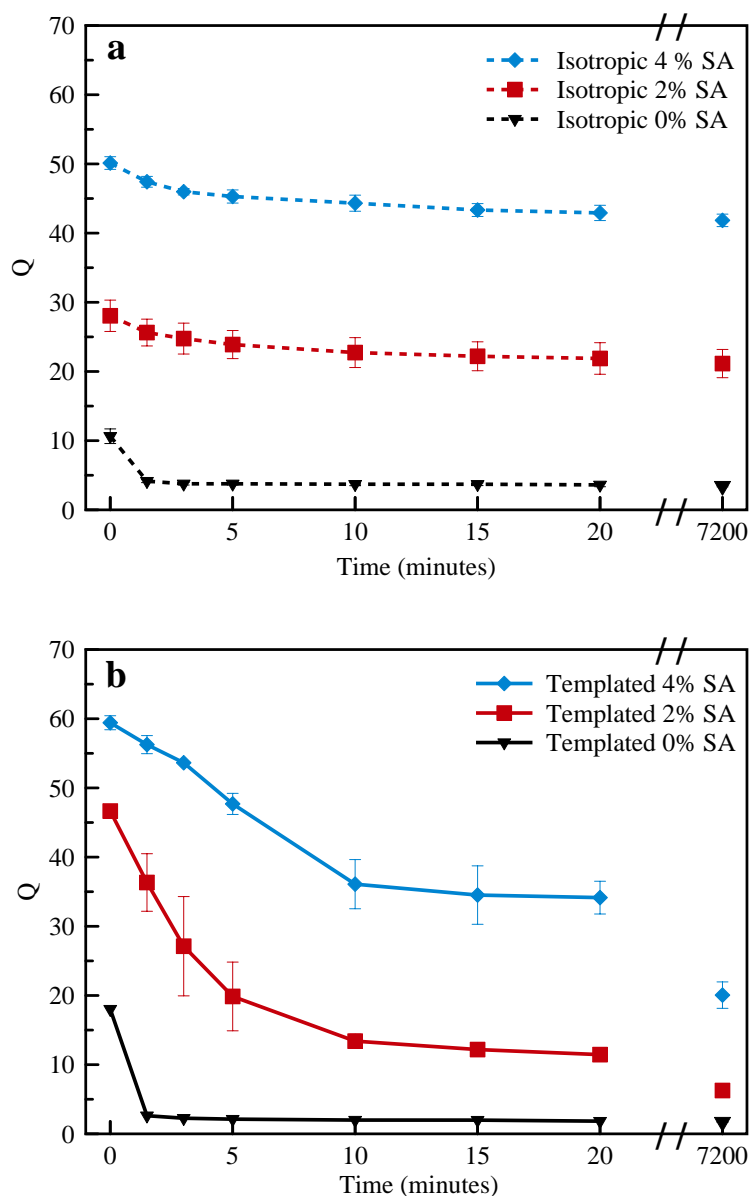
Figure 4.6. Equilibrium swelling data showing the rate of stimuli-response for a) isotropic and b) LLC-templated materials with varying concentrations of SA placed in 50 ˚C water after initial equilibration at 22 ˚C.

isotropic samples, this results in a dense polymer 'shell' on the outside, which slows water expulsion from the inside of the bulk material and reduces water transport to the interior. This behavior is observed with the gradual deswelling of the isotropic samples. However, the ordered nanostructure and porosity of the LLC-templated materials allows
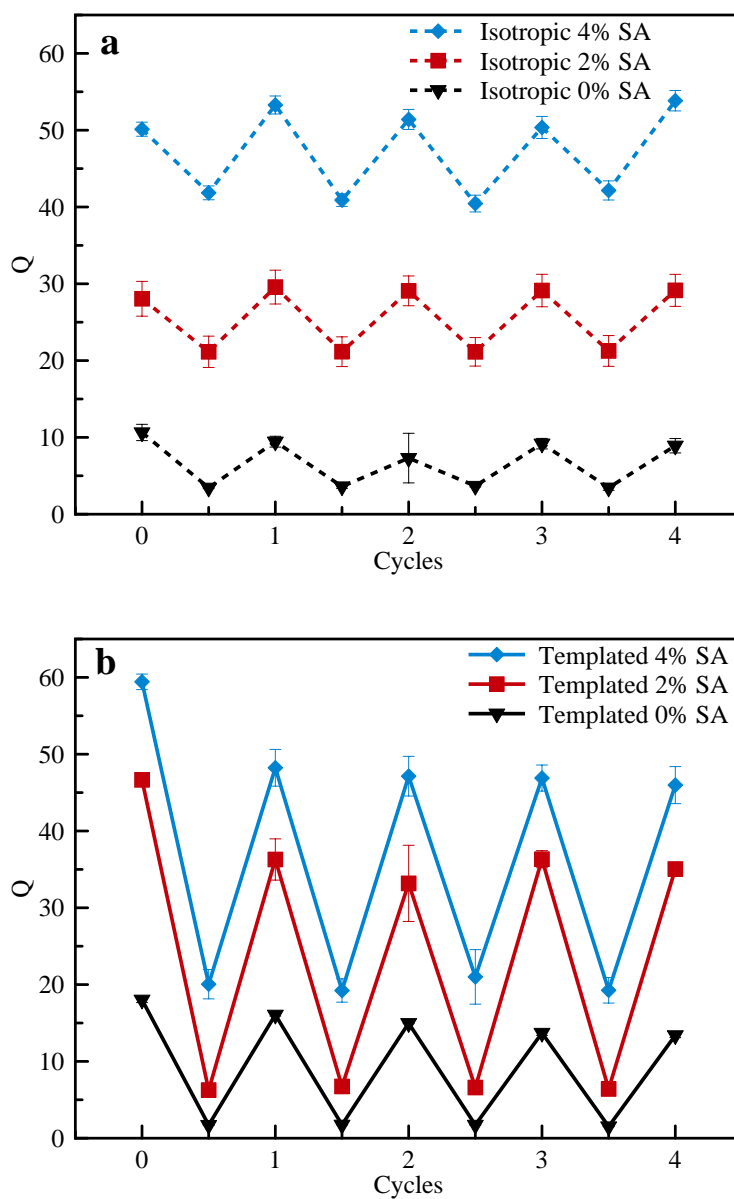
Figure 4.7. Swelling ratios of a) isotropic and b) LLC-templated materials with varying concentrations of SA during 24-h cycling from 22 ˚C to 50 ˚C. Discs were equilibrated at each temperature for 24 h. Average peak-to-valley change from cycles 2-4 were used to calculate the reversible dynamic range (RDR).

water to flow from the material quickly and more completely, unhindered by a dense polymer layer. Heat may also transport more efficiently through the disc via the increased water transport and water content, allowing for more rapid stimuli-response from the

transition. Increased transport from LLC templated nanostructure is essential to the rapid response rate of these materials. The slower response of templated NIPAM/SA is also not surprising given the lower degrees of order as the SA disrupts the LLC-structure.

Reversibility of the thermoresponsive transition for linear PNIPAM chains in solution is well understood; similar cycling studies of templated hydrogel materials would reveal if the templated structure is stable or collapses over repeated cycles.[34] It is also important to understand how the content of SA will affect the repeated swelling and

deswelling of LLC templated materials. To demonstrate the hydrogel copolymer stimuli-response reversibility, materials were cycled between 22 ˚C and 50 ˚C (Figure 4.7). After 24 h at each temperature, mass was determined. Cycling experiments also allowed the reversible dynamic range (RDR), i.e., the average of the difference from the swollen to deswollen state from a 24-h cycle, of stimuli-response to be measured, demonstrating the repeatability of the process. Isotropic samples show a relatively small RDR for the four cycles measured (Figure 4.7a). The isotropic 0 wt% and 2 wt% SA samples exhibit an RDR of 8 with an increase to approximately 10 for 4 wt% SA loading. Isotropic formulations swell and deswell consistently and reversibly, demonstrating the material structure and dynamics are not changing after several cycles.

The LLC-templated materials also demonstrate reversibility but with much higher RDR (Figure 4.7b). The templated 0 wt% SA control responds to temperature by expelling 16 times its dry mass of water after several cycles, double the RDR of the isotropic material. When SA loading is increased to 2 wt% in the templated sample, an RDR of approximately 32 which represent a total of 4 times more water released per cycle than observed from its isotropic counterpart. Increasing SA further to 4 wt% results

in a slightly lower RDR, about 28 times the dry mass, but one which is still 3 times larger than the isotropic analogue. Repeated cycling of both isotropic and templated samples shows no indication of attenuated swelling capacity or loss of stimuli-response for the cycles tested. A reduction in maximum swelling over cycles is also not observed, which is evidence that the templated structure is not changing. The initial higher equilibrium swelling ratio before the first cycle of the templated materials arises as full equilibrium swelling takes over two days, whereas the samples for subsequent cycles were only allowed 24 h to swell. The isotropic samples do not exhibit the same initial difference due to the much smaller amount of water that absorbs.

4.4: Conclusions

Herein, we demonstrate that effective temperature-responsive, superabsorbent materials are produced through photopolymerization of NIPAM with SA in LLC templates. The ordered LLC-template significantly influences the structure of NIPAM-*co*-SA polymer networks. As SA loading is increased, decreased structure definition and retention of LLC phase morphology are observed as SA interferes with LLC self-assembly, thereby providing a less stable template. At intermediate concentrations (e.g., 2 wt% SA), significant pore structure is still observed. With further increases in SA loading, LLC phase morphology changes during polymerization, resulting in a less defined and almost amorphous polymer structure. This changing structure with addition of SA shows interesting effects on swelling and the temperature-response of these hydrogel materials. Higher equilibrium swelling ratios are obtained with addition of SA to both isotropic and templated copolymers as would be expected. In isotropic, non-templated materials, the addition of SA increases swelling but only slightly increases the

75

amount of water released above the LCST. On the other hand, with templated systems the addition of SA dramatically increases both the degree of swelling and the water release. For example, with incorporation of 2 wt% SA, templated materials release over 4 times more water than isotropic analogues. Additionally, LLC-templated materials exhibit faster and more complete volume transitions. This volume transition is reversible upon repeated swelling and deswelling cycles. The enhanced dynamic range and faster release properties of the LLC-templated materials is likely due to the continuous pore network imparted to the polymer by LLC templating. As pore network becomes less defined with higher loadings of SA, the decrease in structure definition corresponds to a significant reduction in temperature-induced volume transitions. These superabsorbent, temperature-sensitive materials could prove useful for applications that require large, rapid, and reversible changes in volume and water content such as drug delivery and water remediation.

4.5: References

(1)   Zhu, C. H.; Lu, Y.; Peng, J.; Chen, J. F.; Yu, S. H. Photothermally Sensitive poly(N-Isopropylacrylamide)/graphene Oxide Nanocomposite Hydrogels as Remote Light-Controlled Liquid Microvalves. *Adv. Funct. Mater.* **2012**, *22* (19), 4017–4022.

(2)   Mondal, S.; Wickramasinghe, S. R. Photo-Induced Graft Polymerization of N-Isopropyl Acrylamide on Thin Film Composite Membrane: Produced Water Treatment and Antifouling Properties. *Sep. Purif. Technol.* **2012**, *90*, 231–238.

(3)   Zhang, H.; Cooper, A. I. Thermoresponsive "particle Pumps": Activated Release of Organic Nanoparticles from Open-Cell Macroporous Polymers. *Adv. Mater.* **2007**, *19* (18), 2439–2444.

(4)   Pelton, R. Poly(N-Isopropylacrylamide) (PNIPAM) Is Never Hydrophobic. *J. Colloid Interface Sci.* **2010**, *348* (2), 673–674.

(5)   Sun, X.; Shi, J.; Zhang, Z.; Cao, S. Dual-Responsive Semi-Interpenetrating Network Beads Based on Calcium Alginate / Poly (N -Isopropylacrylamide)/ Poly (Sodium Acrylate) for Sustained Drug Release. *J. Appl. Polym. Sci.* **2011**, *122*, 729–737.

(6)   Roy, D.; Cambre, J. N.; Sumerlin, B. S. Future Perspectives and Recent Advances in Stimuli-Responsive Materials. *Prog. Polym. Sci.* **2010**, *35* (1–2), 278–301.

(7)   Cai, Y.; Shen, W.; Loo, S. L.; Krantz, W. B.; Wang, R.; Fane, A. G.; Hu, X. Towards Temperature Driven Forward Osmosis Desalination Using Semi-IPN Hydrogels as Reversible Draw Agents. *Water Res.* **2013**, *47* (11), 3773–3781.

(8)   Yang, S.; Park, K.; Rocca, J. G. Semi-Interpenetrating Polymer Network Superporous Hydrogels Based on Poly(3-Sulfopropyl Acrylate, Potassium Salt) and Poly(Vinyl Alcohol): Synthesis and Characterization. *J. Bioact. Compat. Polym.* **2004**, *19* (2), 81–100.

(9)   Janovák, L.; Varga, J.; Kemény, L.; Dékány, I. Investigation of the Structure and Swelling of poly(N-Isopropyl-Acrylamide-Acrylamide) and poly(N-Isopropyl-Acrylamide-Acrylic Acid) Based Copolymer and Composite Hydrogels. *Colloid Polym. Sci.* **2008**, *286* (14–15), 1575–1585.

(10)   Hertle, Y.; Zeiser, M.; Hasenöhrl, C.; Busch, P.; Hellweg, T. Responsive P(NIPAM-Co-NtBAM) Microgels: Flory-Rehner Description of the Swelling Behaviour. *Colloid Polym. Sci.* **2010**, *288* (10–11), 1047–1059.

(11) Mohan, Y. M.; Premkumar, T.; Joseph, D. K.; Geckeler, K. E. Stimuli-Responsive Poly (N -Isopropylacrylamide-Co-Sodium Acrylate) Hydrogels : A Swelling Study in Surfactant and Polymer Solutions. **2007**, *67*, 844–858.

(12) Huang, H.; Zhang, D.; Mao, Z.; Yu, W.; Yan, H. Fast Responsive and Strong Swelling Hydrogels Based on N -Isopropylacrylamide with Sodium Acrylate. *J. Appl. Polym. Sci.* **2008**, *112*, 123–128.

(13) Buchholz, F. L.; Graham, A. T. *Modern Superabsorbent Polymer Technology*, 1st ed.; Buchholz, F. L., Graham, A. T., Eds.; WILEY-VCH Verlag: New York, 1997.

(14) Brannon-Peppas, L.; Harland, R. S. *Absorbent Polymer Technology*, 1st ed.; Brannon-Peppas, L., Harland, R. S., Eds.; Elsevier Inc.: Amsterdam, 1990.

(15) Muzzalupo, R.; Tavano, L.; Rossi, C. O.; Cassano, R.; Trombino, S.; Picci, N. Synthesis and Properties of Methacrylic-Functionalized Tween Monomer Networks. *Langmuir* **2009**, *25* (3), 1800–1806.

(16) Zohuriaan-mehr, M. J.; Kabiri, K. Superabsorbent Polymer Materials: A Review. **2008**, *17* (6), 451–477.

(17) Anseth, K. S.; Bowman, C. N.; Brannon-Peppas, L. Mechanical Properties of Hydrogels and Their Experimental Determination. *Biomaterials* **1996**, *17* (17), 1647–1657.

(18) Zhang, H.; Li, J.; Cui, H.; Li, H.; Yang, F. Forward Osmosis Using Electric-Responsive Polymer Hydrogels as Draw Agents: Influence of Freezing–thawing Cycles, Voltage, Feed Solutions on Process Performance. *Chem. Eng. J.* **2015**, *259*, 814–819.

(19) Li, D.; Zhang, X.; Yao, J.; Simon, G. P.; Wang, H. Stimuli-Responsive Polymer Hydrogels as a New Class of Draw Agent for Forward Osmosis Desalination. *Chemical Communications*, 2011, *47*, 1710–1712.

(20) Zhao, S.; Zou, L.; Tang, C. Y.; Mulcahy, D. Recent Developments in Forward Osmosis: Opportunities and Challenges. *J. Memb. Sci.* **2012**, *396*, 1–21.

(21) Li, D.; Zhang, X.; Yao, J.; Zeng, Y.; Simon, G. P.; Wang, H. Composite Polymer Hydrogels as Draw Agents in Forward Osmosis and Solar Dewatering. *Soft Matter* **2011**, *7* (21), 10048.

(22) Forney, B. S.; Guymon, C. A. Fast Deswelling Kinetics of Nanostructured poly(N-Isopropylacrylamide) Photopolymerized in a Lyotropic Liquid Crystal Template. *Macromol. Rapid Commun.* **2011**, *32* (9–10), 765–769.

(23) Depierro, M. A.; Guymon, C. A. Polymer Structure Development in Lyotropic Liquid Crystalline Solutions. *Macromolecules* **2014**, *47*, 5728–5738.

(24) DePierro, M. A.; Baguenard, C.; Guymon, C. A. Radical Polymerization Behavior and Molecular Weight Development of Homologous Monoacrylate Monomers in Lyotropic Liquid Crystal Phases. *Polym. Chem.* **2016**, *54*, 144–154.

(25) Worthington, K. S.; Baguenard, C.; Forney, B. S.; Guymon, C. A. Photopolymerization Kinetics in and of Self-Assembling Lyotropic Liquid Crystal Templates. *J. Polym. Sci. Part B Polym. Phys.* **2017**, *55* (6), 471–489.

(26) Forney, B. S.; Baguenard, C.; Guymon, C. A. Effects of Controlling Polymer Nanostructure Using Photopolymerization within Lyotropic Liquid Crystalline Templates. *Chem. Mater.* **2013**, *25* (15), 2950–2960.

(27) Lester, C. L.; Colson, C. D.; Guymon, C. A. Photopolymerization Kinetics and Structure Development of Templated Lyotropic Liquid Crystalline Systems. *Macromolecules* **2001**, *34* (13), 4430–4438.

(28) Forney, B. S.; Baguenard, C.; Guymon, C. A. Improved Stimuli-Response and Mechanical Properties of Nanostructured poly(N-Isopropylacrylamide-Co-Dimethylsiloxane) Hydrogels Generated through Photopolymerization in Lyotropic Liquid Crystal Templates. *Soft Matter* **2013**, *9* (31), 7458–7467.

(29) Clapper, J. D.; Sievens-Figueroa, L.; Guymon, C. A. Photopolymerization in Polymer Templating. *Chem. Mater.* **2008**, *20* (3), 768–781.

(30) Xu, Y.; Gu, W.; Gin, D. L. Heterogeneous Catalysis Using a Nanostructured Solid Acid Resin Based on Lyotropic Liquid Crystals. *J. Am. Chem. Soc.* **2004**, *126* (6), 1616–1617.

(31) Zhou, A.; Luo, H.; Wang, Q.; Chen, L.; Zhang, T. C.; Tao, T. Magnetic Thermoresponsive Ionic Nanogels as Novel Draw Agents in Forward Osmosis. *RSC Adv.* **2015**, *5* (20), 15359–15365.

(32) Clapper, J. D.; Guymon, C. A. Physical Behavior of Cross-Linked PEG Hydrogels Photopolymerized within Nanostructured Lyotropic Liquid Crystalline Templates. *Macromolecules* **2007**, *40* (4), 1101–1107.

(33) Bäcker, M.; Raue, M.; Schusser, S.; Jeitner, C.; Breuer, L.; Wagner, P.; Poghossian, A.; Förster, A.; Mang, T.; Schöning, M. J. Microfluidic Chip with Integrated Microvalves Based on Temperature- and pH-Responsive Hydrogel Thin Films. *Phys. Status Solidi Appl. Mater. Sci.* **2012**, *209* (5), 839–845.

(34) Ni, C.; Zhu, X.-X. X. Synthesis and Swelling Behavior of Thermosensitive Hydrogels Based on N-Substituted Acrylamides and Sodium Acrylate. *Eur. Polym. J.* **2004**, *40* (6), 1075–1080.

(35) Hyde, S. T. Identification of Lyotropic Liquid Crystalline Mesophases. In *Handbook of Applied Surface and Colloid Chemistry*; Holmberg, K., Ed.; John Wiley & Sons, Inc., 2001; pp 299–332.

(36) DePierro, M. A.; Carpenter, K. G.; Guymon, C. A. Influence of Polymerization Conditions on Nanostructure and Properties of Polyacrylamide Hydrogels Templated from Lyotropic Liquid Crystals. *Chem. Mater.* **2006**, *18* (23), 5609–5617.

(37) Liu, H. Y.; Zhu, X. X. Lower Critical Solution Temperatures of N -Substituted Acrylamide Copolymers in Aqueous Solutions. **1999**, *40*, 6985–6990.

(38) Ahn, S.; Kasi, R. M.; Kim, S.-C.; Sharma, N.; Zhou, Y. Stimuli-Responsive Polymer Gels. *Soft Matter* **2008**, *4* (6), 1151–1157.

5: SUPERABSORBENT, NANOSTRUCTURED, AND STIMULI-RESPONSIVE HYDROGELS AS FORWARD OSMOSIS DRAW AGENTS

Utilizing forward osmosis (FO) to purify water has gained much attention recently based on its low energy requirements and simplicity. Appropriate agents must draw water through a membrane efficiently. Additionally, effective separation of the draw agent from the processed water is critical for large scale applications. The use of stimuli-responsive hydrogels as draw agents has been studied by several research groups in recent years. The reusable and solid nature of hydrogels permits materials to be easily separated during regeneration. The goal of the work presented here is to examine the efficacy of stimuli-responsive hydrogels created with lyotropic liquid crystal (LLC) templating to induce nanostructure in copolymers prepared from stimuli-responsive N-isopropyl acrylamide (NIPAM) and superabsorbent sodium acrylate (SA). Hydrogel nanostructure through LLC templating increases swelling while maintaining stimuli-response, permitting materials suitable as draw agents to be produced. To determine the efficacy of materials as FO draw agents, osmotic pressure was measured indirectly by determining the ability to swell against solutions with different concentration. This process was performed on templated and non-templated materials with varying amounts of SA. Templated hydrogels absorb more water at lower osmotic pressures than isotropic controls. At osmotic pressures greater than 3.35 atm, the swelling ratio of all materials tends to converge at low swelling ratios. Additionally, the rate at which the hydrogels absorbed water against an osmotic solution through an FO membrane was compared for nanostructured and isotropic materials. The increased resistance from the FO membrane combined with the osmotic pressure causes materials of all compositions and structures to

draw at similar rates. Flux measurements examining the rate at which pure water is absorbed through an FO membrane were carried out using powdered samples of the materials. Templated materials exhibit much greater flux rates with only the membrane resisting swelling. In addition, a proof-of-concept device examined the suitability of nanostructured hydrogels as FO draw agents; water from a local river was drawn through an FO membrane using hydrogel draw agents. It was determined that the rate and amount of water that was absorbed was not significantly different between the templated and isotropic samples. However, theoretical water yields for templated materials were much higher than isotropic.

5.1: Introduction

Billions of people in the world do not have access to clean, reliable water.[1] As a result, providing a low cost, simple method for purifying water has been a major area of research in the scientific community for many years.[2–4] One promising strategy for energy efficient water purification is forward osmosis (FO). FO is an alternative to reverse osmosis (RO), a technique that uses high pressure pumps to force water through an RO membrane to purify the water of ions and organisms. RO membranes are typically thick, consisting of many active and support layers to resist these high pressures, which reduces throughput. In addition, forcing water through a membrane results in fouling. Consequently, large amounts of energy are required to pressurize water for purification.[5]

In addition to water purification, FO may be applied in a wide variety of industrial processes.[5,6] Concentrating waste streams to reduce volume by dehydration is one such application.[5] The concentrated waste may then be more easily transported for disposal or treatment. Another application of FO is in the concentration of heat sensitive products,

82

such as fruit juices and other food products.[6] In these examples, the heat used in distillation or other separations would damage the product. FO is an excellent solution as it uses relatively low amounts of energy and heat. Additionally, the membranes will be less affected by fouling due to solids or particulates in the juice products.

In contrast to RO, FO pulls water through a semi-permeable membrane utilizing a high osmotic pressure draw agent (Figure 5.1). The milder pulling action of FO means that membranes can be thinner, fouling is less of a concern, and energy requirements may be greatly reduced.[2] FO membranes can consist of only a thin polymer support layer and the active membrane layer, which rejects impurities.
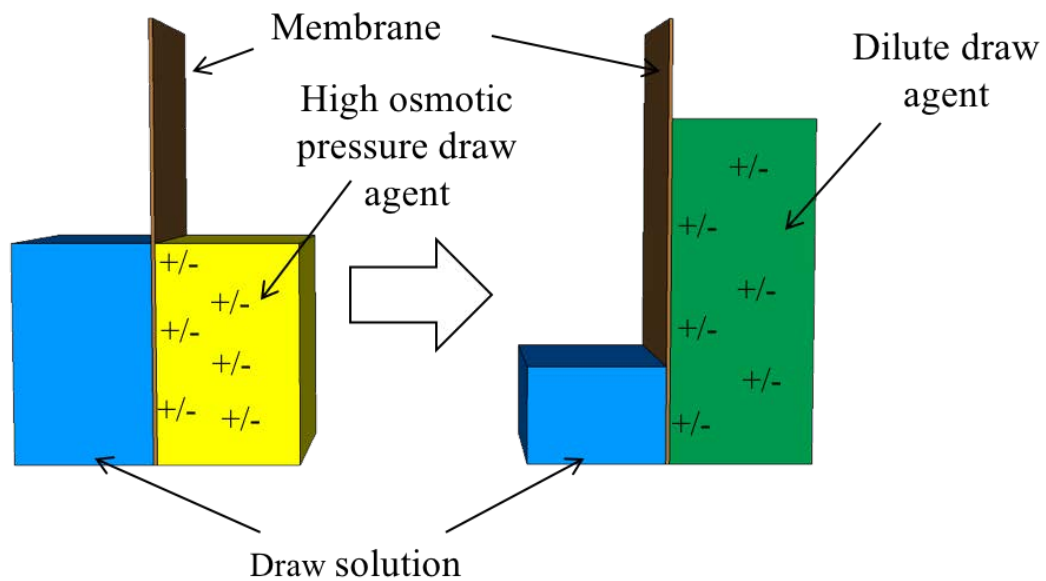
Figure 5.1. A simplified schematic illustrating a forward osmosis process. A semi-permeable membrane separates the draw agent from a draw solution. The high osmotic pressure draw agent pulls water from the draw solution through the membrane preventing solutes from crossing. The draw agent is diluted during this process.

FO utilizes the osmotic pressure of a draw agent to passively pull water across a membrane. The draw agent is diluted during the osmotic diffusion process. Therefore, an ideal draw agent would have a high osmotic pressure to draw water effectively.[7] After water is drawn through the membrane, the water can be recovered and the draw agent may be regenerated. One advantage of FO is that its low energy requirements enable FO water purification to be used in areas that have expensive or scarce electrical power.[8]

Although it boasts many advantages, FO has engineering challenges that must be addressed to further its adoption as a widespread method. One is that draw agents must have high osmotic pressures to draw water across a membrane from a brine or other solution. Osmotic pressure draw agents with pressures more than 30 atm are desirable for purifying sea water which has an osmotic pressure of roughly 22 atm.[9,10] Another challenge is that the water must be recovered and the draw agent regenerated following the purification process. Finding draw agents that pull large amounts of water across a membrane as well as release that water upon application of a stimulus is a complex problem, especially as hydrophilic materials with high osmotic pressures do not typically expel water readily. Multiple strategies have been pursued to find a draw agent with high osmotic pressure and the ability to absorb a large quantity of water and then release it upon introduction of a stimulus. One promising method is the use of ammonium carbonate salt solutions as an osmotic draw agent. Ammonium carbonate salts can be thermally degraded and distilled out of a purified water solution with application of modest heat. Challenges associated with this method include poor water taste due to residual salts and ammonia in recovered water.[4] Additionally, the ammonium carbonate draw agent regeneration is complicated due to the extensive equipment required for the

84

collection of carbon dioxide and ammonia gas.[3] In applications where water collected from the draw agent was not required to be potable, other approaches have utilized simple NaCl brine or high concentration solutions.[6]

Recent research has examined stimuli-responsive polymer hydrogels as draw agents.[11,12] Thermo-responsive polymers, such as poly(n-isopropylacrylamide) (PNIPAM), undergo a volume transition upon heating. At the lower critical solution temperature (LCST), the temperature at which polymer chains become less soluble in water, PNIPAM undergoes a coil-to-globule transition.[13,14] During this transition, the polymer becomes much less hydrophilic and will separate from water.[15] With a transition temperature of 32 ˚C, PNIPAM is an attractive option for drug delivery applications due to its proximity to biological temperatures.[16] In an aqueous solution of linear polymer, the change is observed when the polymer chains become insoluble and 'cloud' the liquid.[17] Thus, the term 'cloud point' is often used when discussing stimuli-responsive materials in solution. Therefore, a crosslinked hydrogel consisting of PNIPAM will expel water and shrink, releasing water. A shortcoming of these materials is that the osmotic pressure of PNIPAM is often lower than ideal for drawing against a contaminated source. Thus, research on hydrogel based materials often focuses on increasing the osmotic pressure of the materials.[18]

Recent work has explored the use of sodium acrylate (SA) as a comonomer or as a secondary network in stimuli-responsive materials to increase osmotic pressure and overall swelling capacity.[19] Copolymerizing PNIPAM with SA has resulted in increases in the overall swelling of the materials but at the expense of stimuli-responsive ranges.[20] Higher osmotic pressure increases the hydrophilicity of a material but decreases stimuli-

85

response. The stimuli-responsive nature of these copolymers relies on balancing between very hydrophilic and nearly hydrophobic so that upon stimulus the material expels water. The addition of a high osmotic pressure moiety can upset this delicate balance by increasing the hydrophilicity of the hydrogel, reducing the desired water expulsion response. Materials for which the swelling ability and osmotic pressure may be increased without attenuation of stimuli-response are very desirable for FO applications.

One strategy for increasing the swelling of materials without a corresponding decrease in stimuli-response is by the addition of a templated nanostructure via lyotropic liquid crystal (LLC) templating.[21,22] LLC templating utilizes surfactant and water mixtures, which may self-assemble into ordered nanostructures when surfactants are present in high concentrations. The various structures observed are dependent upon the concentration and type of surfactant, as shown in Figure 1.1. Templating of a polymer is achieved via mixing a monomer into LLC mixtures where the monomer can segregate into different regions depending upon its hydrophilic/hydrophobic nature. The materials are then polymerized and the LLC template removed, leaving a nanostructured polymer material (Figure 1.3).[23]

Photopolymerization is utilized because it occurs at ambient temperatures. Elevated temperatures influence and eventually melt the LLC order. Photopolymerized, nanostructured materials have been shown to increase diffusional, swelling, and stimuli-responsive properties of various hydrogels when compared to their isotropic counterparts.[23] Forney and Guymon demonstrated that the addition of bicontinuous cubic nanostructure to a PNIPAM hydrogel allowed swelling ratios of ten times the dry mass, an increase of nearly double that of an isotropic material of identical chemical

86

composition.[22] The LLC templated materials also exhibit faster and more complete deswelling at 40 ˚C. This more complete and rapid response was attributed to nanostructure allowing increased transport of water out of the hydrogel and the prevention of a dense outer deswollen layer. Additionally, the mechanical properties of nanostructured materials were not adversely affected by the increased water capacity. Modulus of swollen nanostructured and isotropic materials were nearly identical.

Further improvements to LLC templated materials for potential use as FO agents may be achieved by copolymerizing with SA. The results of combining the improved stimuli-response of LLC templating with a high swelling superabsorbent monomer are described in Chapter 4. The LLC templated materials described previously exhibit equilibrium swelling ratios of up to 50 and expel 40 times their dry mass upon application of heat. These ratios represent a five times increase in both metrics as compared to the isotropic counterparts. Additionally, material swelling and deswelling is reversible. The templated materials exhibit thermo-responsive volume transitions through multiple cycles that are approximately 400% greater than the isotropic materials. The increase in swelling combined with a large stimuli-response makes these nanostrucutred superabsorbents promising for use as draw agents.

In this chapter, copolymerization of PNIPAM with SA will be combined with LLC templating to create nanostructured stimuli-responsive FO draw agents. To investigate if an LLC templated nanostructure within hydrogels affects the suitability of the materials for draw agents, various strategies for measuring the efficacy of hydrogels are utilized. Both isotropic and LLC templated nanostructured materials are prepared with varying concentrations of SA. Flux across an FO membrane is measured to

determine FO efficacy. By comparing swelling ratios to known osmotic pressure solutions, the osmotic pressure of hydrogel materials is evaluated. Finally, pouches are created to simulate a practical configuration to test the ability of the material as a draw agent.

5.2: Experimental

Monomers used to synthesize copolymers include N-isopropyl acrylamide (NIPAM, Sigma-Aldrich) at 20% of solution mass, N-N' methylene bisacrylamide (MBA) (Sigma-Aldrich) at 1% prepolymer solution mass, and sodium acrylate (SA) (Sigma-Aldrich) at varying concentrations from 0-5% prepolymer mass with water making up the difference. The photoinitiator used was 2,2-Dimethoxy-2-phenylacetophenone (DMPA) photoinitiator (Ciba) at 1 mass% with respect to monomer. Poly(oxyethylene)-2 cetyl ether (Brij® 52, Sigma-Aldrich) was utilized as the templating surfactant at 40% by weight and ethanol used as a rinse solvent. Figure 5.2 shows the chemical structures of materials used. All materials were used as received. Synthesis of hydrogel materials was carried out as described in Chapter 4.

5.2.1: Real-time Swelling

Real-time swelling of materials was measured using the apparatus in Figure 5.3, which was based on a device used for similar experiments that measured the absorptivity of clay soils by Dieng *et al*. [24,25] As water is drawn into the hydrogel through a membrane, the increase in mass is recorded by the balance. Drawing performance was analyzed by measuring flux through a membrane in real-time into a powdered polymer material. Powdered material was prepared by grating polymer discs in a coffee grinder and sieving to a particle size between 250 and 700 µm. The device consists of a balance

88

with a mounted dead-end FO membrane holder. A tube runs from a reservoir of water to

a membrane mounted in the holder. The apparatus is filled so that water is in constant

contact with the bottom of the FO membrane (Hydration Technology Innovations (HTI))

and the balance is tared for the mass of water, tubing, and membrane holder. Powdered
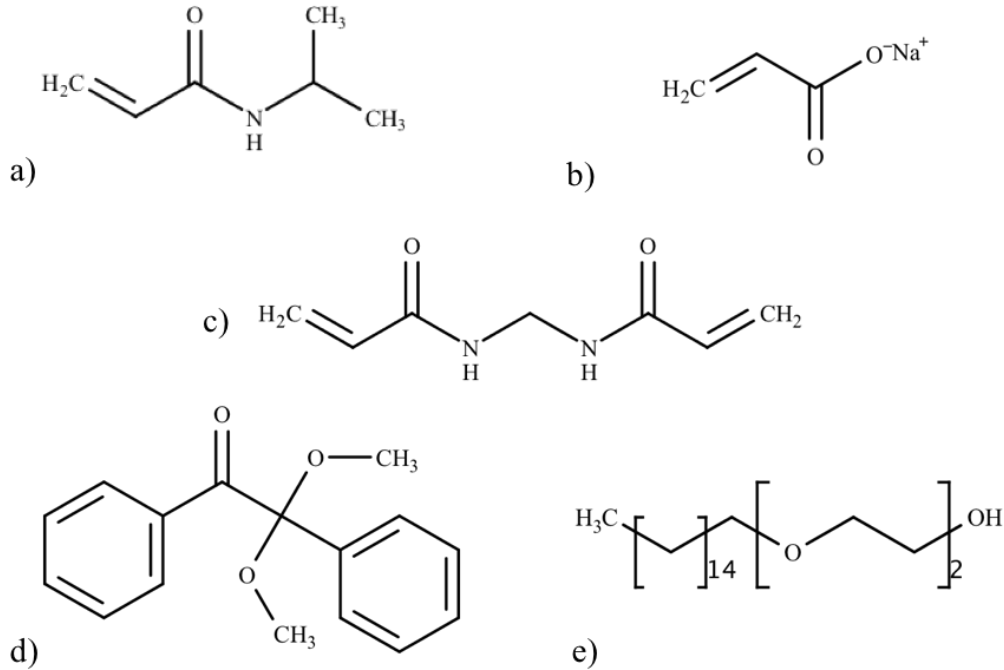
Figure 5.2. Materials used in this work include: a) *N*-isopropyl acrylamide, b) 2,2-
Dimethoxy-2-phenylacetophenone (DMPA), c) *N-N'* methylene bisacrylamide, d)
Sodium acrylate (SA), and e) Polyoxyethylene (10) cetyl ether (Brij 52).

polymer (0.3 g) is placed on top of the membrane and the mass of water drawn through

the membrane into the powder is measured to determine the water flux across the

membrane. The balance is connected to a computer, allowing for mass to be measured in

real-time. Flux was calculated by dividing the volume of water absorbed by the

membrane surface area over time.
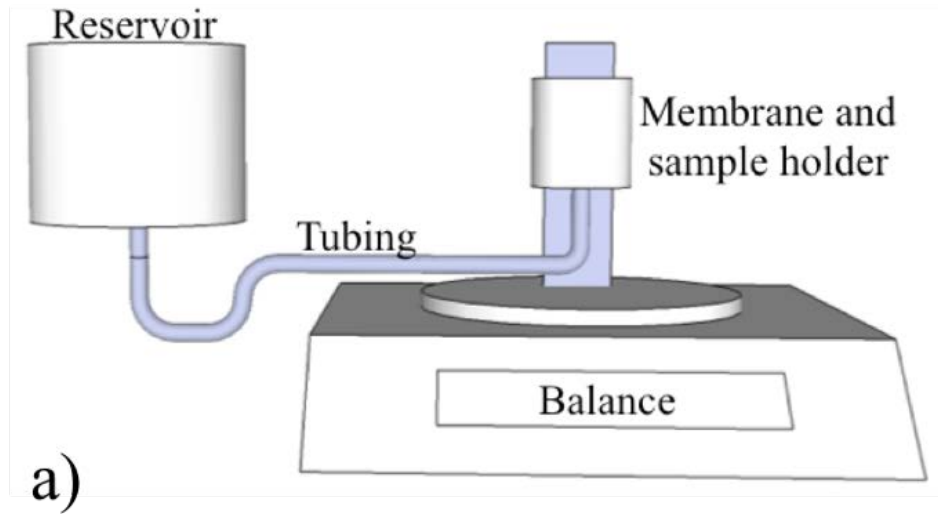
Figure 5.3. Schematic a) describing the apparatus used to perform real-time flux and water absorption measurements and b) image of the experimental setup.

5.2.2: Osmotic Solutions

Solutions consisting of PEG6000, PEG20K, or sucrose were mixed at varying concentrations to compare swelling of hydrogel discs against solutions with varying osmotic pressures. Swelling ratios were calculated using Equation 3.2.

.

Osmotic pressures were determined using data from Frazer and Myrick for the sucrose solutions and Money for the PEG6000 and PEG20K .[26,27] The osmotic pressure of the hydrogels was calculated by linearizing the swelling curve and calculating the x-intercept.

5.2.3: Membranes

Tubular dialysis tubing with MW cutoff of 12,000 g/mol was used as a barrier between sucrose and the hydrogel discs. Discs were placed in dialysis tubing, which was sealed by knotting one end and using clips on the other. The samples were removed from the dialysis tubing, lightly dabbed with a laboratory napkin to remove excess water from the surface and then weighed at regular intervals. The disc was then replaced in the tubing and the clip used to reseal the sample before being placed back into solution.

A cellulose acetate membrane on a non-woven polyethylene support donated by HTI was used as the FO membrane for swelling studies. Pouches were constructed of polyethylene film and FO membrane (Figure 5.4). Membrane material with the active FO side facing outward was heat sealed into a pouch with 150 µm thick polyethylene film similar to the construction of the HTI pouches shown previously. The pouch was constructed around the hydrogel sample of a known mass (3 g). The pouch was then immersed in a well-stirred osmotic solution. PEG20K solutions with osmotic pressures from 0.04 to 10 atm were used. Pouch mass was recorded at specified intervals.

5.2.4: River Water Absorption Prototype

Pouches filled with 3 g of hydrogel 2% SA powder were swollen in water collected from the Iowa River. Water samples were taken from the Iowa River on a calm August day. Sediment levels in the water were assumed to be low as there was no

precipitation in the previous week. Pouches were swollen for 90 days with pouch mass

recorded at regular intervals to determine water uptake.

Figure 5.4. A single-use water purification device manufactured by Hydration
Technology Innovations. The pouch is constructed with one side forward osmosis
membrane and the other poly(ethylene). It is then filled with a sports drink powder
and sealed. Water passes through the membrane, is purified, and then mixes with the
drink mixture for consumption. *Image courtesy of Hydration Technology
Innovations and Eastman Chemical.*

5.3: Results and Discussion

Previous work has shown that imparting ordered structure to hydrogels allows for

increased water absorption. However, this characteristic only reveals the equilibrated

nature of the swelling event. By measuring the flux of water through a membrane as it is

drawn through a membrane by a hydrogel, the kinetics of the swelling process are better

understood. Flux is defined as the volume of water that passes through an area of

membrane over time. High flux of water with good rejection of contaminants is an

important consideration for successful membrane application. A real-time balance was

used to measure flux and mass of water absorbed for 0, 2, and 5% SA for LLC templated

and isotropic formulations (Figure 5.5). The swelling and flux of 0% SA control samples are greater for the templated samples. Additionally, due to better consistency in materials, templated samples exhibit lower standard deviations between samples tested. Templated sample synthesis results in more uniform properties than isotropic materials due to surfactant compatibilization of the monomers. The flux of isotropic and templated samples increases initially as hydrogel swelling improves the contact between membrane and powder, reaching a maximum soon after measurements begin. Samples containing 2% and 5% SA exhibit similar trends, however with increased flux. The maximum flux was reached at roughly 30 min for the 2% and 5% samples. Samples containing more SA absorb more water and draw water through the membrane at a higher apparent flux.

Increased water flux indicates that the materials may be capable of FO processes across an FO membrane. However, applications for FO will require drawing water from a solution with osmotic pressure, which resists extraction through the membrane. The unstirred nature of solution side means that the inclusion of a solute into the water side of the membrane will lead to the rapid concentration of solution on the membrane surface, creating a highly concentrated boundary condition that prevents accurate flux measurements. As such, more realistic methods of measuring suitability of hydrogels for forward osmosis are required.

Measuring the absorption characteristics of hydrogels against an osmotic draw is highly desirable for the determination of suitability for FO applications. Prior work has shown that the osmotic pressure of hydrogels may be determined by swelling a hydrogel against a solution with a known osmotic pressure.[28,29] To evaluate the osmotic pressure of

93
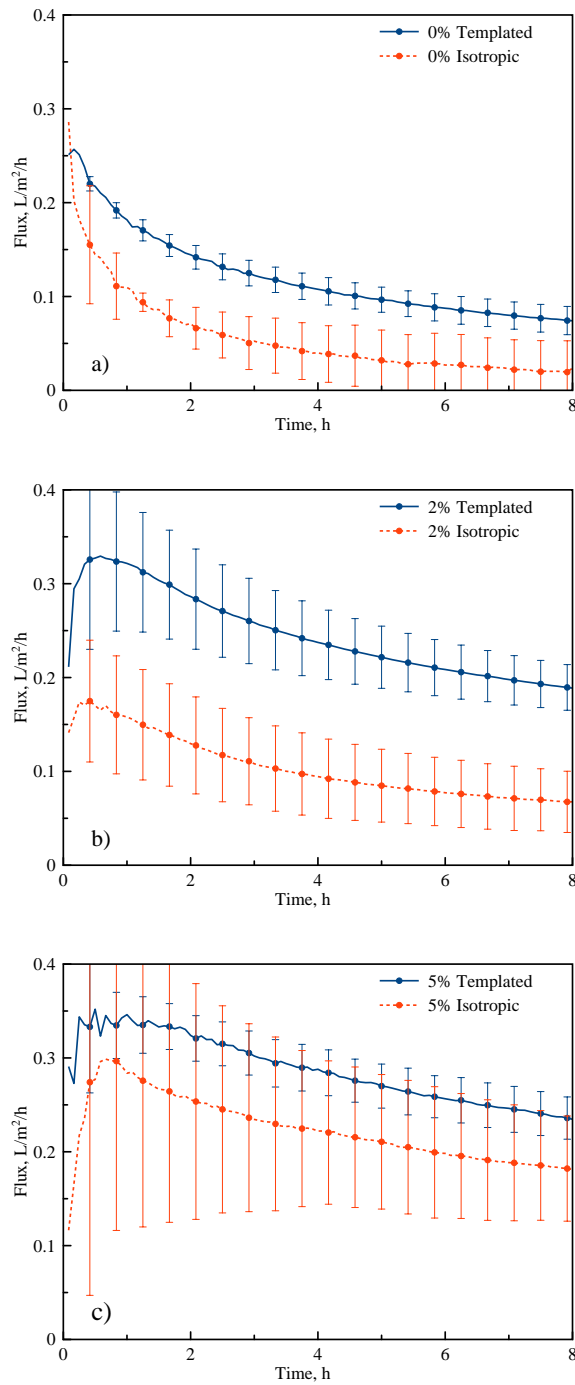
Figure 5.5. Flux of pure water absorbed by isotropic (—) and templated (---) NIPAM-co-SA powdered samples at a) 0%, b) 2%, and c) 5% SA through FO membrane. Measurements were made with the device described in Figure 5.3.

templated and isotropic copolymerized hydrogels, swelling experiments were carried out with hydrogels encased in dialysis tubing. The tubing was then immersed in sucrose solutions at various osmotic pressures between 0 and 10 atm, achieved by changing the concentration (Figure 5.6).

By measuring hydrogel swelling at varying concentrations, the osmotic pressure may be indirectly measured. For distilled water, swelling is much greater for LLC structured materials. The swelling ratio as compared to the dry mass (Q) of templated SA 0% is nearly double that of the isotropic material. When the SA content is increased to 2%, the templated sample swells to a Q approximately 20 greater than the isotropic system, meaning that it increases the water absorbed on the order of 20 times the dry mass of the copolymer. Further increasing SA to 4%, causes a reduction in the difference between final Q for the templated and isotropic samples and the hydrogel has an equilibrium swelling ratio of 10 more than the isotropic material. As osmotic pressure is increased to 0.04 atm, a marked decrease in swelling is observed for all materials. Swelling still increases as a function of SA content but there is a greater convergence in swelling for templated and isotropic samples. Further increasing osmotic pressure of the sucrose solution to 3.35 atm causes a decrease in swelling for all samples. As observed in Figure 5.5 the more uniform sample properties of LLC templated materials allow for less variation between samples runs. Templated materials with 2% SA loading swell to greater ratios than isotropic materials through 3.35 atm.

A decrease in equilibrium swelling ratio is expected when a draw agent is swollen against a solution possessing an osmotic pressure. This osmotic pressure creates a resistance to water passing across the membrane. When drawing against a solution with

95

an osmotic pressure of 10 atm, swelling is further decreased. Samples containing no SA swell to a Q of nearly 2, and samples containing SA do not swell significantly more. No significant differences between isotropic and templated materials are observed once a
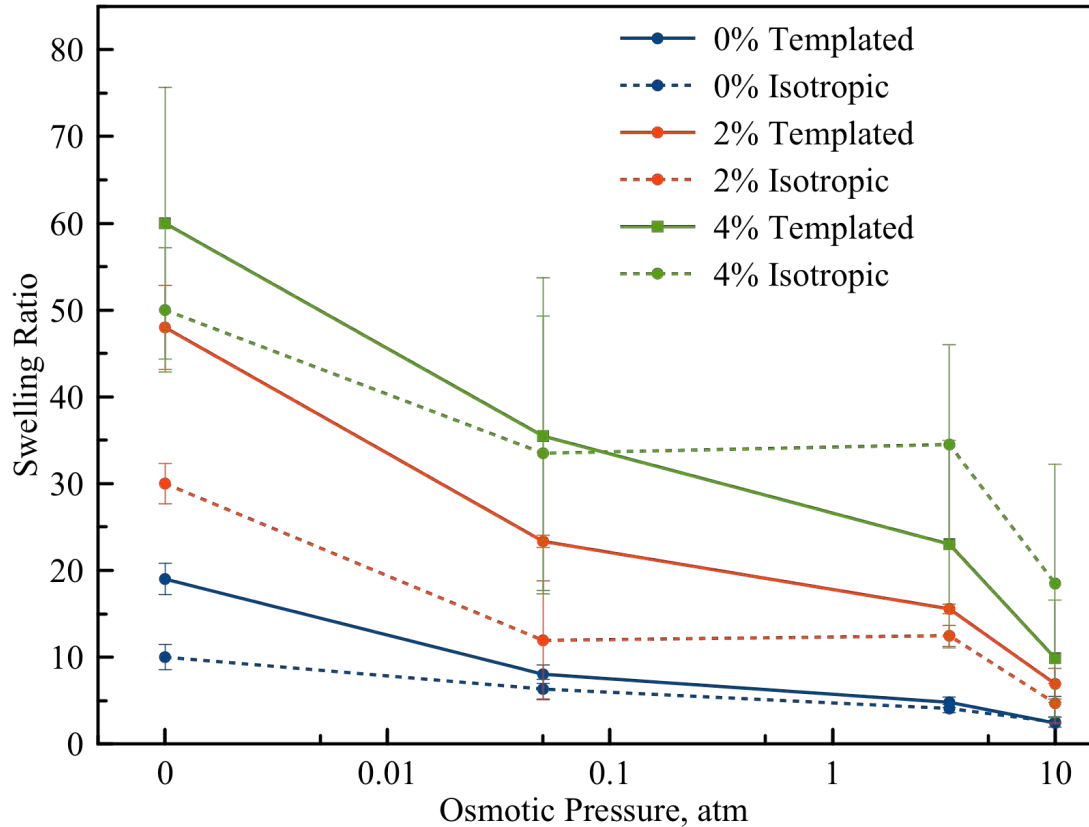
Figure 5.6. Equilibrium swelling ratios of isotropic (—) and templated (---) NIPAM-co-SA samples at varying osmotic pressure sucrose solutions swollen in dialysis tubing.

suitably high osmotic pressure of draw solution is reached. While free-swelling of hydrogels increases with the addition of SA, significant increases in hydrogel osmotic pressure are not realized. Upon examination of the components contributing to osmotic pressure in Equation 5.1; these results are not unexpected. [30]

$$\prod_{ion} + \prod_{elastic} + \prod_{solv} = \prod_{tot} \qquad (5.1)$$

The chemical mixing or solvation (solv) osmotic pressure of a hydrogel can be expected to be much larger than the other two contributing factors due to the non-ionic polymer chains making up the bulk of the hydrogel. Imparting structure, which modifies the elastic term, to a hydrogel is sufficient to swell an already hydrophilic material in DI water more than an isotropic counterpart. By increasing osmotic pressure, swelling ratios fall dramatically. The high swelling ratios observed in LLC templated materials for pure water but not for sucrose solutions is evidence that osmotic pressure is affected by chemical potential more than the increased transport due to the continuous pore network structure in LLC templated hydrogels.[22,23]

The rate of water drawn across a membrane is also an important consideration for FO draw agents, especially at higher osmotic pressures. In a reusable batch process, the rate of water through the membrane and draw agent regeneration are the two potential rate limiting steps of the cycle time. To observe the rate at which water was absorbed through an HTI FO membrane into templated and isotropic systems with varying SA, FO pouches were created. Hydrogel materials were heat sealed in FO pouches and were immersed in a 2 atm solution of PEG20K (134 g/L). The mass of water absorbed through the membrane was recorded at specific intervals (Figure 5.7). Overall swelling was approximately equal for templated and isotropic samples at all SA concentrations. This result is consistent with the varied osmotic pressure studies discussed in Figure 5.7. The rate of swelling was also not significantly different for any tested samples due to the increased resistance of the FO membrane combined with the osmotic pressure of the solution. A noteworthy result was the reduced consistency of swelling at longer times for higher SA concentrations. This result is attributed to structural loss and heterogeneities

97

observed for higher SA concentration samples. These results do not directly measure water flux into the hydrogel since surface area changes as the materials swell. The contact with the membrane surface is changing, particularly during the early swelling period.

Swelling pouched hydrogels using river water will allow the materials to be tested in a real-world problem. Powdered samples (3 g) of an isotropic and a templated 2% SA hydrogel were heat sealed into pouches and immersed in the beakers containing river water. Water absorption was measured by weight over a period of 90 days (Figure 5.8). Rates of absorption are roughly equal for both templated and isotropic samples throughout the initial rapid swelling and continue to remain statistically the same throughout the experiment.

The river water prevents the enhanced swelling previously observed in LLC templated materials. This behavior is due to the slight osmotic pressure present in unpurified water. After five days, both samples exhibit swelling ratios of 15, significantly lower ratios than observed for materials swollen in DI water. However, this result is still promising for forward osmosis applications since the templated material surpasses its predetermined swelling ratio of 7 after deswelling at 50 ˚C, as observed in Chapter 4. The isotropic sample never attains its equilibrium swelling ratio post exposure to 50 ˚C, even upon the conclusion of the experiment after nearly three months. However, LLC templated structure could allow the templated material to still release water due to the

98
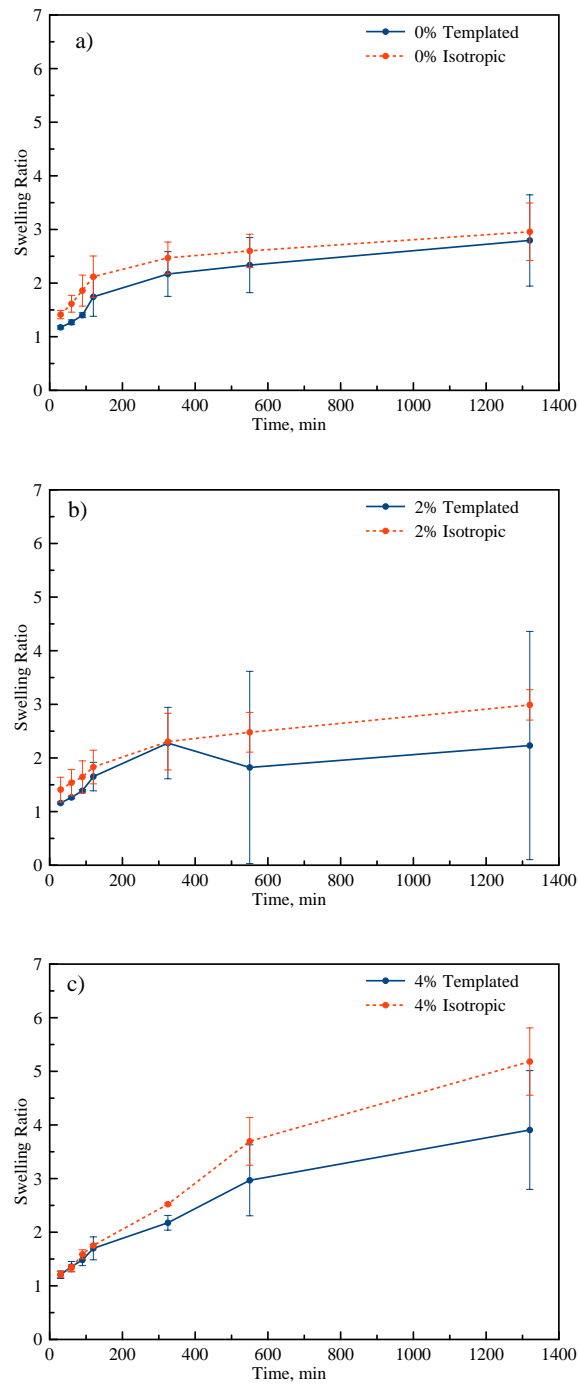
Figure 5.7. Rate of water absorption into isotropic (—) and templated (---) NIPAM-co-SA samples at a) 0%, b) 2%, and c) 4% concentrations of SA from a 2 atm solution of PEG20K through a forward osmosis pouch.

high dynamic range of swelling ratios observed previously in Chapter 4. The isotropic material never attains a sufficiently high swelling ratio for stimuli-response to be observed. The templated material can exhibit stimuli-response after a couple of days and may expel meaningful water amounts after only a week. The FO pouch device is promising, due to the high degree of stimuli-response allowed by the templated structure and the increased amount of water that is released from a templated material.
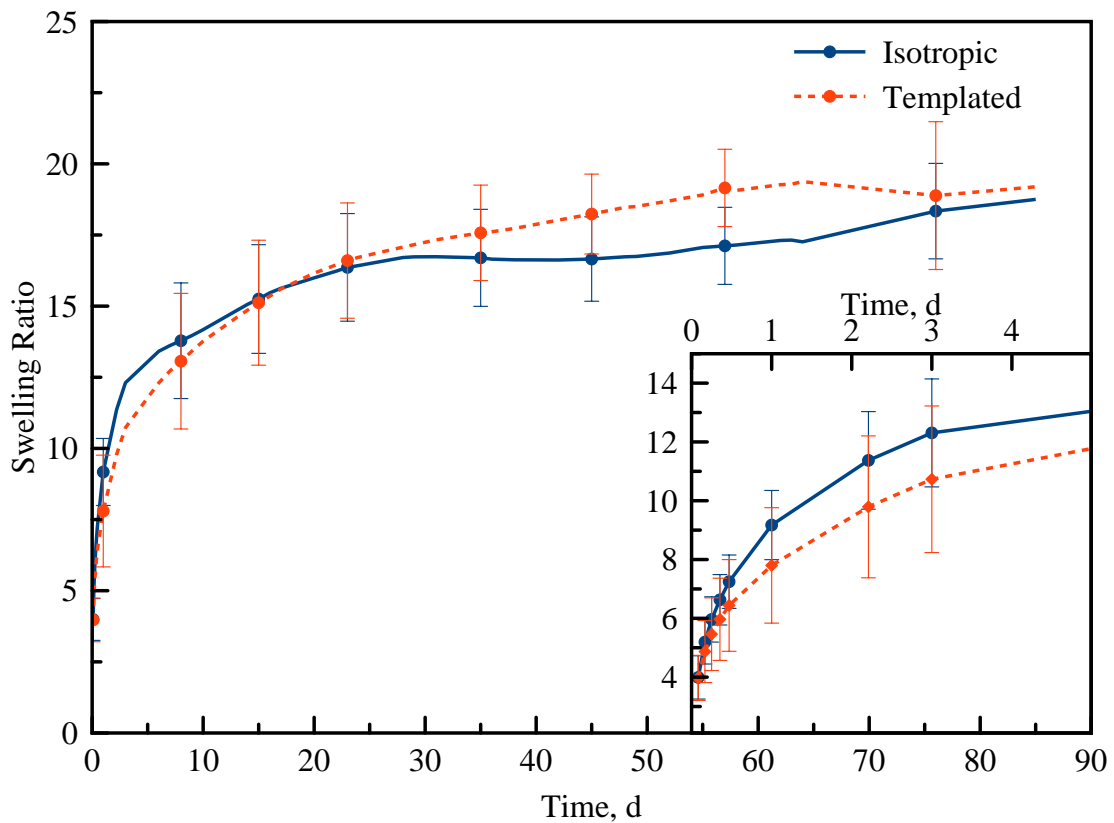
Figure 5.8. Water drawn into forward osmosis membrane pouches by isotropic (—) or templated (---) NIPAM-co-SA 2% powder over 90 days. The rate and amount of water absorbed through the membrane was independent of the structure of the polymer. Lines show the deswelling ratio for templated or isotropic materials.

5.4: Conclusions

Standardized methods of determining FO capabilities of materials are not readily available.[8,31] The methods typically used to characterize superabsorbent stimuli-responsive materials are unable to fully characterize a draw agent. Simple swelling in water, or 'free' swelling, does not consider the resistive forces of an FO membrane or the effects of solutes in the draw agent. In addition, free swelling in a draw solution does not allow reliable determination of how a material will behave opposite a membrane from a draw solution. Solutes in the water may chemically interact with the polymers or may be absorbed into the hydrogel matrix with little to no effect on the overall swelling of the material. LLC nanostructure allows increased swelling of hydrogel materials, which may increase the rate at which water is absorbed into the material.[21,22,32] The creation of nanostructured copolymers of PNIPAM and SA results in materials with increased rates of water drawn across a membrane. These increases are due to higher rates of transport of water through the hydrogel, permitting larger water fluxes through the membrane. For hydrogels swollen with distilled water, the highest resistance to water absorption through the membrane is the saturation of hydrogel at the membrane surface. However, when an osmotic agent is placed opposite the hydrogel draw agents, it results in reduced swelling for all samples regardless of structure or SA content. When an osmotic solution is opposite the hydrogel, the limiting factor becomes the passing of water from the solution side of the membrane to the draw agent. Although LLC-nanostructured materials exhibit higher water swelling and better flux ratios when swollen with DI water, it does not appear that the structure increases osmotic pressure. This result is confirmed with a sample of water from the Iowa River. When hydrogels are encased in an FO membrane

101

and swollen in river water, the osmotic agents in the river water present enough resistance to cause nearly identical swelling ratios and rates between the isotropic and templated materials. The methods explored in this chapter support further investigation of the use of LLC templated materials as FO draw agents by allowing flux and osmotic pressure to be characterized independent of hydrogel water absorption.

5.5: References

(1)   UNICEF; World Health Organization. *Progress on Sanitation and Drinking Water: 2015 Update and MDG Assessment*; 2015.

(2)   Thompson, N. A.; Nicoll, P. G. Forward Osmosis Desalination: A Commercial Reality. In *IDA World Congress*; 2011; pp 1–16.

(3)   McGinnis, R. L.; Elimelech, M. Energy Requirements of Ammonia–carbon Dioxide Forward Osmosis Desalination. *Desalination* **2007**, *207* (1–3), 370–382.

(4)   McCutcheon, J. R.; McGinnis, R. L.; Elimelech, M. Desalination by Ammonia–carbon Dioxide Forward Osmosis: Influence of Draw and Feed Solution Concentrations on Process Performance. *J. Memb. Sci.* **2006**, *278* (1–2), 114–123.

(5)   Coday, B. D.; Xu, P.; Beaudry, E. G.; Herron, J.; Lampi, K.; Hancock, N. T.; Cath, T. Y. The Sweet Spot of Forward Osmosis: Treatment of Produced Water, Drilling Wastewater, and Other Complex and Difficult Liquid Streams. *Desalination* **2014**, *333* (1), 23–35.

(6)   Jiao, B.; Cassano, A.; Drioli, E. Recent Advances on Membrane Processes for the Concentration of Fruit Juices : A Review. *J. Food Eng.* **2004**, *63*, 303–324.

(7)   Lewis, G. N. The Osmotic Pressure of Concentrated Solutions, and the Laws of the Perfect Solution. *J. Am. Chem. Soc.* **1908**, *30* (5), 668–683.

(8)   Cai, Y.; Hu, X. M. A Critical Review on Draw Solutes Development for Forward Osmosis. *Desalination* **2016**, *391*, 16–29.

(9)   Garrey, W. E. The Osmotic Pressure of Sea Water and of the Blood of Marine Animals. *Biol. Bull.* **1905**, *8* (4), 257–270.

(10)   Carmignani, G.; Sitkiewitz, S.; Webley, J. W. Recovery of Retrograde Soluble Solute for Forward Osmosis Water Treatment. US 2012/0267308A1, 2012.

(11)   Razmjou, A.; Barati, M. R.; Simon, G. P.; Suzuki, K.; Wang, H. Fast Deswelling of Nanocomposite Polymer Hydrogels via Magnetic Field-Induced Heating for Emerging FO Desalination. *Environ. Sci. Technol.* **2013**, *47* (12), 6297–6305.

(12)   Zhang, H.; Li, J.; Cui, H.; Li, H.; Yang, F. Forward Osmosis Using Electric-Responsive Polymer Hydrogels as Draw Agents: Influence of Freezing–thawing Cycles, Voltage, Feed Solutions on Process Performance. *Chem. Eng. J.* **2015**, *259*, 814–819.

(13)   Zeng, F.; Tong, Z. N. M. R. Investigation of Phase Separation in Poly (N - Isopropyl Acrylamide)/ Water Solutions. *Polymer (Guildf).* **1997**, *38* (22), 5539–5544.

(14) Mendez, S.; Andrzejewski, B. P.; Canavan, H. E.; Keller, D. J.; Mccoy, J. D.; Lopez, G. P.; Curro, J. G. Understanding the Force-vs-Distance Profiles of Terminally Attached Poly(a-Isopropyl Acrylamide) Thin Films. *Langmuir* **2009**, *25* (18), 10624–10632.

(15) Pelton, R. Poly(N-Isopropylacrylamide) (PNIPAM) Is Never Hydrophobic. *J. Colloid Interface Sci.* **2010**, *348* (2), 673–674.

(16) Roy, D.; Cambre, J. N.; Sumerlin, B. S. Future Perspectives and Recent Advances in Stimuli-Responsive Materials. *Prog. Polym. Sci.* **2010**, *35* (1–2), 278–301.

(17) Sasaki, S.; Okabe, S.; Miyahara, Y. Thermodynamic Properties of N-Isopropylacrylamide in Water: Solubility Transition, Phase Separation of Supersaturated Solution, and Glass Formation. *J. Phys. Chem. B* **2010**, *114*, 14995–15002.

(18) Li, D.; Zhang, X.; Yao, J.; Simon, G. P.; Wang, H. Stimuli-Responsive Polymer Hydrogels as a New Class of Draw Agent for Forward Osmosis Desalination. *Chemical Communications*, 2011, *47*, 1710–1712.

(19) Cai, Y.; Shen, W.; Loo, S. L.; Krantz, W. B.; Wang, R.; Fane, A. G.; Hu, X. Towards Temperature Driven Forward Osmosis Desalination Using Semi-IPN Hydrogels as Reversible Draw Agents. *Water Res.* **2013**, *47* (11), 3773–3781.

(20) Huang, H.; Zhang, D.; Mao, Z.; Yu, W.; Yan, H. Fast Responsive and Strong Swelling Hydrogels Based on N -Isopropylacrylamide with Sodium Acrylate. *J. Appl. Polym. Sci.* **2008**, *112*, 123–128.

(21) Forney, B. S.; Baguenard, C.; Guymon, C. A. Improved Stimuli-Response and Mechanical Properties of Nanostructured poly(N-Isopropylacrylamide-Co-Dimethylsiloxane) Hydrogels Generated through Photopolymerization in Lyotropic Liquid Crystal Templates. *Soft Matter* **2013**, *9* (31), 7458–7467.

(22) Forney, B. S.; Guymon, C. A. Fast Deswelling Kinetics of Nanostructured poly(N-Isopropylacrylamide) Photopolymerized in a Lyotropic Liquid Crystal Template. *Macromol. Rapid Commun.* **2011**, *32* (9–10), 765–769.

(23) Clapper, J. D.; Guymon, C. A. Physical Behavior of Cross-Linked PEG Hydrogels Photopolymerized within Nanostructured Lyotropic Liquid Crystalline Templates. *Macromolecules* **2007**, *40* (4), 1101–1107.

(24) Dieng, M. a. Der Wasseraufnahmeversuch Nach DIN 18132 in Einem Neu Entwickelten Gerät. *Bautechnik* **2005**, *82* (1), 28–32.

(25) Kaufhold, S.; Dohrmann, R. Comparison of the Traditional Enslin-Neff Method and the Modified Dieng Method for Measuring Water-Uptake Capacity. *Clays Clay Miner.* **2008**, *56* (6), 686–692.

(26) Money, N. P. Osmotic Pressure of Aqueous Polyethylene Glycols ' Relationship between Molecular Weight and Vapor Pressure Deficit. *Plant Physiol.* **1989**, *91*, 766–769.

(27) Frazer, J. C. W.; Myrick, R. T. The Osmotic Pressure of Sucrose Solutions at 30˚. *J. Am. Chem. Soc.* **1916**, *XXXVIII* (10).

(28) Horkay, F.; Tasaki, I.; Basser, P. J. Osmotic Swelling of Polyacrylate Hydrogels in Physiological Salt Solutions. *Biomacromolecules* **2000**, *1* (1), 84–90.

(29) Granik, V. T.; Smith, B. R.; Lee, S. C.; Ferrari, M. Osmotic Pressures for Binary Solutions of Non-Electrolytes. *Biomed. Microdevices* **2002**, *4* (4), 309–321.

(30) Han, I. S.; Han, M.-H. H.; Kim, J.; Lew, S.; Lee, Y. J.; Horkay, F.; Magda, J. J. Constant-Volume Hydrogel Osmometer: A New Device Concept for Miniature Biosensors. *Biomacromolecules* **2002**, *3* (6), 1271–1275.

(31) Manek, E.; Tombácz, E.; Geissler, E.; László, K. Search for the Origin of Discrepancies in Osmotic Measurements of the PNIPAM - Water System. *Period. Polytech. Chem. Eng.* **2017**, *61* (1), 39–50.

(32) Clapper, J. D.; Sievens-Figueroa, L.; Guymon, C. A. Photopolymerization in Polymer Templating. *Chem. Mater.* **2008**, *20* (3), 768–781.

6: POLY(*N*-ISOPROPYL ACRYLAMIDE) HYDROGELS TEMPLATED WITH POLYOXYETHYLENE ALKYL ETHERS IN NORMAL AND INVERSE LYOTROPIC LIQUID CRYSTAL MESOPHASES

Templating ordered nanostructure within hydrogels has been shown to enable control of material swelling and transport. One method of creating these structured materials is to use self-assembled lyotropic liquid crystals (LLCs), which consist of ordered surfactant and water, as a structuring agent for photopolymerization. The type of surfactant used can have large effects on which mesophases are accessible and which monomers may be templated. Despite the importance of the templating surfactant on the mesophase and compatibility in monomer systems, work on this technique has focused on the use of a limited number of surfactants. Expanding the availability of surfactants with a greater variety of hydrophobic and hydrophilic characters that still exhibit LLC mesophases will increase flexibility in monomer choice and structure for templated materials. Surfactants examined in this work were nonionic polyoxyethylene alkyl ether surfactants. Three hydrophobic tail group lengths were examined in combination with three hydrophilic head group lengths. The surfactants were examined for the presence of LLC mesophases and utilized as templates for photopolymerized poly(n-isopropyl acrylamide) (PNIPAM) hydrogels. Isotropic, isotropic surfactant templated, normal nanostructured, and inverse nanostructured were all examined as templates for PNIPAM hydrogels. Swelling ratios are generalized based on the type of structure present during polymerization. The creation of highly ordered nanostructure in a PNIPAM hydrogel results in a roughly two-fold increase in the water uptake as compared to the isotropic control. Samples templated with the surfactant L23, which exhibits no mesophase

behavior, shows almost no increase in swelling when compared to the isotropic sample. Additionally, when PNIPAM is templated using inverse mesophases, no swelling increase is observed. In the inverse phase, the materials no longer exhibit a continuous polymer mesophase, losing the increased transport and swelling properties associated with this structure. By examining surfactants of various head and tail lengths, mesophases and their accessibility can be extended through the use of a variety of polyoxyethylene alkyl ether surfactants. PNIPAM hydrogels templated with different surfactants are also examined for mesophase retention. In this study, we demonstrate that PNIPAM templated in a normal nanostructured mesophase will exhibit double the swelling compared to an isotropic polymer. Due to the lack of continuous polymer within the structure, templating in an inverse mesophase does not allow these increases in swelling ratio. The influence on surfactant choice in monomer compatibility, mesophase availability, and final material swelling properties are examined

6.1: Introduction

Imparting structure to hydrogels using lyotropic liquid crystals (LLCs) and photopolymerization has been demonstrated to allow control over swelling, stimuli-response, and mechanical properties in numerous studies.[1–6] The nanostructured network templated by the LLC mesophase permits increased transport of liquid through the hydrogel and can act to reinforce the material. Templating with self-assembled monomers and surfactant mesophases creates an ordered network within the bulk material. As

surfactant concentration is increased, the mesophases become increasingly complex (Figure 6.1).
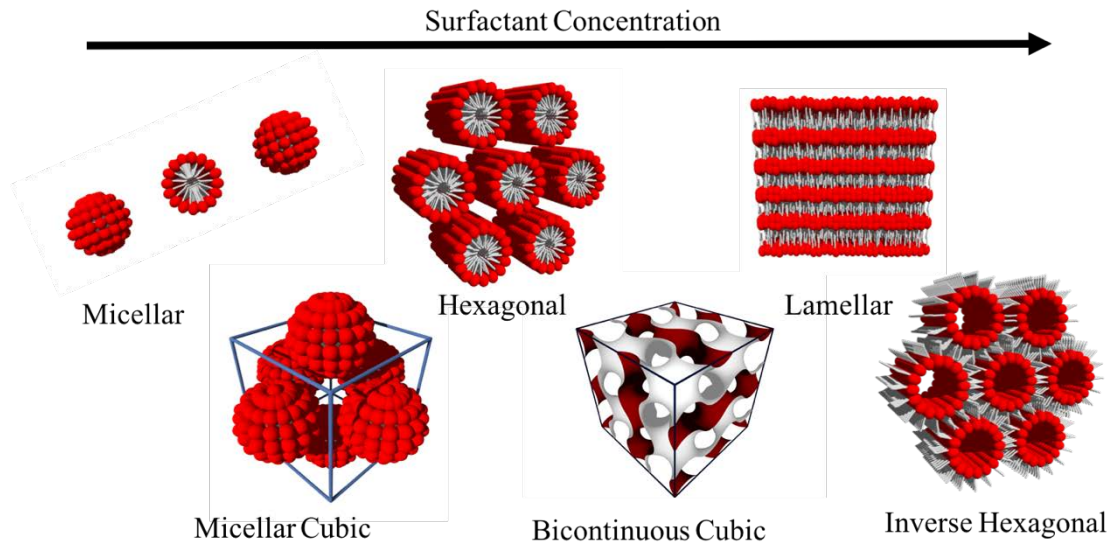
Figure 6.1. A schematic illustrating LLC mesophases and their progression as surfactant concentration is increased. Hydrophillic head groups are represented by red and hydrophobic tail groups by gray.

Low concentrations of surfactant result in spherical micelles forming within the solvent. Further increases in surfactant concentration may cause the micelles to begin to aggregate into cubic structures.[7] Eventually as concentration is further increased, a hexagonal (columnar) mesophase can form based on the specific surfactant system. Bicontinuous cubic mesophases (primitive, gyroid, and diamond) may form if conditions and surfactants permit. These bicontinuous mesophases are uncommon and usually only form for a narrow range of concentrations. At higher surfactant concentrations, lamellar mesophases are often observed. Lamellar structures consist of alternating layers of surfactant and solvent. Further increases in surfactant concentrations may result in the formation of inverse mesophases that proceed in the opposite order. The normal

mesophases are considered oil-in-water (O/W), whereas the inverse mesophases are water-in-oil (W/O).[8–10] The type and geometry of the surfactant chosen for use as a templating agent has a great influence on the type of mesophase present and the compatibility with various monomers.[11] The variety of mesophases available and the ability to control which structures are accessible with increasing concentration enables LLC templating to be a highly flexible, simple tool for imparting structure to polymer materials.

To create an LLC templated polymer, monomer and photoinitiator are incorporated into an LLC mesophase and will assemble within the mesophase depending the relative hydrophilicity of monomer and surfactant (Figure 6.2). The prepolymer mixture is then irradiated with UV-light to initiate the photopolymerization.
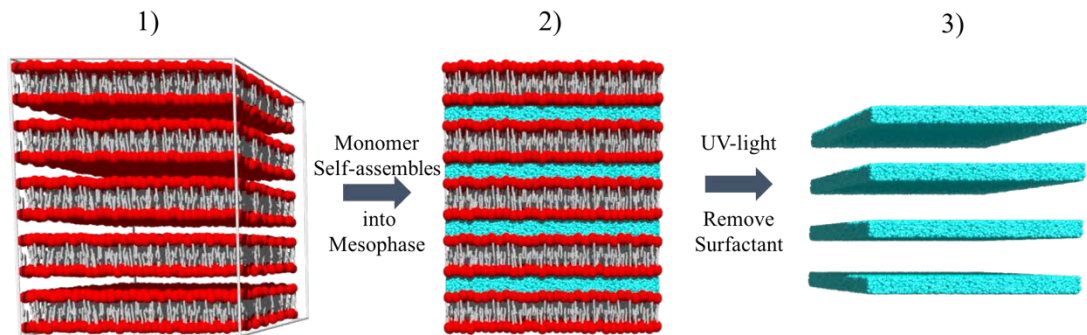
Figure 6.2. A schematic illustrating the LLC templating process. 1) A lamellar LLC mesophase is used as a template after which 2) hydrophilic monomer (blue) is added to the mesophase. 3) After polymerization and removal of the LLC surfactant mesophase, a templated polymer remains.

Photopolymerization is instrumental in LLC templating processes for two reasons: fast initiation kinetics and low temperature (room temperature) polymerization.[2] The rapid initiation of a photoinitiator by interaction with a photon creates large

quantities of radicals. The propagation reactions proceed rapidly in in the free-radical polymerization. A significant advantage of photopolymerization is that the reactions may be initiated at room temperature. In the case of LLC templating, polymerization at room temperature, where mesophases are typically formed, is particularly important. DePierro demonstrated that utilizing photoinitiators rather than thermal initiation enables better mesophase retention and the inclusion of smaller features templated into the material.[12]

It is hypothesized that polymerization with surfactants that do not exhibit highly ordered mesophases or templating with inverse mesophases will not have the same effects on hydrogel properties as highly ordered mesophases. This chapter will elucidate the differences when non-LLC forming surfactants are used as monomer templates as compared to highly ordered LLC systems. Comparing various surfactant and mesophase effects on the swelling of hydrogels will lead to a better understanding of the consequences that templating agents have on the properties of materials. The methods for LLC templating hydrogels are simple in practice, but have only been utilized with a relatively small number of monomers and surfactant. Exploring different head and tail length surfactants may allow the templating of additional monomer systems. A system of surfactants was examined to determine trends in mesophase availability, structure retention, and how swelling is affected by the type of templating structure.

This work explores a range of polyoxyethylene alkyl ether surfactants for LLC templating, many of which have not been utilized as templating agents previously. We use a systematic approach for surfactant choice to examine the effects of mesophase and surfactant on the swelling properties of LLC templated hydrogels. We first examine binary systems of surfactant and water to better understand mesophase availability in

these materials. Then PNIPAM templated in LLC mesophase is characterized using small-angle X-ray scattering (SAXS). PNIPAM hydrogels templated with different surfactants and mesophases were swollen in water to determine the effects on swelling that are induced by changing surfactant, mesophase, and concentration. Additionally, surfactant systems observed that do not exhibit mesophase during the binary screening experiments are utilized as controls for LLC templated polymers. Exploring and characterizing various templating surfactants and their effect on polymer properties will enable greater application and control over nanostructure created through photopolymerization in LLC templates.

6.2: Experimental

6.2.1: Materials

To systematically examine the relationship between surfactant structure, mesophase, and swelling, a surfactant system available with many head/tail length combinations was chosen. The Brij series of polyoxyethylene alkyl ether surfactants (Figure 6.3), from CRODA Chemical is available with three tail group lengths (lauryl/12, cetyl/16, and steryl/18 chains) and three ethylene oxide head group lengths (short, medium, and long) for a total of nine combinations of surfactant head/tails, (Table 6.1). For simplicity, the surfactants in this chapter will be described using the Brij (Croda Chemicals) naming convention, consisting of a letter designating the alkyl chain followed by the number of ethylene oxide groups in the head group. The letter is derived from the

long chain alcohol the surfactant originated from. For example, L10 consists of a lauryl alcohol joined to a 10-unit ethylene oxide.
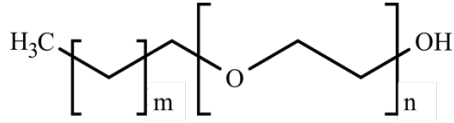
Figure 6.3. A generic polyoxytheylene alkyl surfactant where *m* designates the number of alkyl repeat units (12, 16, or 18) and *n* the number of oxyethylenes present.

N-isopropyl acrylamide (Sigma-Aldrich, St. Louis, MO) and N-N' methylene bisacrylamide (MBA) (crosslinker, Sigma-Aldrich, St. Louis, MO) were used as monomers for the creation of hydrogels, while the photoinitiator used was 2,2-

Table 6.1. Surfactants used in the study.

Designation	Alkyl Units *(m)*	Ethylene Oxide Units *(n)*	Head MW	Tail MW	Total MW
L4	12	4	192.67	169.33	362
L10	12	10	457.53	169.33	626.86
L23	12	23	1030.21	169.33	1199.54
C2	16	2	104.56	225.44	330
C10	16	10	457.56	225.44	683
C20	16	20	898.56	225.44	1124
S2	18	2	104.51	253.49	358
S10	18	10	457.51	253.49	711
S20	18	20	896.51	253.49	1150

dimethoxy-2-phenylacetophenone (DMPA, Ciba, location). Surfactants (Sigma-Aldrich, St. Louis, MO) used for LLC templating are shown in Table 6.1. Ethanol was utilized to remove surfactant from the cured hydrogel material. All materials were used as received.

6.2.2: Hydrogel Preparation

LLC templated copolymer discs were prepared by heating and vortex mixing the prepolymer mixture consisting of 20% NIPAM, 1% crosslinker, surfactant, 1% photoinitiator, and water. The surfactant templated mixtures were poured into 12 mm (outside diameter) x 3 mm thick circular Teflon®-impregnated Delrin® molds while warm and were cooled before photocuring. Isotropic mixtures were cooled to room temperature while being vortex mixed aggressively and then poured into Teflon®-impregnated Delrin® molds. Photopolymerization of both mixtures was performed using 10 mW/cm^2 of 365 nm light from an Omnicure 1500 high-pressure mercury arc UV-lamp for 20 min. The resulting discs were then rinsed in ethanol for at least 24 h to remove surfactant and unreacted monomers before being vacuum dried. It is important to note that some surfactants do not mix well with the NIPAM monomer or form discontinuous micellar mesophases, which do not permit a cohesive gel to form. When a non-viable sample is swollen in water, it disintegrates. If this occurred, then a second sample set was attempted. If the sample was again not viable for testing, it was concluded that the surfactant is incompatible for LLC templating of PNIPAM at that concentration.

6.2.3: Characterization

Previous work in LLC templating has relied heavily on SAXS to characterize structure before and after polymerization. SAXS is utilized as a semi-quantitative way to determine mesophases in LLC mixtures. As X-rays pass through a sample, they interact

113

with the electrons in the ordered molecules and scatter. An ordered sample will scatter photons in recognizable patterns, the peak ratios of which are used to determine mesophase.[7] These peaks can also be used to measure characteristic distances in the mesophase structure (D-spacing).[13,14]

SAXS was used to measure structure by collecting diffraction profiles of materials before and after polymerization. The SAXS instrument used was a Heccus M-Braun with a Kratky-type collimator, Nonius FR590 with copper target Röntgen tube with a Ni-filtered Cu Kα line of 0.154 nm as the radiation source and a linear PSD-50 detector. Profiles had backgrounds subtracted and were smoothed. The instrument was calibrated using a silver stearate sample.

Polarized light microscopy (PLM) is also used as a qualitative method for mesophase determination. When polarized light passes through an optically anisotropic structure, such as most LLC mesophases, a textured pattern will be visible. These patterns generally correlate to the various structures and can be used to aid in confirming the presence of mesophases. For screening samples for LLC mesophase behavior, a small amount of surfactant was placed upon a glass microscope slide. A glass cover slip was then placed upon the surfactant and gently pressed to distribute sample over slide. Water was pipetted onto the opposite side of the cover slip from the surfactant. Capillary action draws the water under the slip and across the slide. The slide is then heated gently with a heat gun, melting the surfactant. At the interface between the water and surfactant, mixing occurs. PLM is then used to observe the mesophases that occur in the concentration gradient between the surfactant and water. This method is useful for

114

obtaining a qualitative understanding of what mesophases may be available for a given surfactant and water.

<div align="center">6.2.4: Swelling Studies</div>

Swelling studies of PNIPAM hydrogels were performed by swelling the material to equilibrium in deionized water for 48 h. Samples were then removed from water and gently patted dry before being weighed. The mass was recorded and compared to the dry mass of the polymer. The swelling ratio is the quotient of the mass from the swollen material and the dried sample.

<div align="center">*6.3: Results and Discussion*</div>

Prior work has demonstrated mesophase availability in several surfactant systems. We believe that other similar surfactants may also exhibit mesophase behavior and that access to a variety of mesophases, ranges, and surfactant hydrophilicity/hydrophobicity may be useful for LLC templating polymer materials. To this end, a system of surfactants of varying head and tail lengths were screened for mesophase availability in a binary water system.

The surfactants used in this work were screened to ascertain the presence and type of mesophases without the addition of a monomer in simple water/surfactant binary systems. To rapidly screen each mixture, surfactant and water were placed at opposite ends of a glass slide before being heated gently on the hot stage. At the interface of mixing between the two, a gradient of mesophases is observed (Figure 6.4). This method

115

does not result in quantitative data, but does give a qualitative sense of what phases are available for each water-surfactant system.
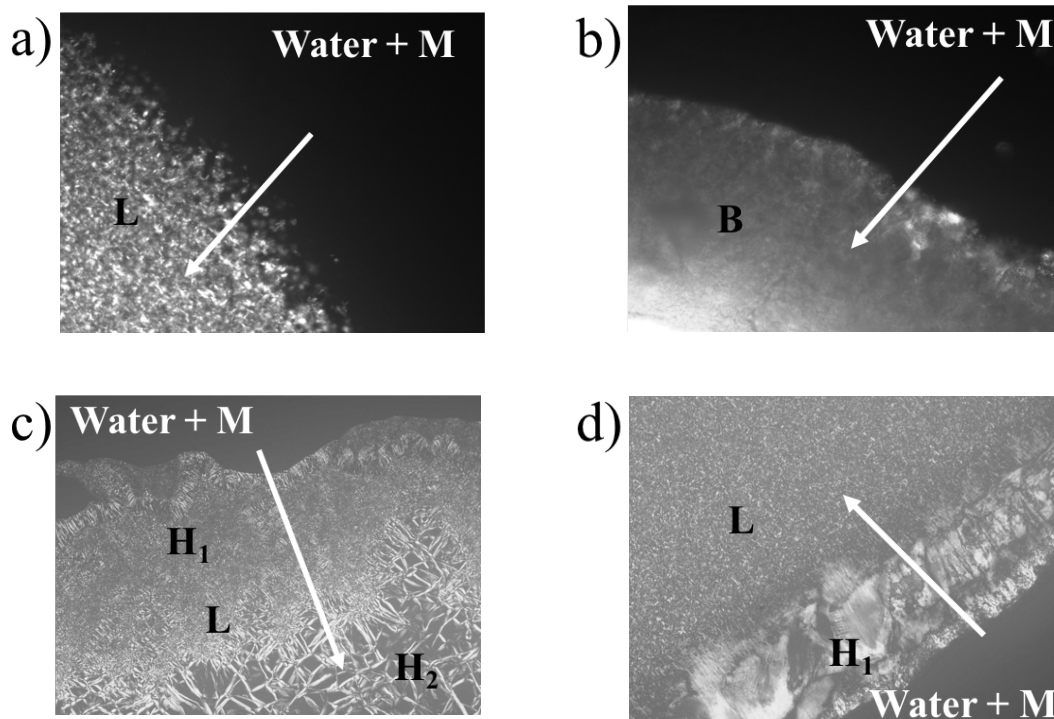
Figure 6.4. Representative gradient mesophases of a) L10, b) L23, c) S2, and d) S20 binary mixtures with H_2O from polarized light microscopy. The arrow indicates increasing surfactant concentration. Observed are water or oil in water micelles (Water + M), Hexagonal normal (H_1), Hexagonal inverse (H_2), and Lamellar (L). Bulk (B) indicates that the solid surfactant exhibits enough light scattering on the microscope to appear, but no order is apparent.

The width of these mesophases observed by PLM can be used to predict the availability of a mesophase over a range of surfactant compositions. However, upon the addition of a monomer, some shifts in both range and type of mesophase present are expected.[15] The mesophase data generated from these screenings was also used to inform a surfactant without structure to be utilized as a control. The mesophases observed for

binary gradient systems are listed in Table 6.2. The representative micrographs presented
in Figure 6.4 are for surfactants for which there is scarce mesophase information
available. However, mesophase behaviors have been well documented for the cetyl-
surfactants and S10.[9,16]

Table 6.2. Summary of mesophases observed by PLM in binary water/surfactant
screens.

Surfactant	Hexagonal	Bicontinuous	Lamellar	Inverse	None
L4					*x*
L10			*x*		
L23					*x*
C2	*x*	*x*			
C10	*x*	*x*	*x*	*x*	
C20	*x*	*x*	*x*		
S2	*x*		*x*	*x*	
S10	*x*	*x*	*x*		
S20	*x*		*x*		

Most polyoxyethylene alkyl ether surfactants follow the typical progression of
micelle (M), hexagonal (H_1), bicontinuous (Q) (if present), lamellar (L), and then inverse
mesophases (i.e., H_2).[7] As surfactant concentration increases, surfactants S2 and S20 are
observed to progress through a variety of hexagonal mesophases to lamellar. S2 and C10
are the only surfactants that show a clear transition to an inverse hexagonal mesophase in
the surfactant screen. Interestingly, L10 mixtures appear to only contain a single lamellar

117

mesophase. Surfactant L23 does not exhibit any mesophase behavior in the PLM screen micrographs, as only the bulk surfactant scatters any light. For this reason, L23 is used in control samples, which contain surfactant but not LLC structure.

For templated mixtures containing monomer, photoinitiator, and crosslinker, small-angle X-ray scattering (SAXS) was used to examine structure both pre- and postpolymerization. Figure 6.5 shows SAXS profiles of pre- and postpolymerization systems of L10, L23, S2, and S20 at multiple surfactant concentrations. L10 is observed to weakly display a mixed phase of lamellar and hexagonal mesophases throughout most of its range before becoming inverse micellar (Figure 6.5a). The similarity of pre- and postpolymerization profiles for the concentrations tested indicates good retention of the template. Figure 6.5b shows that surfactant L23 exhibits non-LLC mesophase behavior throughout its range of compositions. This lack of mesophase behavior may be due to the combination of a very bulky head group and short 12-carbon alkyl chain, which may prevent organization mesophases. Samples templated with S2 are micellar at lower surfactant loads and then progress to lamellar mesophases at 40 and 50% surfactant (Figure 6.5c). Retention of templated structure is good for the lamellar mesophases. At 60%, the material indexes to an inverse hexagonal mesophase, which retains structure with less fidelity than lower concentrations before transitioning to an inverse micellar mixture at 65%. In Figure 6.5d, it is observed that S20 also begins with micelle formation in lower mesophases, but then transitions to lamellar mesophases at 30 to 40% surfactant. From 50 to 60%, a mixture of lamellar and hexagonal inverse mesophases is observed, and finally micelles are observed at 65%

118
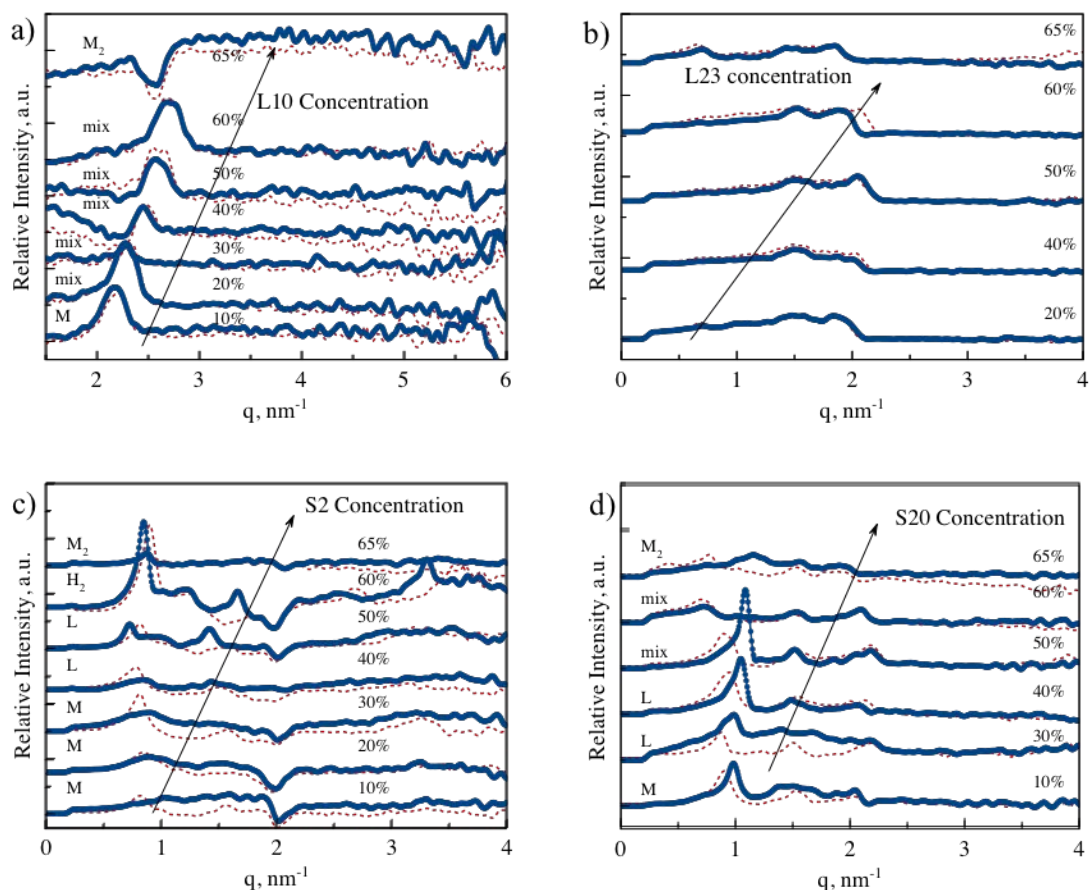
Figure 6.5. SAXS profiles of 20% NIPAM, 1% crosslinker, 1% phototiniator, and water combined with a) L10, b) L23, c) S2, and d) S20 pre (—) and post (----) polymerization at varying surfactant concentrations. Samples were polymerized with 10 mW/cm^2 at 365 nm.

Increased swelling due to structure imparted by LLC templated hydrogels has been well documented. Conversely, the reduction in structure has been noted to correspond to a loss of these properties.[17] Many monomers have been templated with LLCs and most have exhibited increased swelling. Increased swelling in templated hydrogels is a simple method of observing evidence of ordered nanostructure. Increased swelling, or the lack thereof, can help inform what type of structure may be present in a hydrogel. Increased equilibrium swelling has typically been correlated with successful

transfer of the LLC template to the hydrogel. Hydrogels were swollen to equilibrium in deionized water for 48 h. Then, mass was recorded and compared to the dry mass of the polymer. This measurement is reported as the swelling ratio.

Figure 6.6 shows the swelling ratio for crosslinked PNIPAM templated with each surfactant at various compositions. Shading is used to indicate the type of structure the material was templated with: blue for no structure or isotropic, no shading for normal nanostructure, and orange for inverse nanostructured mesophases. For PNIPAM systems templated with L23, no augmented swelling is observed (Figure 6.6a). This is expected since there is no phase observed by SAXS or PLM. PNIPAM templated in L10 retained the normal mesophases that it was templated in and as such exhibited increased swelling to 12 times the dry mass, climbing slowly to nearly 15 times at 50% surfactant compared to the 6.5 times swelling ratio of the isotropic control. In the inverse mesophase, swelling is greatly reduced by the lack of continuous polymer structure to roughly 10 times the dry mass. Samples created with L4 were unable to be tested for swelling in water. The surfactant was determined to be incompatible with PNIPAM at all concentrations. Hydrogels templated with the C-series of surfactants are known to template monomer in normal mesophases from 30 to 60% surfactant loading; hexagonal, bicontinuous, lamellar, and mixed have all been observed..[4,16–19] Even with only 10% surfactant loaded in the sample, all three systems exhibit increased swelling as compared to the isotropic control (Figure 6.6b). C10 and C20 swell to 12 times the dry mass and C2 to 16 times the dry mass. Materials templated in the normal nanostructure exhibit greatly increased swelling compared to isotropic controls. As concentration increases and mesophases shift, swelling ratios change for each surfactant. The highest swelling ratios were

120

observed in 20% C10, 30% C10 and 50% C20, which all swell around 16 times their dry mass. The variation in swelling between head group sizes, surfactant loads, and mesophases throughout the normal nanostructure range is not very large. No trend in mesophase, head, and tail group is observed. As the template transitions into the inverse, swelling of the hydrogels is reduced to similar levels as the micellar templated samples. In Figure 6.6c, when S2 is utilized as the template for PNIPAM, increases in swelling are observed beginning at 10% loading. These results are similar to the swelling observed with the C-series surfactants of roughly 12 times the dry mass. At 40 and 50% surfactant loading, when SAXS indicates that the samples are in a lamellar phase, there is a significant drop off in the swelling observed for the 50% sample from 17 times to less than ten. This suggests that the system is perhaps becoming inverse and is reinforced by the appearance of an inverse hexagonal mesophase at 60%. As the surfactant template progresses to inverse structures, swelling decreases to below isotropic levels. Samples templated with S20 exhibit swelling ratios only slightly higher than the isotropic control at 10 and 20% loading. Hydrogels templated with the middle range of S20 loading were unable to be tested for swelling due to incompatibility with PNIPAM. Swelling ratios slightly higher than the isotropic control are observed for 60 and 65% surfactant loaded samples.

An interesting trend is observed for surfactants when hydrogels are templated in an inverse mesophase. Materials in the inverse mesophase (hexagonal or lamellar) or inverse micellar show a marked reduction in swelling, nearing or becoming less than the swelling ratios observed for isotropic samples. The reduction in swelling in the inverse

121
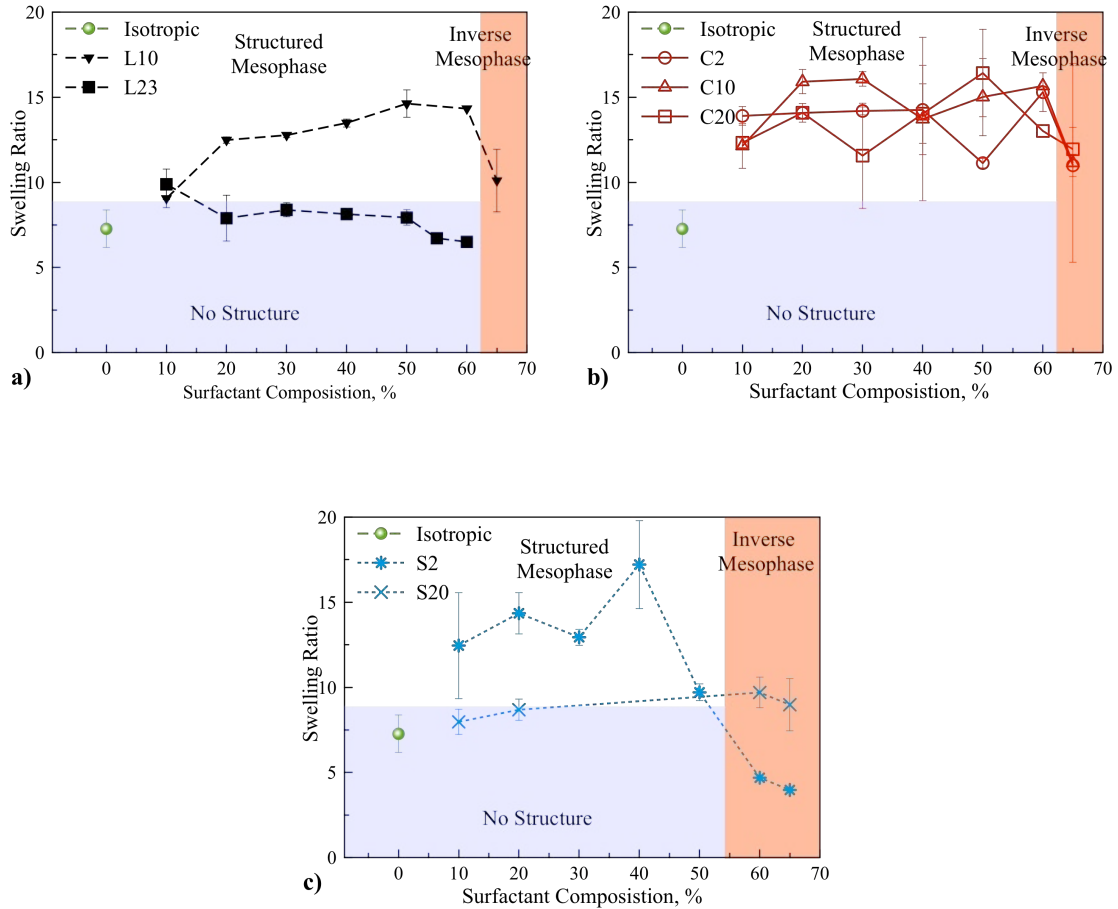
Figure 6.6. Swelling ratios of hydrated 20% PNIPAM hydrogel samples at various surfactant concentrations. The blue shaded areas represent no structure, the unshaded regions represent structured mesophase, and the orange areas represent inverse mesophase. The isotropic sample (⊙) is shown as a reference for all surfactant families. Shown are: a) L10 (▼), L23 (■), b) C2 (○), C10 (△), C20 (□), and c) S2(◆), S20 (X) surfactant template systems. Samples were cured at 10 mW/cm^2 for 10 min.

mesophase is attributed to a reduction in or the removal of the continuous network. Where there were once 'open' channels filled with the hydrophobic tails of surfactant during polymerization of a hydrophilic material, the inverse is now true. The 'channels' are now discrete and formed of hydrogel, (see Figure 6.1 for the difference between the normal and inverse hexagonal mesophases). A similar trend is observed in polyethylene

122

glycol diacrylate hydrogels, but to a lesser degree (Appendix A). The inverse nature of the polymer structure removes the continuous pore network associated with LLC templating. Thereby creating materials that act more like an isotropic material with no ordered structure. The importance of an interconnected network is emphasized by the absence of swelling increase for PNIPAM materials polymerized in the presence of a non-ordered L23 surfactant. Though the surfactant is present within the prepolymer mixture, the lack of LLC structure prevents any ordering of the hydrogel.

6.4: Conclusions

The LLC templating process relies upon the surfactant compatibility and type of mesophase present to create nanostructured materials. By understanding how templating structures affect the final properties of hydrogel materials, greater control and a wider variety of materials can be templated. To this end, a matrix of surfactants was selected with alkyl chains of 12, 16, and 18 carbons and short (~2), medium (~10), and long (~20) polyoxyethylene (PEO) units. The surfactants were observed to show a range of LLC mesophases in water, which progressed in the typical micelle, hexagonal, bicontinuous, lamellar, and inverse phases with increasing surfactant content. Structural characterization of the surfactant systems revealed that retention of structure was generally good and that hexagonal, lamellar, and mixed mesophases were available for templating. L10, S2, and S20, surfactants not previously utilized as LLC templates, allowed good retention of structure in PNIPAM systems. Surfactant polyoxythylene (23) lauryl ether (L23) did not exhibit mesophase behavior at any concentration and was utilized for the synthesis of isotropic, surfactant loaded controls. This surfactant was ideal for use as a control because the lack of structure allows it to be compared to structured

123

surfactant templated systems. Swelling was observed for each surfactant through a range of concentrations and was correlated to the nanostructure used to template the material. Swelling was observed to increase markedly in hydrogels templated in a normal LLC mesophase up to 17 times the dry mass compared to 6.5 times for the isotropic. When the templated structures are inverse mesophases, swelling is reduced to near that of an isotropic material. The lack of a continuous polymer network within the hydrogel prevents swelling increases. Swelling is not increased by templating with an unorganized, random system of surfactant micelles or inverse mesophases. A continuous nanostructured material is required for increases in swelling ratio to occur. This is demonstrated by observing materials templated with L23, which exhibit swelling ratios similar to that of the isotropic controls. Lack of any structure, even at high concentrations of surfactant loading, permits L23 to be used as an excellent control for structured LLC systems. The work described here extends the knowledge of surfactants available for use as LLC templates. These surfactants show promise in expanding monomer compatibility with LLC templates, which may be utilized to apply LLCs to a greater variety of polymer materials.

124

6.5: References

(1)   Forney, B. S.; Guymon, C. A. Fast Deswelling Kinetics of Nanostructured poly(N-Isopropylacrylamide) Photopolymerized in a Lyotropic Liquid Crystal Template. *Macromol. Rapid Commun.* **2011**, *32* (9–10), 765–769.

(2)   Worthington, K. S.; Baguenard, C.; Forney, B. S.; Guymon, C. A. Photopolymerization Kinetics in and of Self-Assembling Lyotropic Liquid Crystal Templates. *J. Polym. Sci. Part B Polym. Phys.* **2017**, *55* (6), 471–489.

(3)   Sievens-Figueroa, L.; Guymon, C. A. Cross-Linking of Reactive Lyotropic Liquid Crystals for Nanostructure Retention. *Chem. Mater.* **2009**, *21* (6), 1060–1068.

(4)   Clapper, J. D.; Guymon, C. A. Physical Behavior of Cross-Linked PEG Hydrogels Photopolymerized within Nanostructured Lyotropic Liquid Crystalline Templates. *Macromolecules* **2007**, *40* (4), 1101–1107.

(5)   Forney, B. S.; Guymon, C. A. Nanostructure Evolution during Photopolymerization in Lyotropic Liquid Crystal Templates. *Macromolecules* **2010**, *43* (20), 8502–8510.

(6)   Depierro, M. A.; Guymon, C. A. Polymer Structure Development in Lyotropic Liquid Crystalline Solutions. *Macromolecules* **2014**, *47*, 5728–5738.

(7)   Hyde, S. T. Identification of Lyotropic Liquid Crystalline Mesophases. In *Handbook of Applied Surface and Colloid Chemistry*; Holmberg, K., Ed.; John Wiley & Sons, Inc., 2001; pp 299–332.

(8)   Uddin, M. H.; Yamashita, Y.; Furukawa, H.; Harashima, A.; Kunieda, H. Phase Behavior of Poly (Oxyethylene)-Poly (Dimethylsiloxane) Surfactant (Copolymer) with Water or Silicone Oil. *Trends Colloid ...* **2004**, *123*, 269–274.

(9)   Nandy, D.; Mitra, R. K.; Paul, B. K. Phase Behavior of the Mixtures of Poly(oxyethylene) (10) Stearyl Ether (Brij-76), 1-Butanol, Isooctane, and Mixed Polar Solvents. II. Water and Ethylene Glycol (EG) or Tetraethylene Glycol (TEG). *J. Colloid Interface Sci.* **2007**, *310* (1), 229–239.

(10)   Landh, T. Phase Behavior in the System Pine Oil Monoglycerides-Poloxamer 407-Water at 20°C. *J. Phys. Chem.* **1994**, *98* (34), 8453–8467.

(11)   Nagarajan, R. Molecular Packing Parameter and Surfactant Self-Assembly: The Neglected Role of the Surfactant Tail. *Langmuir* **2002**, *18* (1), 31–38.

(12)   DePierro, M. A.; Guymon, C. A. Photoinitiation and Monomer Segregation Behavior in Polymerization of Lyotropic Liquid Crystalline Systems. *Macromolecules* **2006**, *39* (2), 617–626.

(13) Amar-yuli, I.; Wachtel, E.; Shoshan, E. Ben; Danino, D.; Aserin, A.; Garti, N. Hexosome and Hexagonal Phases Mediated by Hydration and Polymeric Stabilizer. **2007**, No. 12, 3637–3645.

(14) Fontell, K.; Hernqvist, L.; Larsson, K. R. E.; Sjoblom, J. On Structural Relations between Lipid Mesophases and Isotropic Reversed Micellar (L2) Solutions. *J. Colloid Interface Sci.* **1983**, *93* (2), 453–460.

(15) DePierro, M. A.; Carpenter, K. G.; Guymon, C. A. Influence of Polymerization Conditions on Nanostructure and Properties of Polyacrylamide Hydrogels Templated from Lyotropic Liquid Crystals. *Chem. Mater.* **2006**, *18* (23), 5609–5617.

(16) Thorson, T. Phase Behavior and Stimuli Response in Lyotropic Liquid Crystalline Templated Photopolymers, University of Iowa, 2013.

(17) Mclaughlin, J. R.; Abbott, N. L.; Guymon, C. A. Responsive Superabsorbent Hydrogels via Photopolymerization in Lyotropic Liquid Crystal Templates. *Polymer (Guildf).* **2018**.

(18) Lester, C. L.; Smith, S. M.; Jarrett, W. L.; Guymon, C. A. Effects of Monomer Organization on the Photopolymerization Kinetics of Acrylamide in Lyotropic Liquid Crystalline Phases. *Langmuir* **2003**, *19* (22), 9466–9472.

(19) Forney, B. S.; Baguenard, C.; Guymon, C. A. Improved Stimuli-Response and Mechanical Properties of Nanostructured poly(N-Isopropylacrylamide-Co-Dimethylsiloxane) Hydrogels Generated through Photopolymerization in Lyotropic Liquid Crystal Templates. *Soft Matter* **2013**, *9* (31), 7458–7467.

7: CAPACITANCE IN NON-CONDUCTING SILICONE POLYMERS VIA LYOTROPIC LIQUID CRYSTAL TEMPLATED NANOSTRUCTURE

The increasing reliance on energy storage devices and the desire for fast charging power solutions has led to increased examination of capacitive materials. We demonstrate a method of creating capacitive materials from non-conducting silicone polymers utilizing photopolymerization in a self-assembling nanostructured surfactant system. The structured silicone materials exhibit several orders of magnitude larger specific and volumetric capacitance as compared to chemically identical isotropic samples. The surfactant system allows nanostructure to be easily templated within the silicone material. This work shows a method for creating economical, simple, and easily scaled-up capacitive devices from previously unexplored nanostructured polymer materials.

7.1: Introduction

Increasing use of renewable energy sources is changing the way the world thinks about power generation. These sources, such as wind and solar, rarely output constant energy.[1] This variability means that energy storage is required as a method of leveling power output, charging in times of surplus production, and discharging in low production periods. Additionally, the growing number of electronic devices and electric transportation creates an ever-increasing demand for electricity storage.

The fast charge/discharge and high density power characteristics make capacitors a promising technology for energy storage. The most successful capacitors to date require the use of expensive metal oxides.[2] Polymer electrolyte and polymer-based capacitors have received a great deal of attention as a possible method for creating capacitors

without expensive metal oxides. Techniques and materials that can be cheaply and easily made into capacitor devices could be of great value.

A common strategy for controlling and improving electrochemical properties of materials is to create structures within the material on small size scales. Recently silver honeycomb nanostructures were hybridized with poly(methyl methacrylate) to create conductive, semi-transparent thin films for use in sensors.[3] Similarly, solid state membranes were created by utilizing polymerization induced phase separation.[4] These membranes exhibited very high ion conductance and high modulus, due to the nanostructure created. Many studies have demonstrated that the manipulation of materials at the nanoscale is an effective method of improving capacitive characteristics.[1,5] Capacitive performance characteristics are largely governed by creation of nanostructures within or insertion of nanoparticles into a material. These nanoscale features function as a multitude of electric double layer capacitors.[6]

A method of creating potentially relevant nanostructure within polymers employs self-assembling surfactant systems, known as lyotropic liquid crystals (LLCs). Combined with photopolymerization, this method has created ordered nanostructure hydrogel materials with a simple template. A mixture of surfactant and solvent may self-assemble into an LLC mesophase. These mesophases are concentration dependent, and as surfactant concentration increases, the following mesophase progression typically occurs: micelles, hexagonal columns, bicontinuous or sponge, lamellar, followed by inverse phases in the opposite order. When monomer and photoinitiator are added to these mesophases, they may self-assemble into the mesophase based on hydrophilic/hydrophobic character. Photopolymerization allows fast initiation rates,

128

which cure the monomer rapidly. The rapid curing of the templated structure allows for increased template fidelity as thermodynamically unfavorable structures may be kinetically trapped. The monomer is then photopolymerized and the surfactant system potentially leaving a templated structure (Figure 7.1).

LLC Mesophase   LLC Mesophase +   Templated polymer
Monomer

UV-light

Remove surfactant
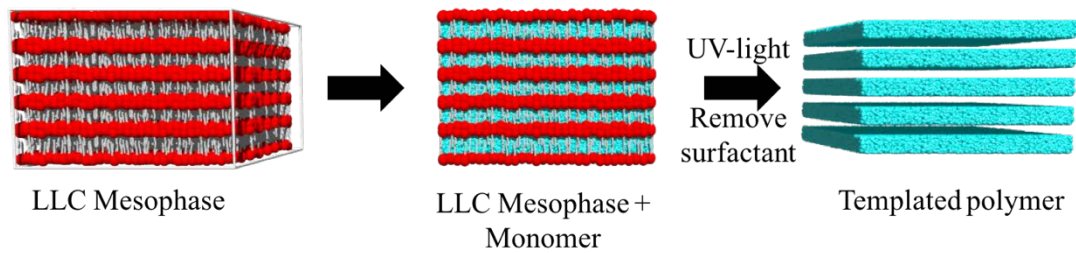
Figure 7.1. Schematic illustrating the LLC templating process. Surfactant (red hydrophilic heads with grey hydrophobic tails) forms a lamellar mesophase. Hydrophobic monomer (blue) self-assembles into the mesophase. After photopolymerization and surfactant removal, a templated polymer remains.

By employing this templating method, swelling and compressive modulus have been modified in several monomer systems.[7–10] Poly(ethylene glycol diacrylate) has shown increases in swelling without a corresponding decrease in compressive modulus despite the increase in water concentration compared to non-templated materials. The retained modulus is attributed to the ordered structure within the material, acting as a network of support channels when filled with fluid.[11] The stimuli-responsive characteristics of poly(n-isopropyl acrylamide) (PNIPAM) are increase greatly by the addition of structure. PNIPAM is a thermo-responsive material, which undergoes a reversible volume transition upon exposure to temperatures greater than 32 ˚C. PNIPAM polymer chains undergo a coil-to-globule transition, which forces water from the hydrogel. LLC templating PNIPAM allows faster, more complete volume transition, due to increased transport of water from the hydrogel.[8] LLC templating has also been utilized

129

as a tool for compatibilizing dual networks of hydrophilic PNIPAM self-assembled in the hydrophilic domain of a poly(oxyethylene) cetyl ether surfactant hexagonal mesophase and hydrophobic polydimethylesilicone segregated to the hydrophobic domain.[9] After photopolymerization, the two interpenetrating networks created materials with stimuli-responsive characteristics of PNIPAM and increased toughness from silicone. Additionally by monitoring dye-released into water as a function of time, coefficients of diffusion 4.5 times greater than non-structured materials have been observed.[11]

The increased diffusion coefficients and the observed structure templated by LLC suggests a highly porous network with a high surface area. High rates of diffusion and large surface areas are desirable characteristics for the creation of capacitor materials. Here we report a facile method of using LLC templating and photopolymerization to create nanostructured silicone materials which exhibit capacitance. Silicone materials were photopolymerized in an LLC template. Structure retention was analyzed using small angle X-ray scattering, and capacitance was measure using cyclic voltammetry.

7.2: Experimental

7.2.1: Materials

Silicone diacrylate 1500 MW (Di-1508, Siltech) was used as the monomer and 2,2-Dimethoxy-2-phenylacetophenone (DMPA, Ciba) as the photoinitiator. Poly(oxyethylene)-20 steryl ether (Brij S20, Sigma-Aldrich) was used as the anhydrous templating surfactant. LLC templated samples were rinsed with deionized water. Isotropic materials were formed by using ethanol to form a solution polymerization. All materials were used as received. Carbon fiber cloth was utilized as the electrode for cyclic voltammetry experiments.

130

7.2.2: Polymer Templating

LLC templated electrode materials were prepared by heating and vortex mixing Di-1508 silicone diacrylate (ρ=1.1 g/cm^3) with DMPA photoinitiator and 50% Brij S20 surfactant (ρ=0.964 g/cm^3). Isotropic mixtures were prepared with ethanol as a replacement for the surfactant, creating a solution polymerization. Samples were created by dabbing a small amount of prepolymer mixture onto carbon cloth. A mold consisting of 50 µm mylar film with a 6 mm hole was placed around the prepolymer. A Rain-X® treated microscope slide was then used to press the mixture onto the carbon cloth (ELAT, E-TEK), filling the mold. The slide and mylar film were then removed and the material was photopolymerized using 10 mW/cm^2 at 365 nm light from an Omnicure 1500 high-pressure mercury arc UV lamp for 10 min. The resulting polymer, now adhered to the electrode, was then rinsed in deionized water for 24 h to remove surfactant and unreacted monomers before being air dried. This method removes over 95% of surfactant.[5,6,8]

7.2.3: Structure Characterization

Small angle X-ray scattering (SAXS) was used to quantify the structure before and after polymerization of the template silicone materials. By measuring the angles at which X-rays are scattered upon passing through an ordered sample, the structure of the sample may be determined. SAXS was performed using a Nonius FR590 with a wavelength of 0.154 nm as the radiation source, a Heccus M-Braun Kratky-type collimator camera body, and a linear PSD-50 detector. Scattering was examined before and after polymerization on samples placed between mylar windows. From the resulting position versus intensity profile, a background profile was subtracted. This profile is then

Lorentz corrected, desmeared, and the resulting peaks analyzed to determine mesophase presence and retention.

7.2.4: Electrochemical Characterization

Capacitance was determined using cyclic voltammetry. A 1 mM aqueous solution of $NaNO_3$ was prepared and degassed using N_2. A three-electrode setup was used with a platinum mesh electrode as the counter electrode. The reference electrode (RE) was a saturated calomel electrode (SCE). The working electrode (WE) consisted of the polymer samples pressed onto carbon cloth.
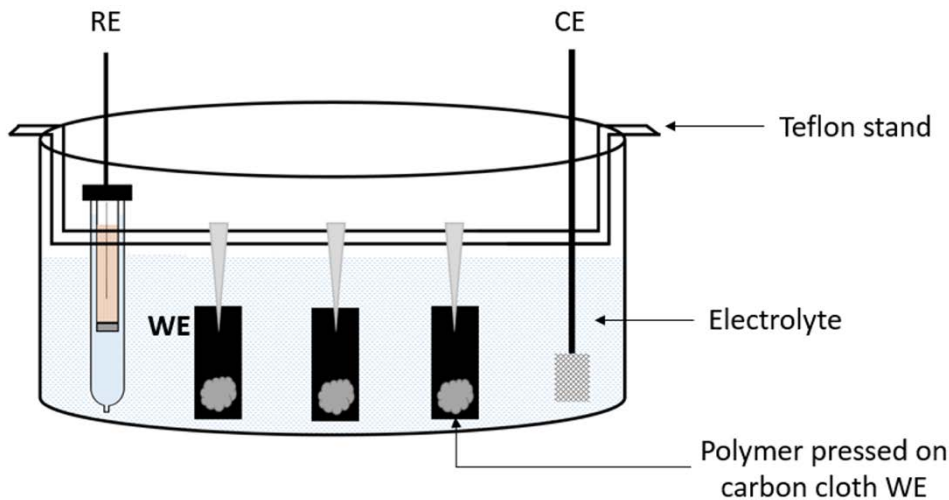
Figure 7.2. Experimental setup for the three-electrode system. A Teflon® stand was used to position three carbon cloth working electrodes (WE), a calomel reference electrode (RE), and the platinum counter electrode (CE).

Cyclic voltammetry was performed (CH instruments 760B potentiostat) at scan rates of 5, 10, 25, 50, 75, 150, and 200 mV/s, in random order from an initial 0.5 V to a

132

high of 1.3 V and a low of -0.4 V. Films equilibrated in the $NaNO_3$ solution for a minimum of 24 h before testing. All measurements were performed in triplicate. The current envelope width from the resulting voltammogram was measured as the difference between the two roughly linear portions of the voltammogram and was used to calculate the capacitance for samples at each scan rate using Equation 3.5.

7.3: Results

The creation of ordered structure polymer materials has been demonstrated to induce changes in material transport properties. Changes in structure on the nanoscale may be expected to induce changes on the electrochemical properties of a material especially those properties that are strongly dependent upon ion diffusion. To examine the structure, small-angle X-ray scattering (SAXS) profiles were completed for samples of Di-1508 templated with Brij S20 pre- and postpolymerization (Figure 7.3). Before polymerization, mixtures exhibit characteristic lamellar peaks of ratio 1:2:3:4:5.[12] The same lamellar structure is well retained postpolymerization as evidenced by the nearly identical peak positions. The lamellar structures appear to extend to larger size scales as was noted by the layered appearance of cooled drops of the mixture shown in the inset image. The formation of a binary monomer/surfactant LLC without the presence of a tertiary solvent (e.g. water) component may give rise to greater flexibility in LLC formulation. The creation of structured silicone material may have a large impact on the electrochemical properties due to the expected large amount of specific surface area from a templated nanostructure
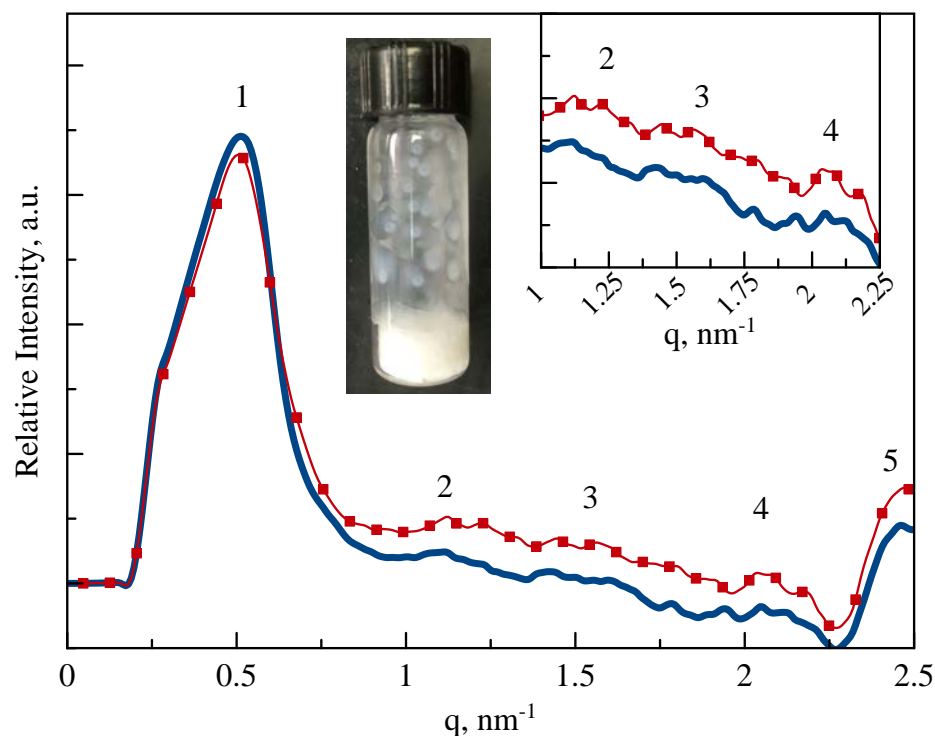
Figure 7.3. Small-angle X-ray scattering profiles of Di-1508 templated with Brij S20, (—) prepolymerization and (■) after polymerization with 10 mW/cm^2 365 nm light. Inset image shows patterning of cooled prepolymer mixture. Inset SAXS profile is zoomed scale of higher order peaks. D-spacing measurements of the primary peak indicate that the lamellar features are roughly 12 nm.

As is expected from a highly insulating polymer, isotropic silicone exhibits almost no observable difference from the bare electrode controls (Figure 7.4). An envelope of current between the two flat portions of the scan (typically 0.5 - 0.75 V) is observed for nanostructured silicone materials in the voltammogram, which becomes larger as voltage scan rate is increased. Intermediate scan rates are left out of figure for clarity. Determining the capacitance from the slope of current versus scan rate at low scan rates (5-20 mV/s) leads
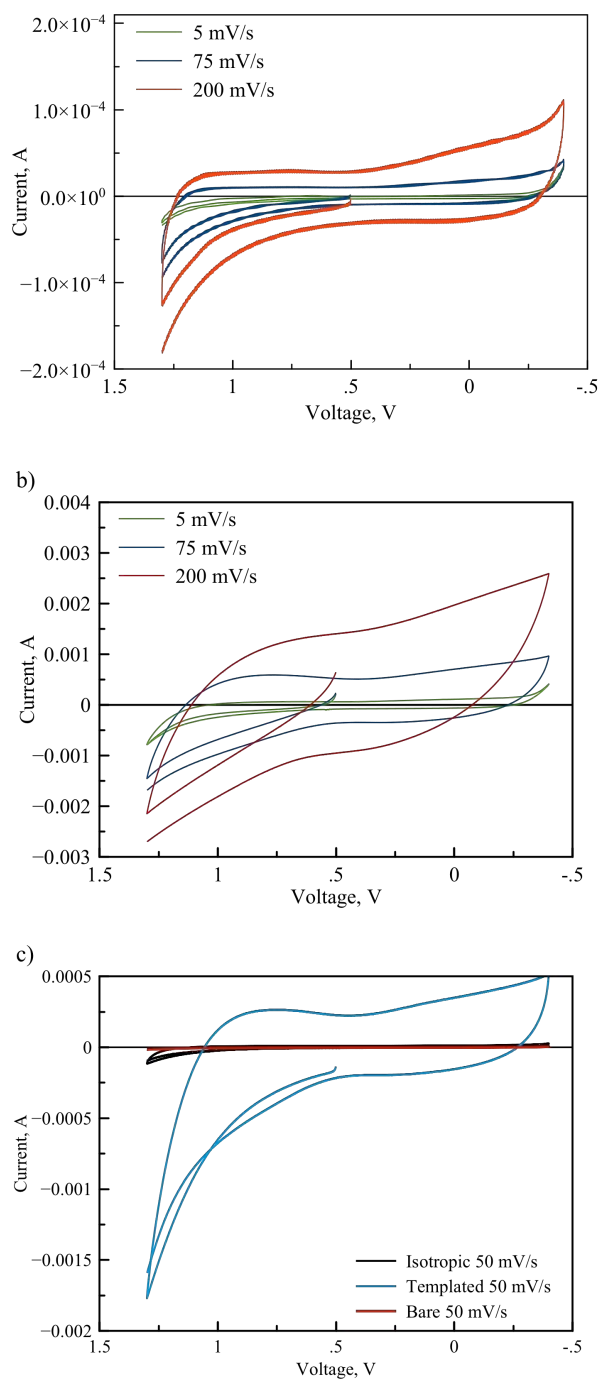
Figure 7.4. Voltammograms of (a) isotropic and (b) templated silicones at various scan rates. A comparison (c) of voltammograms at 50 mV/s of a bare electrode (blue), templated silicone (purple), and isotropic silicone (green) at 50 mV/s scan rate.

to a specific capacitance of approximately 0.27 F/g and 0.60 F/cm^3 (see appendix B for example). Isotropic materials exhibit specific capacitances of 0.007 F/g and 0.0059 F/cm^3.

When the nanostructured silicone materials are compared to state-of-the-art carbon nanomaterials (30-70 F/g), the specific capacitances are low.[3] However, the silicone materials characterized here are analyzed in a neutral ionic solution, whereas carbon nanomaterials are used in highly acidic or basic solutions. The ability to exhibit capacitance under mild conditions is potentially useful in commercial applications. The templated material is assumed to be much less dense due to nanostructure. This lower density allows templated materials to exhibit roughly two orders of magnitude greater capacitance by volume compared to isotropic materials.

Figure 7.5 shows the typical progression of higher capacitance at low scan rates, due to the shortened time window for charge saturation. Lower scan rates allow charge to build in the capacitor, whereas at higher scan rates the device does not have sufficient time to do so. The ordered nanostructure created by LLC templating permits the transfer and collection of charge within an insulating polymer substrate. Capacitance was also observed in two other systems LLC templated to create nanostructure networks. *N*-isopropyl acrylamide and PEGDA were templated with LLCs (Appendix B). Increases in capacitance as

compared to isotropic materials indicate that the method can be extended to other non-conductive polymers.
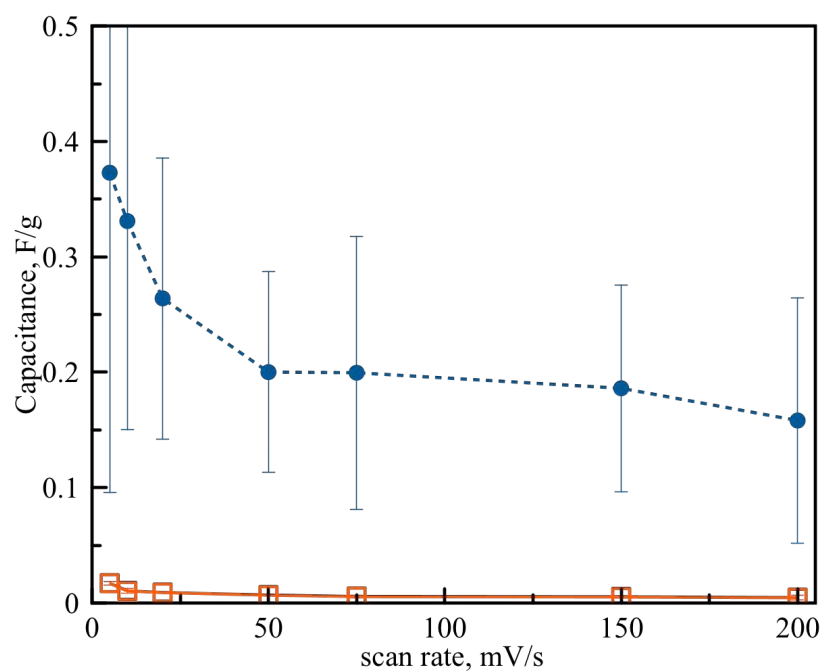
Figure 7.5. Capacitance observed as a function of scan rate for (•) templated silicone diacrylate and (□) isotropic silicone. Templated samples were synthesized with 50% Brij S20, 1% DMPA. Isotropic materials were mixed with ethanol.

7.4: Conclusions

A method of creating nanostructured capacitive materials from silicone diacrylates utilizing LLCs and photopolymerization is described. Anhydrous systems with lamellar order are created using Brij S20 and silicone diacrylate monomer. Structured silicone materials are observed to have specific capacitance on the order of 0.27 F/g and 0.54 F/cm^3, whereas isotropic samples exhibit substantially less capacitance. The advantage of these systems is that the electrochemical behavior is observed in mild conditions where carbon materials are measured in highly basic or acidic solutions. These materials are also easily synthesized, flexible, conformable, and inexpensive. LLC templating polymers allows the creation of many features desirable in capacitive

137

materials, such as large surface areas and compact void spaces. Additionally, the scalability and variety in monomer starting materials afforded by photopolymerization could allow a wide variety of electrochemical devices to be created using this simple method. Creating polymeric capacitors with LLC templated nanostructure may be a powerful method for the creation of inexpensive, easily fabricated power storage devices.

7.5: References

(1)   Yu, G.; Xie, X.; Pan, L.; Bao, Z.; Cui, Y. Hybrid Nanostructured Materials for
        High-Performance Electrochemical Capacitors. *Nano Energy* **2013**, *2* (2), 213–
        234.

(2)   Jang, J. H.; Kato, A.; Machida, K.; Naoi, K. Supercapacitor Performance of
        Hydrous Ruthenium Oxide Electrodes Prepared by Electrophoretic Deposition.
        2006, 321–328.

(3)   Mir, S. H.; Ochiai, B. Conductive Polymer-Ag Honeycomb Thin Film: The
        Factors Affecting the Complexity of the Microstructure. *J. Electrochem. Soc.*
        2018, *165* (8), B3030–B3034.

(4)   Schulze, M. W.; McIntosh, L. D.; Hillmyer, M. A.; Lodge, T. P. High-Modulus,
        High-Conductivity Nanostructured Polymer Electrolyte Membranes via
        Polymerization-Induced Phase Separation. *Nano Lett.* **2014**, *14* (1), 122–126.

(5)   Xiong, P.; Zhu, J.; Wang, X. Recent Advances on Multi-Component Hybrid
        Nanostructures for Electrochemical Capacitors. *J. Power Sources* **2015**, *294*, 31–
        50.

(6)   Simon, P.; Burke, A. Nanostructured Carbons: Double-Layer Capacitance and
        More. *Electrochem. Soc. Interface* **2008**, *17* (1), 38–43.

(7)   Worthington, K. S.; Green, B. J.; Rethwisch, M.; Wiley, L. A.; Tucker, B. A.;
        Guymon, C. A.; Salem, A. K. Neuronal Di Ff Erentiation of Induced Pluripotent
        Stem Cells on Surfactant Templated Chitosan Hydrogels. *Biomacromolecules*
        2016, *17*, 1684–1695.

(8)   Forney, B. S.; Guymon, C. A. Fast Deswelling Kinetics of Nanostructured poly(N-
        Isopropylacrylamide) Photopolymerized in a Lyotropic Liquid Crystal Template.
        Macromol. Rapid Commun. **2011**, *32* (9–10), 765–769.

(9)   Forney, B. S.; Baguenard, C.; Guymon, C. A. Improved Stimuli-Response and
        Mechanical Properties of Nanostructured poly(N-Isopropylacrylamide-Co-
        Dimethylsiloxane) Hydrogels Generated through Photopolymerization in
        Lyotropic Liquid Crystal Templates. *Soft Matter* **2013**, *9* (31), 7458–7467.

(10)   Clapper, J. D.; Iverson, S. L.; Guymon, C. A. Nanostructured Biodegradable
        Polymer Networks Using Lyotropic Liquid Crystalline Templates.
        Biomacromolecules **2007**, *8* (7), 2104–2111.

(11)   Clapper, J. D.; Guymon, C. A. Physical Behavior of Cross-Linked PEG Hydrogels
        Photopolymerized within Nanostructured Lyotropic Liquid Crystalline Templates.
        Macromolecules **2007**, *40* (4), 1101–1107.

(12)   Hyde, S. T. Identification of Lyotropic Liquid Crystalline Mesophases. In
       Handbook of Applied Surface and Colloid Chemistry; Holmberg, K., Ed.; John
       Wiley & Sons, Inc., 2001; pp 299–332.

8: INCREASED ELONGATION OF URETHANE DIACRYLATE FILMS VIA RAFT MEDIATED PHOTOPOLYMERIZATION

Photopolymerization is attractive due to fast polymerization rates, spatial control, and the ability to use low-volatility resins. However, the use of photopolymer materials in commercial applications has typically been limited to thin film coatings and materials for which toughness is not an important design consideration. Increased toughness and elongation of polymer materials could be realized through increased homogeneity in polymer networks using chain-transfer agents. We demonstrate the effects on the thermomechanical properties of photocured urethane acrylate films by controlling network formation with a reversible-addition fragmentation chain-transfer (RAFT) agent. Urethane diacrylate oligomer mixtures are polymerized in the presence of a trithiocarbonate RAFT agent, and thermomechanical properties and reaction kinetics are compared between concentrations of RAFT varying from 0-5 times that of photoinitiator. These films exhibit enhanced elastic properties when polymer propagation is controlled using a RAFT agent to control crosslink density. Adding RAFT slows the rate of polymerization and reduces the conversion. By modifying the reaction kinetics, controlled network growth can occur by chain-transfer of the propagating radical around the RAFT equilibrium bond. This mediation creates networks with lower crosslink density, permitting increased elongation materials to form with lower Young's modulus and higher toughness. RAFT modified materials show toughness up to three times that of controls. Additionally, curing using a high intensity belt lamp system shows that high conversion can be reached even for samples with high RAFT agent content. Adding RAFT agents to photopolymer systems shows promise in facilitating modification of

network formation and final material properties within these increasingly important systems.

8.1: Introduction

Photopolymerization techniques are increasingly being utilized in production methods, such as additive manufacturing and thin films, where fast polymerizations and low volatility starting products are valued.[1] Monomers with acrylate functionality are popular in photopolymerization due to their extremely fast polymerization rates and flexible synthesis. However, due to this rapid polymerization, acrylate-based materials are brittle and may have excessive shrinkage stress which may affect material toughness and durability.[2–5] Toughness is a measurement of the amount of energy a material can absorb before breaking. It is commonly calculated as the area under a stress/strain curve.[6] In traditional photopolymer applications, such as thin films or coatings, these shortcomings may be safely ignored or easily mitigated by modifying the monomer formulation or processing conditions. However, in coatings and larger scale materials the large amount of polymerized material may induce sufficient shrinkage stress to cause short or long-term material failure. Therefore, increased control of toughness and elongation in photopolymerized materials could allow expanded application of photopolymerization in more industries and products.
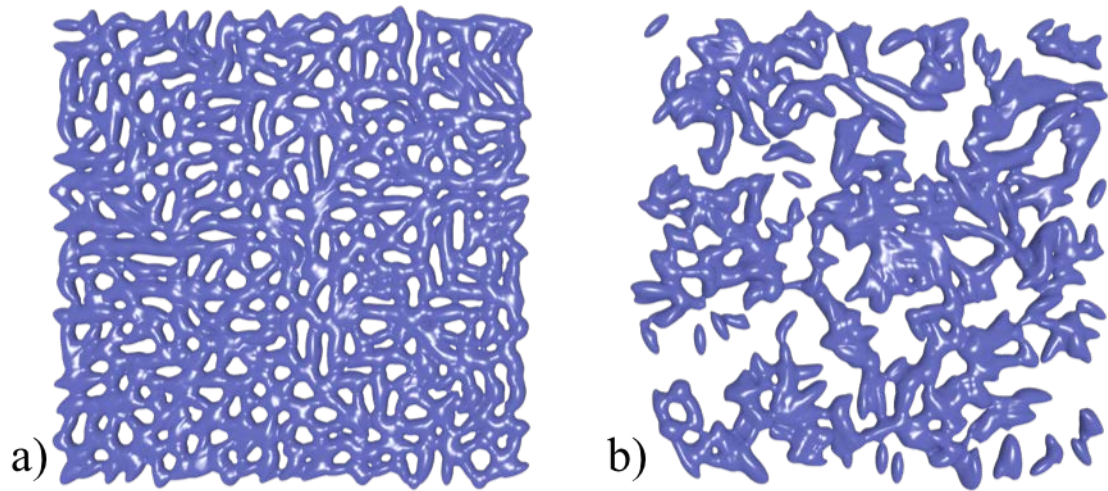
Figure 8.1. Cartoon illustrating a) a homogeneous network with few areas of low crosslink density and b) an inhomogeneous network with many low-density areas.

In a typical photopolymerization, the rapid rate of polymerization causes an increase in microgellation, an abundance of areas of high crosslinking which form due to high rates of localized polymerization. Microgels are known to cause stresses within a polymer network which may reduce the network homogeneity and toughness.[7,8] By modifying the microgellation behavior more homogeneous networks may be permitted to form. Networks that are more homogeneous have fewer weak points and stress risers, resulting in tougher materials, rather than producing traditionally brittle acrylate materials.[2] Figure 8.1 illustrates the concept behind homogeneous networks, the heterogeneous network (a) depicted has larger gaps and a greater variation of network density that could lead to an overall weaker system. In contrast the uniformity of the homogeneous network (b) should allow for a more robust system.

A recent review outlines many strategies for increasing the toughness of photopolymers by controlling network formation to decrease crosslinking inhomogeneities.[2] Thiol-ene/yne polymerization accomplish this by a step-growth

143

reaction which allows for 1:1 reaction of the thiol and the -ene/yne moiety, allowing for low stress, high homogeneity networks to form.[9] Addition fragmentation chain transfer (AFCT) agents such as β-allyl sulfones are utilized to regulate polymerization propagation through the fragmentation and subsequent radical transfer of the AFCT agent.[10] Atom transfer radical polymerization (ATRP) creates a living radical which permits the controlled radical propagation through a reversibly activated/deactivated radical, usually through a transition metal. A common goal of these methods is to control network propagation through various mechanisms. Through this control, more homogeneous networks may be formed in photopolymer systems, by creating monodispersed chains between cross-links, increasing homogeneity of the network. However, one shortcoming of these strategies is that they often require either custom monomer chemistries or are only applicable to a limited set of materials. Therefore, a method for controlling network formation that is extensible to a wide variety of chemistries is very desirable.

Reversible addition fragmentation chain transfer (RAFT) is another method by which network propagation can be controlled. Adding RAFT agents to a photopolymerization may provide a more widely applicable method. RAFT is commonly used in grafting techniques or in functionalization of surfaces or particles for the controlled growth and narrow molecular weight-distribution it creates. These highly controlled polymerization make RAFT attractive for applications requiring low-dispersity linear materials, or for creating branched polymers, which benefit from regulated growth from a polymer backbone.[11–14] A common RAFT chemistry is based upon trithiocarbonates, which control radical polymerization by capturing a radical on the

144

carbon in the thiocarbonate, regulating propagation of the polymer chain. As the radical

transfers to a polymer chain, a double bond reforms between the sulfur and carbon

(Figure 8.2). This interruption of the typical continuous radical polymerization

mechanism allows polymer chains to grow in a controlled manner leading to more

uniform chain growth and molecular weight (MW) distribution.[15] In a crosslinked

material, this control may be due to reduced crosslinking heterogeneities allowing more

homogeneous, less stressed networks to form.[3]
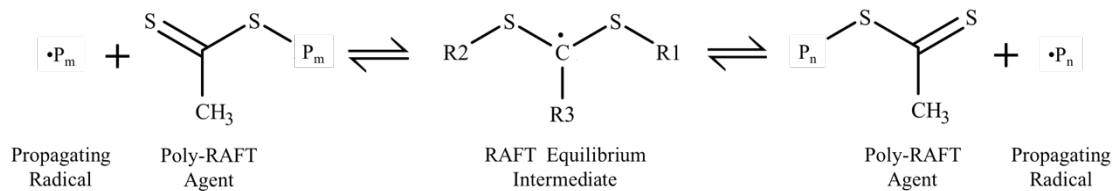
Figure 8.2. A simplified mechanism of the RAFT equilibrium reaction.

Some work has utilized RAFT agents to modify properties in photopolymerized

materials. Leung and Bowman examined the reduction in shrinkage stress by adding a

trithiocarbonate RAFT agent to methacrylate dental materials.[16] Utilizing a RAFT agent

in formulations allowed reduction in shrinkage stress in dental materials through network

rearrangement. In addition, delays in gelation and a slower polymerization rate were also

observed. Henkel and Vana examined the changes that RAFT-addition induces in loosely

crosslinked butyl- and ethyl- acrylate networks. Due to the RAFT agent modifying the

propagation reaction, increases in surface tackiness and elongation at break were

observed.[17,18] The increased tackiness was attributed to a reduction in the formation of

hard microgel domains on the surface of the acrylate formulations with increasing RAFT

concentration. Additionally, butyl acrylate systems polymerized with RAFT agents,

exhibit rate retardation and delayed gel point.

145

Urethane oligomer diacrylates are commonly used in photopolymer formulations due to their inherent toughness, which is attributed to the strong hydrogen bonds that occur between the urethane moieties within the oligomer chains.[19] Uses for these materials include paints, rubberized coatings, adhesives, and additive manufacturing processes such as 3D stereolithography. This work seeks to examine the impact RAFT agents have on relative reaction kinetics and thermomechanical properties of polyurethane diacrylate materials. Systems of urethane diacrylate were photopolymerized with a RAFT chain-transfer agent incorporated at varying concentrations. The effects of RAFT addition on the rate and conversion of the photopolymerization will be observed by Fourier transform infrared spectroscopy (FTIR). The effects on reaction kinetics and material properties of curing under a high-intensity UV-belt lamp system will also be examined. During photopolymerization the number of radicals generated is primarily a function of light intensity. By increasing light intensity observations of how larger radical concentrations interact with RAFT agents, to change material properties. Finally, temperature of glass transition (T_g), modulus, crosslink density, and stress-strain as a function of RAFT concentration will be investigated using dynamic mechanical analysis (DMA). The use of RAFT agents may be a facile method for modifying elastic network formation in a wide variety of materials

8.2: Experimental

8.2.1: Materials

CN-9002 (Sartomer), an aliphatic urethane diacrylate, was chosen as the model oligomer with 2,2-Dimethoxy-2-phenylacetophenone (DMPA, Ciba) was used as a photoinitiator (PI). Both were used as received. The RAFT agent, cyanomethyl dodecyl

146

trithiocarbonate, was prepared using the procedure outlined previously by Aoyagi and Endo.[20] The molar ratios of RAFT:PI are used to describe samples. PI concentration is 1 wt% with respect to the urethane diacrylate oligomer. Samples are also described by the RAFT:acrylate molar ratio.

<div align="center">8.2.2: Methods</div>

Samples for tensile and thermomechanical testing were prepared by placing samples between two microscope slides with a 220-micron spacer. The samples were then gently heated using a heat gun to reduce monomer viscosity, ensuring uniformity of the sample. The materials were cured under a 20 mW/cm^2 medium pressure mercury Omnicure 1500 lamp with collimating head for 30 min.

Polymerization kinetics of various formulations of RAFT agent and photoinitiator were measured by observing the double bond conversion and relative reaction rates using a Thermo-Nicolet Nexus 670 FTIR. Conversion was calculated using the relative C=O peak height of the acrylate group at 810 cm^{-1}.

A UV-belt lamp (Fusion Systems, LC-6B) was utilized to exam effects of high intensity light on the reaction kinetics and mechanical properties. Samples were photopolymerized using a medium pressure mercury bulb with intensity of 1500 mW/cm^2 at a belt speed of 3 in/min. Conversion was monitored between passes under the belt lamp, by comparing peak height ratios of the 810 cm^{-1} acrylate peak to the non-reacting 3400 cm^{-1} region. Dose rate was calculated based on 10 sec of light exposure for each pass.

Dynamic mechanical analysis experiments were performed with a TA Instruments Q800 dynamic mechanical analyzer (DMA) in tensile mode. Temperature sweeps were

performed from -100 to 50 °C at a heating rate of 3 °C/min to determine the T_g of the cured urethane films by recording Tan(δ) versus temperature. Stress and strain of films were evaluated at 30 °C with a force rate of 1.0 N/min. Young's modulus was determined by taking the initial slope of the linear portion of the stress/strain data.

8.3: Results

The addition of RAFT agents to photopolymer systems may allow modification of crosslink and network formation via the reversible chain-transfer mechanism. The chain-transfer will affect the kinetics of the polymerization reaction. With only small modifications to processing conditions and formulation, the modified reaction kinetics may allow materials with increased toughness. To this end, the polymerization kinetics and thermomechanical properties of films modified with varying concentrations of RAFT agent were examined. Additionally, formulations were polymerized at high and low light intensities to investigate the effects on increased radical concentration on polymerization kinetics.

The equilibrium step in the RAFT mechanism creates monodisperse molecular weights between crosslinks. However, this additional reversible chain transfer chain propagation reaction results in a slowing of polymerization propagation due to the additional reversible transfer of radical from RAFT agent back to propagating chain. To determine the effect of RAFT on the polymerization rate on urethane diacrylate systems, double bond conversion was measured using real-time FTIR (Figure 8.3).

148
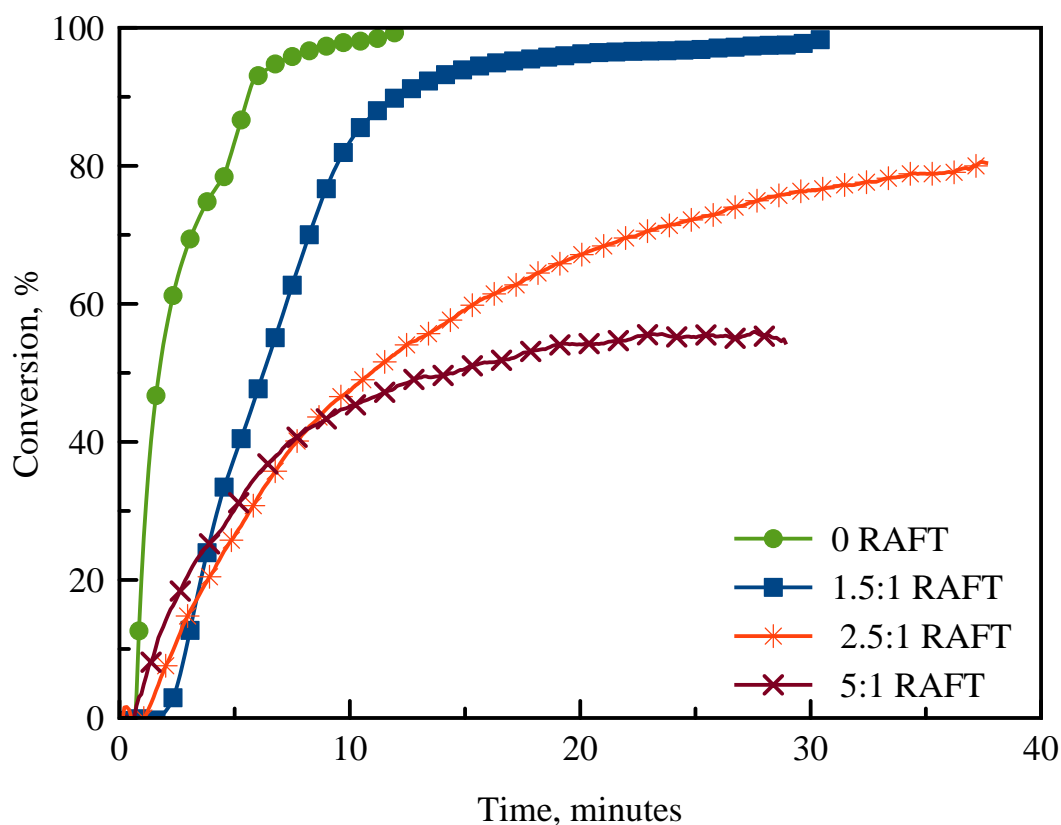
Figure 8.3. Conversion of urethane diacrylate films polymerized with (●) 0, (■) 1.5:1, (*) 2.5:1, and (x) 5:1 RAFT:PI molar ratio of cyanomethyl trithiocarbonate RAFT agent to DMPA photoinitiator. Polymerization was carried out with 10 mW/cm^2 at 365 nm light. Conversion was measured by comparing the peak height at 810cm^{-1} using FTIR.

Samples containing no RAFT exhibit a typical rapid photopolymerization behavior, with conversion approaching completion less than one min after light exposure. The decrease in slope of the conversion profile of formulations containing RAFT:PI concentrations of 1.5:1 indicate that polymerization rate is reduced with complete conversion now not reached around 10 min. Increases in RAFT concentration to 2.5:1 RAFT:PI induce a substantial decrease in conversion to roughly 80% after 40 min. Further increases in RAFT:PI ratio to 5:1 result in a relatively low rate of polymerization

and an apparent final conversion of approximately 50%. The amount of RAFT agent added is sufficient to nearly overwhelm the propagation of radicals and slows the reaction dramatically. Reductions in propagation rate are attributed to the significantly higher number of RAFT agent molecules which form reversible equilibrium products. Compared to formulations without RAFT this results in a lower rate of propagation.

Given the difference in reaction kinetics and conversion via RAFT-addition, it is reasonable to expect network formation of the films will also be different leading to different mechanical properties. To this end, the thermomechanical properties of the materials were examined via temperature sweeps with dynamic mechanical analysis (Figure 8.4). Rubbery modulus, glassy modulus, and T_g were observed for each formulation. Figure 8.4a shows Tan(δ) with respect to temperature for each RAFT composition. Interestingly, when RAFT agent is included in the formulation, T_g shifts roughly 4 ˚C higher, independent of RAFT concentration (Table 8.1).

The increase in T_g indicates that the RAFT agent is not having a plasticizing effect on the material, but appears to be affecting network morphology to some degree. In Figure 8.4b, the rubbery and glassy moduli are observed to follow similar trends as RAFT:PI ratio is increased. The rubbery modulus decreases and glassy modulus increases with RAFT concentration with the exception of the 5:1 RAFT:PI sample which exhibits more rubbery behavior due to lower conversion. Such changes in rubbery and glassy modulus are also consistent with reduced crosslink density in the networks and with
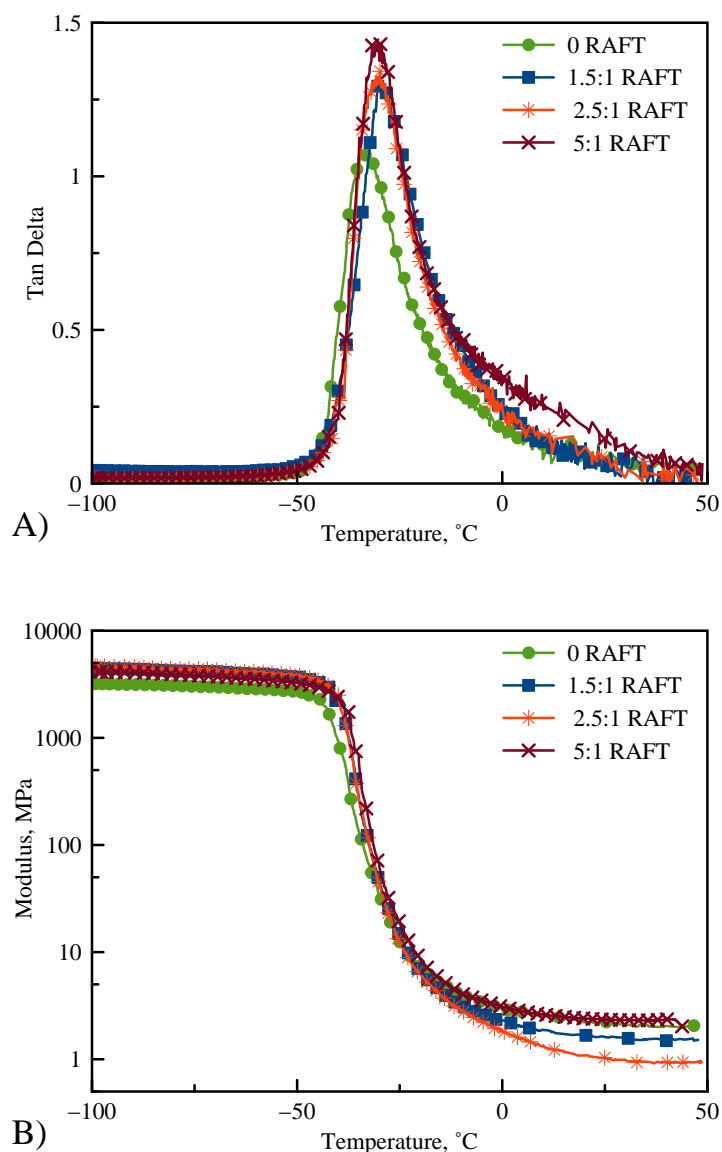
Figure 8.4. Tan(δ) a) and storage modulus b) profiles with respect to temperature for (●) 0, (■) 1.5:1, (*) 2.5:1, and (x) 5:1 RAFT:PI formulations. All samples were polymerized with 1% DMPA at 20 mW/cm^2 for 20 min.

composite theory[21]. If microgels act as hard composite particles within a polymer network, the reduction of such particles would be expected to reduce the overall modulus of a material and increase the elongation.[22]

151

This evidence of decreased rubbery modulus and shifting T_g suggest that the presence of a RAFT agent during photopolymerization decreases the crosslink density of the urethane materials. Differences in crosslink density with RAFT agents would be expected to influence mechanical properties of the urethane films, such as strain at break and Young's modulus. To determine the effect on these thermo-mechanical properties, stress-strain behavior was observed using dynamic mechanical analysis in tensile mode (Figure 8.5).

Figure 8.5. Stress-strain behavior at 30 ˚C of urethane diacrylate formulations (●) 0, (■) 1.5:1, (*) 2.5:1, and (x) 5:1 RAFT:PI. All samples were photopolymerized using 1% DMPA at 20 mW/cm^2 for 30 min.

Addition of 1.5:1 RAFT to the films reduces ultimate stress and modulus, but increases strain at break. Upon increasing the RAFT concentration to 2.5:1, ultimate stress remains roughly the same as the control without any RAFT control while strain roughly doubles. Films containing 5:1 RAFT exhibit a reduction in stress, but further increase elongation with a strain 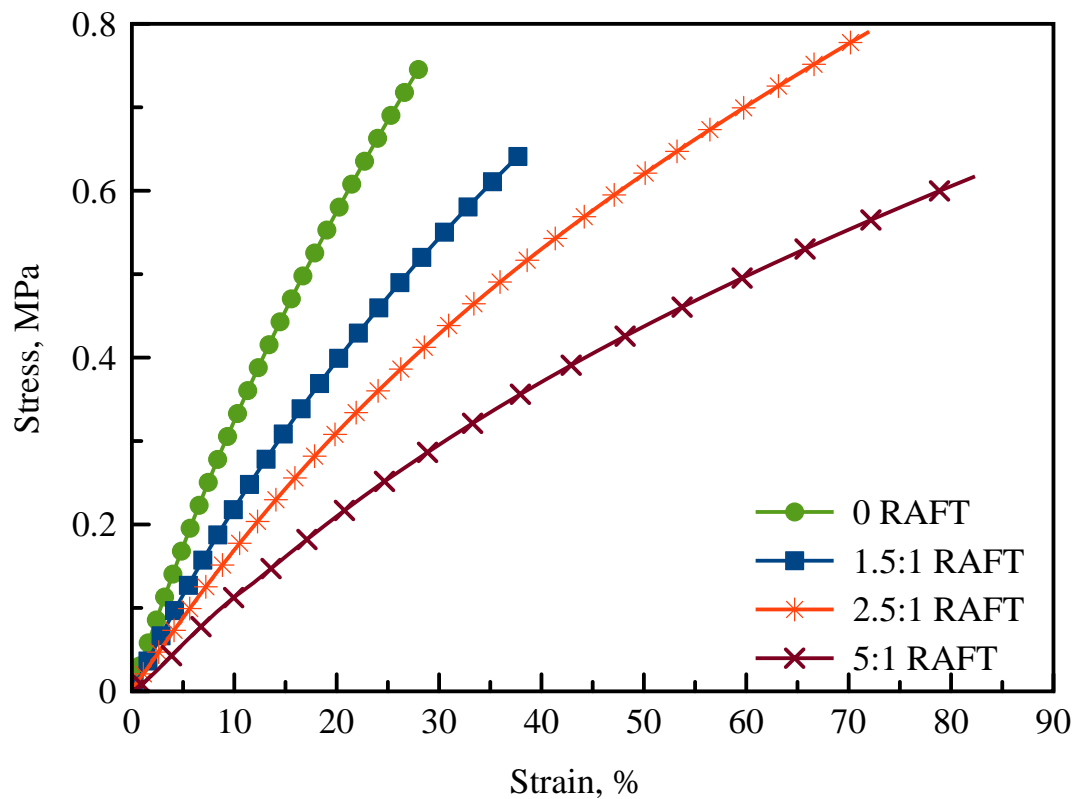at break of approximately 80% (Table 8.1). The increase in strain for all RAFT films is accompanied by a reduction of tensile modulus for the materials. The reduced Young's modulus of RAFT samples is further evidence of reduced crosslink density as, crosslink density is proportional to Young's modulus per Flory elastic theory.[23] This behavior further indicates that higher RAFT concentrations increase of network homogeneity by chain-transfer and increases the toughness of the films. Films containing 5:1 RAFT exhibit the largest increase in elongation, but toughness is limited by the significant decrease in ultimate stress and modulus. Interestingly, the addition of relatively small amounts of a simple chain-transfer agent allows significantly more elongation in these materials.

Most industrial photocuring processes utilize high-intensity UV-lamps to cure materials. Additionally, given the slower rate and lower conversion for RAFT- containing materials, increasing the dose rate of UV radiation using industrial cure lamps could reduce the overall cure time and increase ultimate double bond conversion. To examine the effects of high light intensity (1500 mW/cm^2) on conversion as a function of dose based on number of passes was observed for each formulation, materials were cured using a belt lamp system (Figure 8.6).

Upon polymerization of RAFT-containing materials with high-intensity light, conversion of acrylate bonds is observed to reach near completion for all formulations
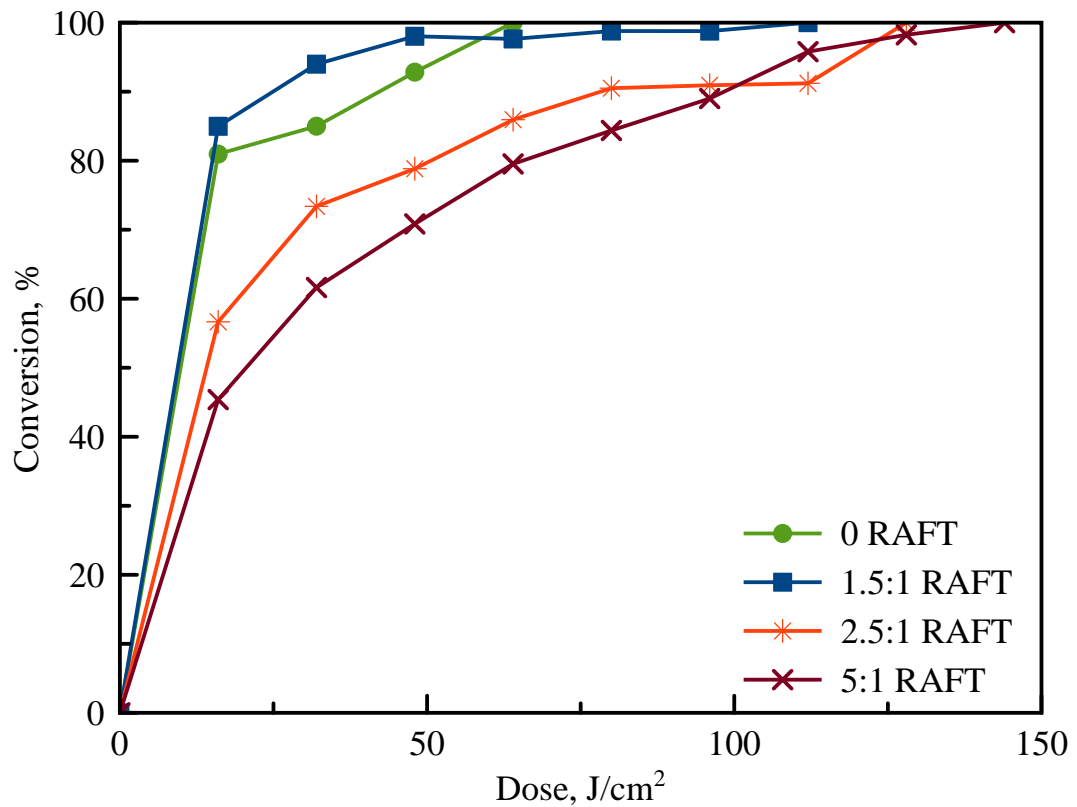
Figure 8.6. Conversion (%) of urethane diacrylate films polymerized with (●) 0, (■) 1.5:1, (*) 2.5:1, and (x) 5:1 RAFT:PI molar ratio of cyanomethyl trithiocarbonate RAFT agent to DMPA photoinitiator at 1500mW/cm^2 in stages on a belt lamp system operating at 3 ft/min.

tested, although more time is required for the high RAFT concentration materials as would be expected. The 1.5:1 RAFT formulation reaches complete conversion after 50 J/cm^2 or three passes under the belt lamp. Formulations containing 2.5:1 and 5:1 RAFT require approximately 125 J/cm^2 to reach full conversion. The increased conversion is likely due to the greater number of radicals formed by the initiator. The additional radicals may allow a greater number of active centers in the polymerization to proceed unchecked by the RAFT agent, resulting in more complete polymerization. Even with higher intensity light, the relative rates of polymerization still decrease upon the addition

154

of RAFT agents. However, the higher radiation dose rate of the belt lamp results in a much faster overall polymerization time with more complete conversion of the double bonds while mitigating the rate retardation associated with the RAFT mechanism.

The faster, more complete polymerization of RAFT films cured under high-intensity light may also influence the material properties. Stress-strain data was examined for samples cured under a high-intensity belt lamp using a DMA in tensile mode (Figure 8.7). Samples containing 1.5:1 RAFT increase in elongation, i.e strain at break and decrease slightly in ultimate stress compared to the 0 RAFT:PI control. Likewise, for 2.5:1 RAFT:PI samples ultimate stress showed further decreases and elongation increased Interestingly at 5:1 RAFT concentrations, the elongation doubles, with a decrease in ultimate stress observed. This shift is attributed to the high ratio of RAFT to acrylate. The abundance of RAFT modifies the rate at which the reaction propagates to such a degree that a loosely crosslinked network of oligomer chains forms, rather than a traditional crosslinked network. The 2.5:1 RAFT concentration appears to be a cut-off for the creation of traditional network structures, with further RAFT addition preventing sufficient crosslink density, resulting in the high flexibility properties of the 5:1 RAFT samples.

Interestingly, when Young's modulus of samples is compared between curing conditions, higher intensity light results in reduced modulus for RAFT containing formulations (Figure 8.8 and Table 8.1).

155
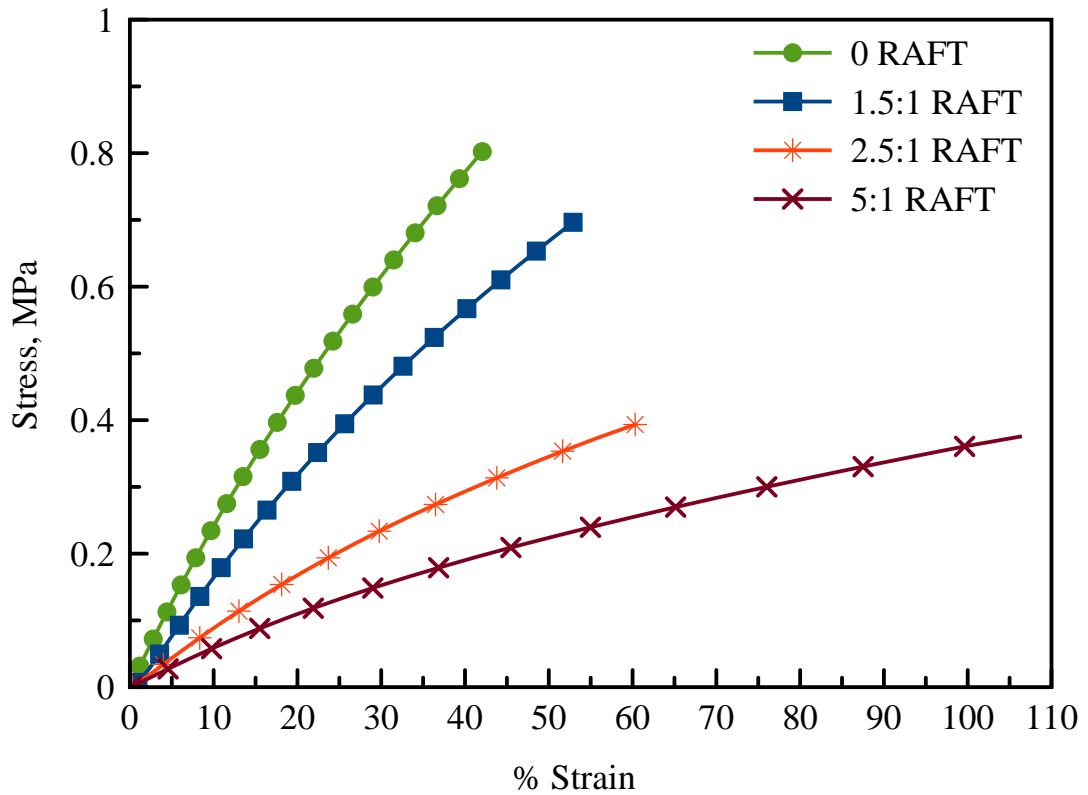
Figure 8.7. Stress-strain behavior at 30 ˚C of urethane diacrylate formulations with (●) 0, (■) 1.5:1, (*) 2.5:1, and (x) 5:1 RAFT:PI ratios of raft. All samples were photopolymerized using 1% DMPA at 1500mW/cm^2 in stages on a belt lamp system operating at 3 ft/min.

This decrease indicates a reduced crosslink density while still converting a high degree of acrylate bonds. The increased number of radicals from the high-intensity light combined with the chain-transfer rearrangement of RAFT results in a reduction of crosslinks in the network, increasing elongation and decreasing modulus.
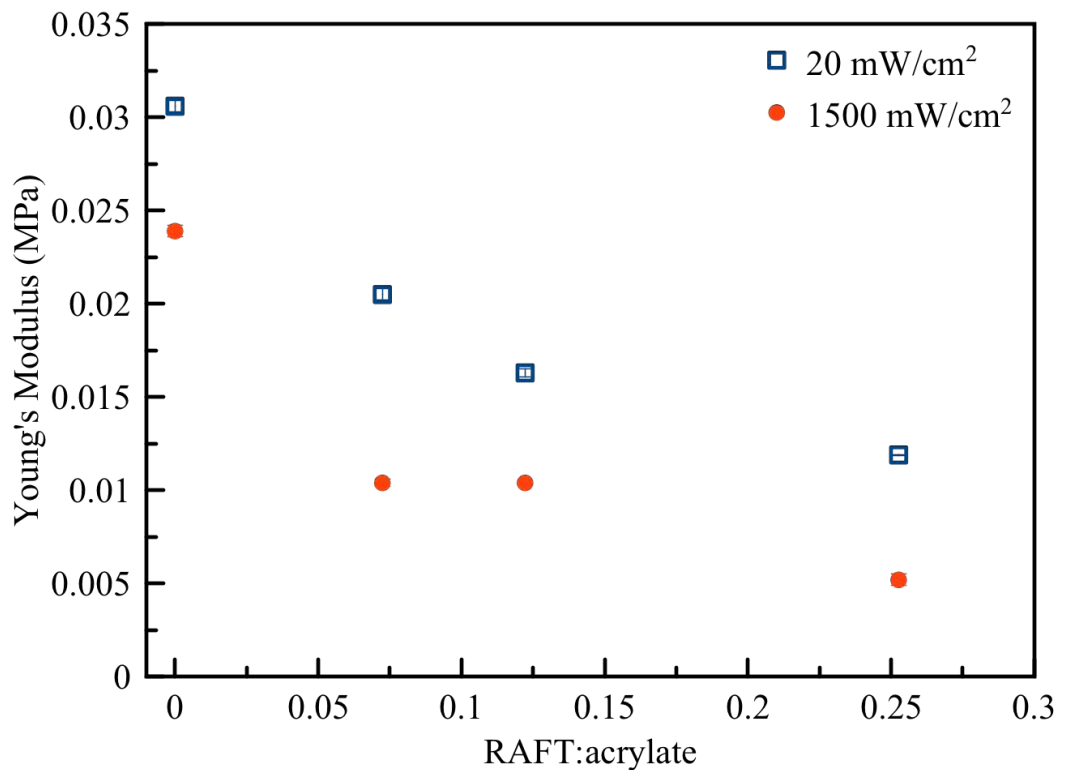
Figure 8.8. Young's modulus as a function of RAFT:Acrylate molar ratio for urethane diacrylate materials polymerized at 20 mW/cm^2 (□) and 1500 mW/cm^2 (●).

Material compositions based on RAFT:acrylate ratios are compared to Young's modulus to clarify the effects of the a high RAFT to double bond ratio. The low number of double bonds compared to moles of RAFT illustrates just how often a radical is likely to react with a RAFT agent. The reduction in modulus between 20 mW/cm^2 and 1500 mW/cm^2 increases with RAFT agent concentration, from a roughly constant 20% reduction for the lower two concentrations to 35% and then 50% for 0.125:1 and 0.25:1, respectively. This proportional reduction modulus is evidence of the controllable network propagation allowed by RAFT addition and of how this technique can be used to control properties in photopolymer materials. Rubbery elastic theory for polymers predicts a

157

Table 8.1. Summary of thermomechanical data for RAFT-modified urethane films.

RAFT:PI	T_g (˚C)	Ultimate Stress (%)	Toughness (MPa)	Young's Modulus 20 mW/cm^2 (MPa)	Young's Modulus 1500 mW/cm^2 (MPa)
0	-34.2 ± 1.0	29.6 ± 2.3	0.07 ± 0.1	0.0306 ± 0.0003	0.0239 ± 0.0003
1.5:1	-32 ± 2	36.4 ± 2.2	0.1 ± 0.01	0.0205 ± 0.0003	0.0104 ± 0.0002
2.5:1	-29.5 ± 0.5	68.6 ± 10.3	0.27 ± 0.07	0.0163 ± 0.0002	0.0104 ± 0.0001
5:1	-34.4 ± 0.3	81.7 ± 17.1	0.26 ± 0.12	0.01185 ± 0.00003	0.0052 ± 0.0003

reduced crosslink density for the observed lower tensile modulus (Young's).[24] The RAFT controlled polymerization reaction allows long loosely crosslinked oligomeric chains to form rather than a network of high crosslink density increasing elongation of the photopolymer system.

8.4: Conclusions

This work utilizes addition of RAFT agents in small amounts to control the elongation and toughness of urethane acrylate materials. The addition of the RAFT agent allows reversible chain-transfer during polymerization, slowing the reaction and creating a more elastic network by reducing crosslink density. The reversible chain transfer leads to increased network rearrangement, creating materials with increased elongation and lower modulus. RAFT modified systems containing 1.5:1 and 2.5:1 RAFT:PI molar ratios exhibit ultimate stress and strain values higher than the control, leading to

increased toughness albeit with a lower modulus. Materials with 5:1 RAFT:PI molar ratios exhibit greatly increased elongation, but with slow polymerization kinetics. By increasing radical concentrations, high-intensity lamps allow polymerization to proceed to high conversion at much lower polymerization times. The addition of RAFT agent to photopolymers allows control propagation of polymer chains via a reversible chain transfer mechanism. The modulus of polymers is reduced with increasing RAFT agent, indicating that crosslink density is decreasing. The technique allows increases in elongation through control of the polymer propagation with a RAFT agent. The ability of the RAFT chemistry to interact with a wide variety of monomers permits greater flexibility in the use of these agents as toughness modifiers in photopolymer systems.

(1)   Liska, R.; Schuster, M.; Infu, R.; Turecek, C.; Fritscher, C.; Seidl, B.; Schmidt, V.; Kuna, L.; Haase, A.; Varga, F.; et al. Photopolymers for Rapid Prototyping. **2007**, *4* (4), 505–510.

(2)   Ligon-Auer, S. C.; Schwentenwein, M.; Gorsche, C.; Stampfl, J.; Liska, R. Toughening of Photo-Curable Polymer Networks: A Review. *Polym. Chem.* **2016**, *7* (2), 257–286.

(3)   Gorsche, C.; Seidler, K.; Knaack, P.; Dorfinger, P.; Koch, T.; Stampfl, J.; Moszner, N.; Liska, R. Rapid Formation of Regulated Methacrylate Networks Yielding Tough Materials for Lithography-Based 3D Printing. *Polym. Chem.* **2016**, *7* (11), 2009–2014.

(4)   Park, H. Y.; Kloxin, C. J.; Fordney, M. F.; Bowman, C. N. Stress Relaxation of Trithiocarbonate-Dimethacrylate-Based Dental Composites. *Dent. Mater.* **2012**, *28* (8), 888–893.

(5)   Park, H. Y.; Kloxin, C. J.; Scott, T. F.; Bowman, C. N. Stress Relaxation by Addition-Fragmentation Chain Transfer in Highly Cross-Linked Thiol-Yne Networks. *Macromolecules* **2010**, *43* (24), 10188–10190.

(6)   Brazel, C. L.; Rosen, S. L. *Fundamental Principles of Polymeric Materials*; John Wiley & Sons, Inc.: Hoboken, New Jersey, 2012.

(7)   Anseth, K. S.; Wang, C. M.; Bowman, C. N. Kinetic Evidence of Reaction Diffusion during the Polymerization of Multi (Meth) Acrylate Monomers. **1994**, 650–655.

(8)   Yu, Q.; Zhu, Y.; Ding, Y.; Zhu, S. Reaction Behavior and Network Development in RAFT Radical Polymerization of Dimethacrylates. *Macromol. Chem. Phys.* **2008**, *209* (5), 551–556.

(9)   Hoyle, C. E.; Bowman, C. N. Thiol-Ene Click Chemistry. *Angew. Chem. Int. Ed. Engl.* **2010**, *49* (9), 1540–1573.

(10)   Gorsche, C.; Griesser, M.; Gescheidt, G.; Moszner, N.; Liska, R. β-Allyl Sulfones as Addition-Fragmentation Chain Transfer Reagents: A Tool for Adjusting Thermal and Mechanical Properties of Dimethacrylate Networks. *Macromolecules* **2014**, *47* (21), 7327–7336.

(11)   Moehrke, J.; Vana, P. The Kinetics of Surface-Initiated RAFT Polymerization of Butyl Acrylate Mediated by Trithiocarbonates. *1600506*, 1–11.

(12)   Hendrich, M.; Vana, P. Tuning the Mechanical Properties of Multiblock Copolymers Generated by Polyfunctional RAFT Agents. **2017**, *201700018*, 1–12.

(13)   Scherf, R.; Müller, L. S.; Grosch, D.; Hübner, E. G.; Oppermann, W. Investigation on the Homogeneity of PMMA Gels Synthesized via RAFT Polymerization. *Polym. (United Kingdom)* **2015**, *58*, 36–42.

(14)   Scholte, J. P.; Ki Kim, S.; Lester, C. L.; Guymon, C. A. Effects of Directed Architecture in Epoxy Functionalized Prepolymers for Photocurable Thin Films. *J. Polym. Sci. Part A Polym. Chem.* **2017**, *55* (1), 144–154.

(15)   Christopher Barner-Kowollik. *Handbook of RAFT Polymerization*; WILEY-VCH Verlag, 2008.

(16)   Leung, D.; Bowman, C. N. Reducing Shrinkage Stress of Dimethacrylate Networks by Reversible Addition-Fragmentation Chain Transfer. *Macromol. Chem. Phys.* **2012**, *213* (2), 198–204.

(17)   Henkel, R.; Vana, P. Increasing the Tackiness of Statistical poly(Butyl Acrylate) and poly(Ethyl Acrylate) Network Materials via RAFT Polymerization. *Macromol. Mater. Eng.* **2015**, *300* (5), 551–561.

(18)   Henkel, R.; Vana, P. The Influence of RAFT on the Microstructure and the Mechanical Properties of Photopolymerized Poly(butyl Acrylate) Networks. *Macromol. Chem. Phys.* **2014**, *215* (2), 182–189.

(19)   Ha, C.-S.; Jung, S.; Kim, E.-S.; Kim, W.; Lee, S.; Cho, W. Properties of UV-Curable Polyurethane Acrylates Using Nonyellowing Polyisocyanate. *J. Appl. Polym. Sci.* **1996**, *62*, 1011–1021.

(20)   Aoyagi, N.; Endo, T. Functional RAFT Agents for Radical-Controlled Polymerization : Quantitative Synthesis of Trithiocarbonates Containing Functional Groups as RAFT Agents Using Equivalent Amount of CS 2. *J. Polym. Sci. Part A Polym. Chem.* **2009**, *47*, 3702–3709.

(21)   Anseth, K. S.; Bowman, C. N. Kinetic Gelation Predictions of Species Aggregation in Tetrafunctional Monomer Polymerizations. *J. Polym. Sci. Part A Polym. Chem.* **1995**, *33*, 1769–1780.

(22)   Ahmed, S.; Jones, F. R. A Review of Particulate Reinforcing Theories for Polymer Composites. *J. Mater. Sci.* **1990**, *25* (12), 4933–4942.

(23)   Flory, P. J. Molecular Theory of Rubber Elasticity. *Polym. J.* **1985**, *17* (1), 1–12.

(24)   Nakanishi, E.; Hamada, K.; Sugiyama, E.; Hibi, S.; Hayashi, T. Estimation of Effective Crosslink Density in Poly(nhydroxyalkyl L Glutamine) Hydrogels.pdf. *Polym. J.* **1991**, *23* (9), 1503–1060.

9: CONCLUSIONS AND RECOMMENDATIONS

Controlling structure of polymeric materials at the nano- and microscale levels allows the manipulation of stimuli-responsive, swelling, elongation, and electrochemical properties, creating opportunities for a wide variety of applications. The ability to control this structure through understanding fundamental processes during polymerization permits polymer properties to be tailored. In this work, photopolymer material structure is modified by lyotropic liquid crystal (LLC) templating and reversible addition fragmentation chain transfer (RAFT).

Imparting structure to stimuli-responsive materials using LLC templates has induced increases in the kinetics and magnitude of stimuli-responsive transitions. The enhancement of thermoresponsive water expulsive properties is enabled by templating nanostructure within poly(*n*-isopropyl acrylamide)-co-sodium acrylate (PNIPAM-*co*-SA) hydrogels. Materials were templated in a bicontinuous mesophase, which exhibits efficient transport of water through interconnected pores and high degrees of swelling. LLC templated polymers are characterized by large dynamic ranges of thermoresponsive volume transition, up to eight times larger than their chemically identical isotropic counterparts. Isotropic materials exhibit increased swelling with higher SA loading, but do not display the large volumetric response after application of thermal energy.

As SA loading increases for templated materials, the observed LLC mesophase shifts from bicontinuous to hexagonal after polymerization. The structures become less complex and no longer retain the original template. This reduction in structure retention results in a decrease in the dynamic range of volumetric response. In LLC templated

162

materials loaded with 2% SA, dynamic ranges of 36 times dry mass are observed. With load levels of 4% SA, the range decreases to 32 times the dry mass.

Thermoresponse was reversible for all samples tested. Samples were swollen and deswollen to the same levels repeatedly over 24 h cycles. This reversibility shows promise for many applications seeking to use responsive hydrogels as actuators, switches, or valves. The addition of structure to PNIPAM-*co*-SA hydrogels allows high degrees of swelling with retention of the stimuli-responsive volume transition. This combination of characteristics creates materials that are capable of expelling very large amounts of water when exposed to elevated temperatures (50 ˚C).

These materials were also examined for use as forward osmosis (FO) draw agents. Flux of water through a semi-permeable membrane was shown to be greater for LLC templated materials and those containing superabsorbent SA. Flux increases for templated materials due to the interconnectivity of pore structures, allowing more effective transport of water through the hydrogel. Osmotic pressure was characterized for copolymer materials as a measure of their suitability for purifying salt water or other contaminated effluents. It was determined that the LLC templated structure did not change the osmotic pressure significantly, as the structure and not the chemistry is influenced by LLC templating. In conclusion, the increase in dynamic range and the much lower ratio level of water release at elevated temperatures indicate that there is promise for utilizing LLC templated materials as FO draw agents.

Polyoxyethylene alkyl ether surfactants have long been known to form LLC mesophases when mixed with water. As such, the materials are a logical choice for LLC templating processes. However, their availability in a wide range of head and tail lengths

163

has not been fully characterized or explored as a potential tool for expanding monomer compatibility or available mesophases. A system of nine polyoxyethylene alkyl ether surfactants was screened for mesophase behavior when mixed with water. Of those nine, eight were observed to form LLC mesophases. The surfactants exhibited a wide range of mesophase behaviors over the tested concentration ranges, suggesting that additional tailoring of surfactant and concentration may allow further control over polymer structure.

The non-ionic surfactants were then used as templates for NIPAM hydrogels. The differences in swelling between isotropic, isotropic surfactant templated, normal nanostructured, and inverse nanostructured templates were observed. In general, imparting nanostructure to hydrogels results in swelling increases of roughly three times that of the isotropic system. A polymer templated with surfactant that does not demonstrate LLC mesophase behavior swells to statistically the same ratio as an isotropic sample. Interestingly, LLC templating in the inverse mesophases does not increase the swelling of hydrogels. The discontinuous nature of inverse structure does not confer the interconnected system of nanostructured pores when templating a hydrophilic monomer.

Creating nanostructured polymers for electrochemical devices is another potential application for LLC templating. Increasing the internal surface area of capacitive materials in a controllable, consistent manner is a potential means to improve capacitor technology. LLC templating combined with photopolymerization is a method by which the structure of new and non-traditional capacitors can be explored. By LLC templating silicone diacrylates, it is possible to create capacitors from non-conductive materials. Specific capacitances for materials templated in the lamellar LLC mesophase are 0.27 F/g

164

and 0.60 F/cm^3, while isotropic materials are two orders of magnitude less capacitive with capacitances of 0.007 F/g and 0.0059 F/cm^3. The large amount of surface area generated by the templating process acts as a number of electric double layer capacitors. The nanostructured capacitances are not comparable to state of the art metal oxide or carbon composite capacitors. However, the ease of fabrication combined with the gentle electrolyte medium required for capacitance to occur could make these materials a valuable method for creating ordered nanostructure for electrochemical devices.

In Chapter 8, the modification of polymer propagation by RAFT agents is shown to affect the thermomechanical properties of a material. Through the reversible chain transfer mechanism of RAFT, the modified polymer network reduces material modulus and increases elongation and thus, toughness, to over three times that of control samples. These changes are attributed to lower crosslink density as evidenced by the reduction in modulus. Due to the exceedingly large number of RAFT molecules compared to functional acrylates, increases in molecular weight of chains between crosslinks are suspected. By increasing radical concentration during polymerization with high intensity light, RAFT-modified materials reach near total conversion. By adding small amounts of RAFT agent, polymer toughness can be augmented. This simple addition could allow the increased application of photopolymer materials.

Using the fundamentals explored in this work, control of material structure can be extended to different material classes. The exploration of new materials and applications will offer challenges to explore with LLC templating and photopolymerization fundamentals. Through this expansion, a greater body of understanding and control will be realized for structuring processes.

Previous LLC templating endeavors have focused on hydrophilic, soft photopolymer materials. Many photopolymer materials that are hydrophobic or are high modulus with low elongation exist. Expanding the use of LLC templating to more durable materials could have interesting applications in the energy storage, catalyst, and composite fields. Successful LLC templating of hydrophobic materials requires the use of inverse mesophases. As was shown in Chapter 6, polymerization in the discontinuous domain of an LLC material does not allow the same benefits in material properties as templating in the continuous domain. It follows that this will hold true for hydrophobic materials as well. Templating in the inverse mesophase generally requires higher surfactant loads than in normal mesophases.

Silicone surfactants may offer an attractive method of templating hydrophobic monomers in a continuous (inverse) mesophase. Surfactants have been demonstrated which exhibit hexagonal, lamellar, and even bicontinuous mesophases.[1] Additionally, the flexible silicone tail allows fluidity of mixtures to be maintained at the high surfactant concentrations required to form LLC mesophases. Templating polymer pre-ceramics is a possible application of silicone surfactants. Pre-ceramic polymers typically consist of a silicone backbone monomer polymerized using either free radical acrylate-based or thiol-ene polymerizations.[2,3] After polymerization, the materials are sintered at high temperatures to convert the silicone polymer into a ceramic material. Photopolymerization of silicone monomers has been used with success in 3D printing complex ceramic materials. Silicone surfactants could permit LLC templating of a wide variety of pre-ceramic silicone monomers. Combining pre-ceramic monomers with LLC templated materials could allow for nanostructured ceramics to be created. Such materials

could find applications in high performance catalysts and electronics due to high surface area and diffusion. Additionally, nanostructured ceramics could find application in the creation of insulating materials due to low density and low thermal conductivity.[4]

The large amount of stimuli-response volume transition observed previously for templated copolymers of PNIPAM and SA indicates that imparting structure may still have an important role to play in FO research. Since the templated nanostructure does not appear to greatly affect osmotic pressure, future LLC templating FO research should focus on utilizing materials with extremely high osmotic pressures. Work should improve stimuli-response of high osmotic pressure materials through surfactant templated nanostructure and copolymerization. The combination of these traits may result in crosslinked FO draw agents for use in many water purification and stream concentration applications.

Polymerizable ionic liquids (PIL) or molten salts are materials which have very low volatility due to the high molecular affinity of their ionic character. These materials have been examined for use in FO applications due to their high osmotic pressures. Work on 'smart' PILs has been carried out with tributyl-4-vinylbenzylphosphonium (TVBP)-based IL monomers and poly(propylene glycol) diacrylate (PPG) and poly(ethylene glycol) diacrylate (PEG) as crosslinkers.[5] These materials were demonstrated to induce flux against brackish salt water and upon application of warm temperatures release water. However, deswelling rates were low. Improvements to both swelling ratios and response kinetics could be realized with LLC templating techniques.

Mixtures of a PIL, surfactant, and water have been reported to display LLC mesophases of the columnar, bicontinuous, and lamellar types.[6,7] The synthesis of

167

nanostructured PILs using these materials should be straightforward, only requiring the addition of a photoinitiator and perhaps modification of the reactive bond of the PIL. Additionally, ionic liquids dissolved in supercritical CO_2 (sCO_2) have been observed to self-assemble into micro- and nanostructures. The combination of a polymerizable ionic liquid and a photoinitiator into sCO_2 could allow for a new avenue of 'solventless' LLC templating. After polymerization, the system is depressurized, leaving only the templated PIL behind.

As was demonstrated in Chapter 7, the nanostructure imparted by LLC templating shows promise for utilization in electrochemical devices. The ordered nanostructure within LLC templated polymer lends itself well to applications where high permeability is desirable. Battery separators are one such application. Separators function within batteries or fuel cells as a type of membrane. The separator must allow the efficient transport of charge and separate the conductive components of the device physically.[8] High temperature stability and a large resistance to voltage breakdown are additional requirements. Polyethylene is a common separator material due to its low cost and ease of pore fabrication in the films. The use of LLC templating could be extended to other photopolymerized films, especially silicone materials, where high electrical impedance and resistance to voltage breakdown make them an attractive separator.[9]

Continuing work on capacitive materials could focus on creating LLC structured carbon composites. The high porosity of carbon nanomaterials can be combined with LLC templating to create composites with ordered carbon particles intercalated within the templated polymer. Pseudocapacitance exhibited by a polymer material may be combined

168

with carbon nanomaterials, allowing for improvement in the very promising use of carbon nanomaterials as capacitors.[10]

Chapter 8 details the modifications in elongation and toughness that occur during photopolymerization in the presence of a RAFT agent. However, only a low-modulus elastomer was modified. Another direction would modify the network formation of a high-modulus or glassy polymer. If the network can be homogenized to permit increased elongation and toughness, a new avenue to toughen photocured materials can be developed. This may be especially useful in high functionality urethane-acrylate systems used for many 3D printing applications. RAFT techniques may create additional improvements to 3D printing, such as better interlayer adhesion. RAFT agents can induce longer radical lifetimes and increase the conversion percentage at which gelation occurs.[11] Combining these changes could allow for higher rates of monomer and reactive center migration between printed layers, thus improving the mechanical properties of the print-as-a-whole.

Due to their thiol or xanthate base, RAFT agents are often heavily pigmented. For colored or opaque systems, this is typically not an issue. In transparent photopolymer systems, this natural pigmentation could present a complication. Exploration of non-colored RAFT agents, such as 2-(dodecylthiocarbonothioylthio)-2-methylpropionic acid pentafluorophenyl ester, would eliminate this concern.

In conclusion, the work here demonstrates the power of manipulating and understanding polymer structure on different size scales. Changes in polymer properties, including toughness, stimuli-response, and capacitance, are all modified by imparting different structure to prepolymer mixtures combined with photopolymerization. LLC

templating, with proper consideration of monomer and surfactant compatibility, can be extended to a much greater range of monomers and systems. Similarly, the simple addition of only a few weight percent of RAFT agent can be easily applied to many systems in which greater control of network homogeneity is desired. Due to the flexibility of these techniques, applications utilizing structural modifications of polymers is virtually unlimited.

References

(1)   Uddin, M. H.; Yamashita, Y.; Furukawa, H.; Harashima, A.; Kunieda, H. Phase Behavior of Poly (Oxyethylene)-Poly (Dimethylsiloxane) Surfactant (Copolymer) with Water or Silicone Oil. *Trends Colloid …* **2004**, *123*, 269–274.

(2)   Eckel, Z. C.; Zhou, C.; Martin, J. H.; Jacobsen, A. J.; Carter, W. B.; Schaedler, T. A. Additive Manufacturing of Polymer-Derived Ceramics. *Science (80-.).* **2015**, *351* (6268), 58–62.

(3)   Bernardo, E.; Fiocco, L.; Parcianello, G.; Storti, E.; Colombo, P. Advanced Ceramics from Preceramic Polymers Modified at the Nano-Scale: A Review. *Materials (Basel).* **2014**, *7* (3), 1927–1956.

(4)   Hsueh, H.; Ho, R. Bicontinuous Ceramics with High Surface Area from Block Copolymer Templates. **2012**.

(5)   Fan, X.; Liu, H.; Gao, Y.; Zou, Z.; Craig, V. S. J.; Zhang, G. Forward-Osmosis Desalination with Poly (Ionic Liquid) Hydrogels as Smart Draw Agents. **2016**, 1–6.

(6)   Lester, C. L.; Guymon, C. A. Phase Behavior and Polymerization Kinetics of a Semifluorinated Lyotropic Liquid Crystal. *Macromolecules* **2000**, *33* (15), 5448–5454.

(7)   Zhang, J.; Peng, L.; Han, B. Amphiphile Self-Assemblies in Supercritical CO2 and Ionic Liquids. *Soft Matter* **2014**, *10* (32), 5861.

(8)   Darling, R.; Gallagher, K.; Xie, W.; Su, L.; Brushett, F. Transport Property Requirements for Flow Battery Separators. *J. Electrochem. Soc.* **2016**, *163* (1), A5029–A5040.

(9)   Ferrão, P.; Fournier, J.; Lacarrière, B.; Corre, O. Le. Epoxy/Silicone Rubber Blends for Voltage Insulators and Capacitors Applications. *Energy Procedia* **2017**, *119*, 501–506.

(10)   Simon, P.; Burke, A. Nanostructured Carbons: Double-Layer Capacitance and More. *Electrochem. Soc. Interface* **2008**, *17* (1), 38–43.

(11)   Park, H. Y.; Kloxin, C. J.; Scott, T. F.; Bowman, C. N. Stress Relaxation by Addition-Fragmentation Chain Transfer in Highly Cross-Linked Thiol-Yne Networks. *Macromolecules* **2010**, *43* (24), 10188–10190.

A: Swelling Ratio of PEGDA Hydrogels with Various Polyoxyethylene Alkyl Ether
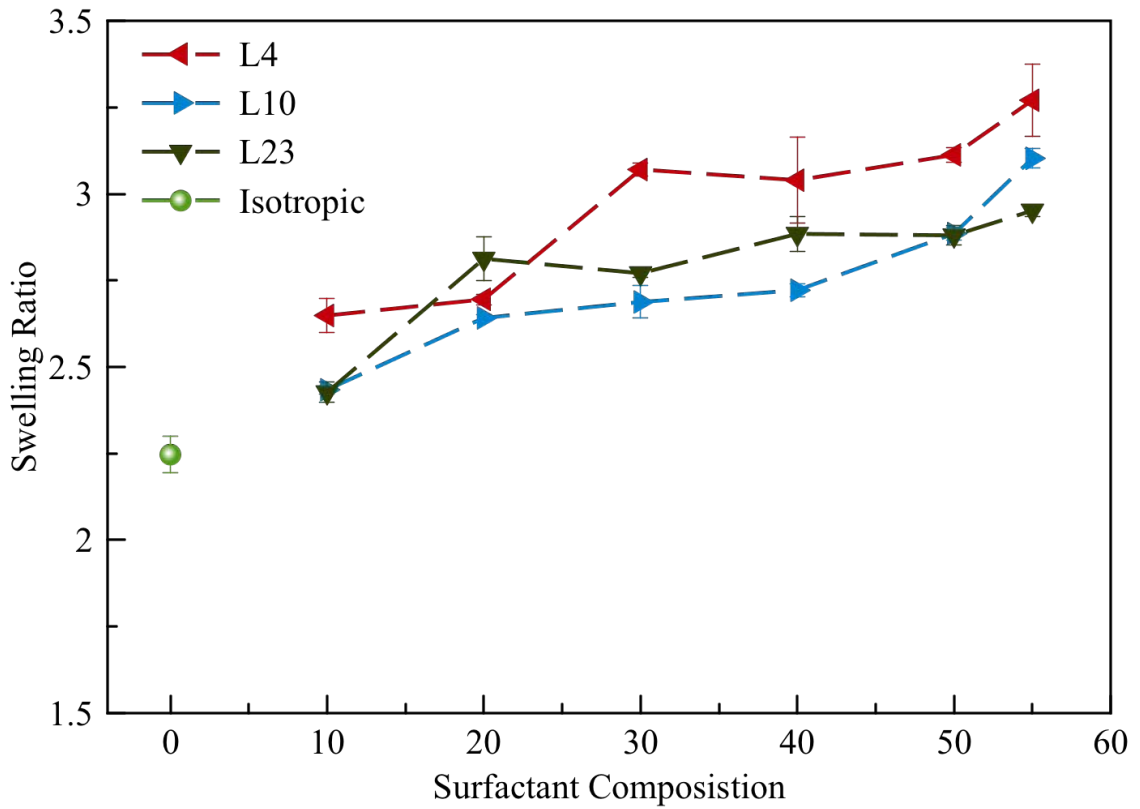
Surfactants.

Figure A.1. Swelling ratios of hydrated 40% polyethylene glycol diacrylate hydrogel samples at various surfactant concentrations. The isotropic sample (◉) is shown as a reference. Shown are: L4 (◀) L10 (▶), L23 (▼). Samples were cured at 10 mW/cm^2 for 10 min with 1% weight DMPA photoinitiator.

Figure A.2. Swelling ratios of hydrated 40% polyethylene glycol diacrylate hydrogel samples at various surfactant concentrations. The isotropic sample (⊙) is shown as a reference. Shown are: C2 (■), C10 (●), and C20 (◆). Samples were cured at 10 mW/cm^2 for 10 min with 1% weight DMPA photoinitiator.
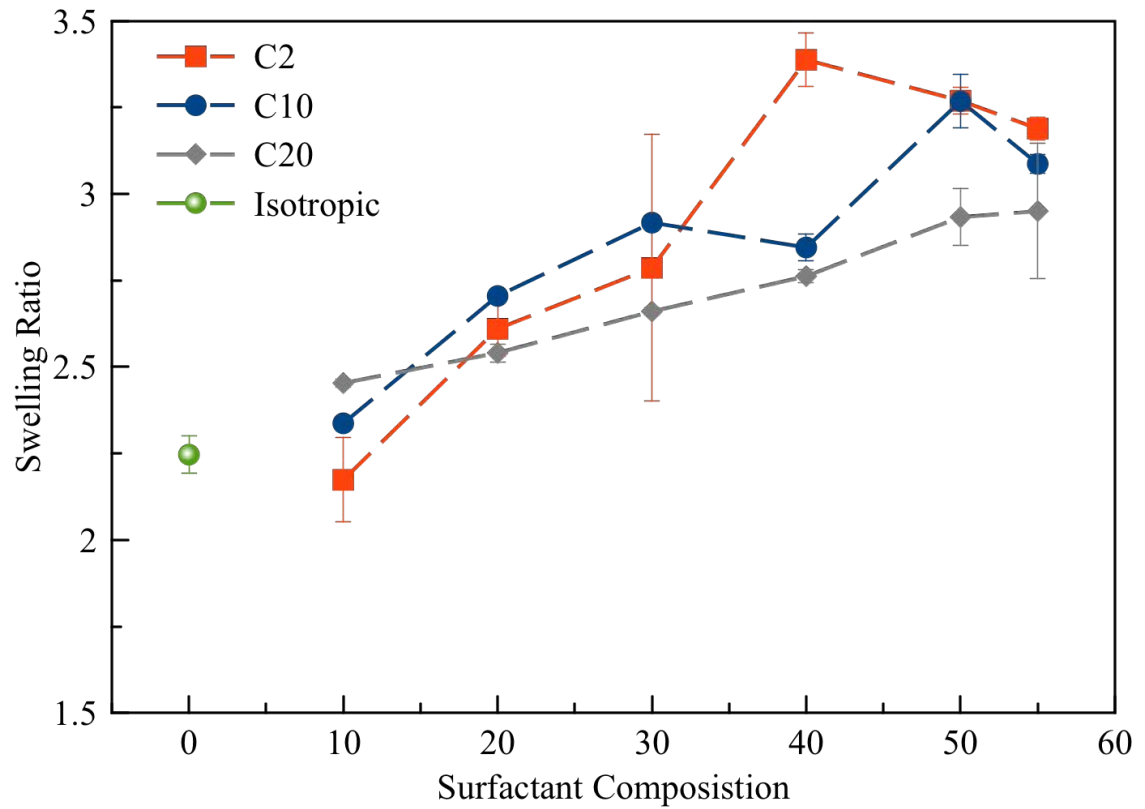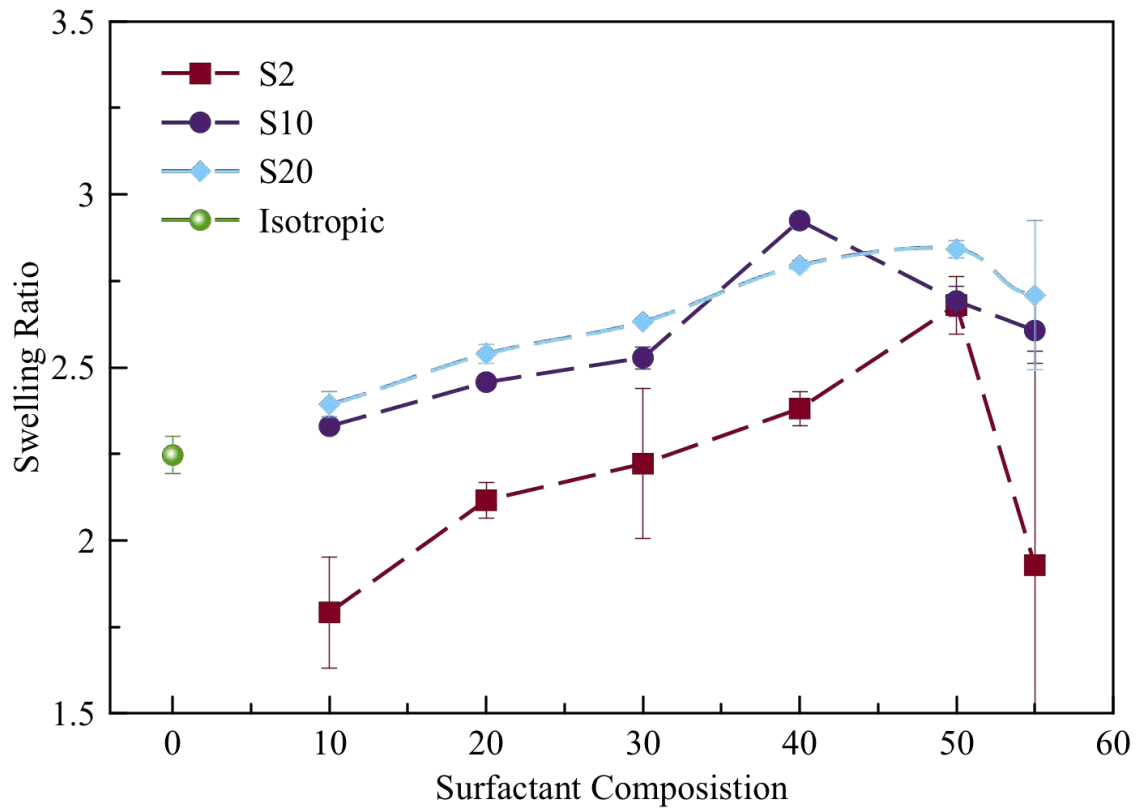
Figure A.3 Swelling ratios of hydrated 40% polyethylene glycol diacrylate hydrogel samples at various surfactant concentrations. The isotropic sample (⊙) is shown as a reference. Shown are: S2 (■), S10 (●), and S20 (◆). Samples were cured at 10 mW/cm^2 for 10 min with 1% weight DMPA photoinitiator.

Figure B.1. Analysis of current versus voltage scan rate in silicone films. The slope is equal to capacitance (F). A linear curve was fit to the lower three scan rates of a) isotropic silicone and b) templated silicone.

Figure B.3. Voltammograms of (a) isotropic and (b) templated PEGDA at various scan rates. Note the difference in scale bars on the y-axis.
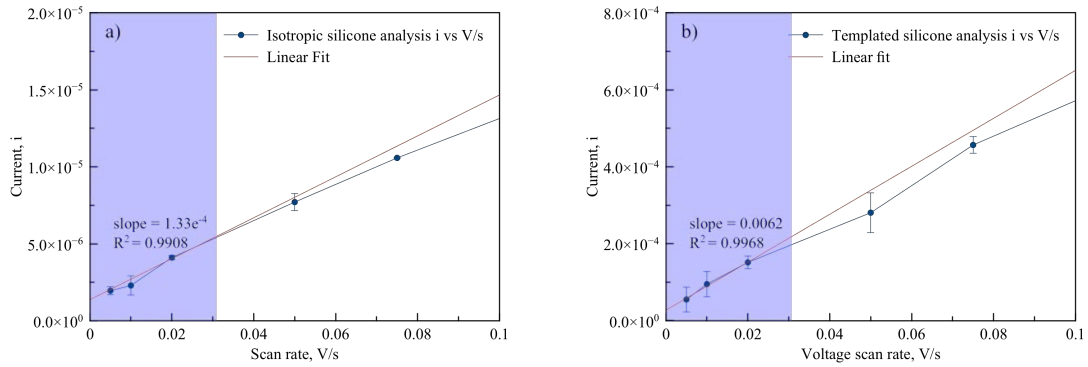
Figure B.4. Analysis of current versus voltage scan rate in silicone films. The slope is equal to capacitance (F). A linear curve was fit to the lower three scan rates of a) isotropic PEGDA and b) templated PEGDA.

Figure B.5. Capacitance observed as a function of scan rate for (•) templated PEGDA
and (□) isotropic PEGDA. Samples of 40% PEGDA were templated with Brij C10,
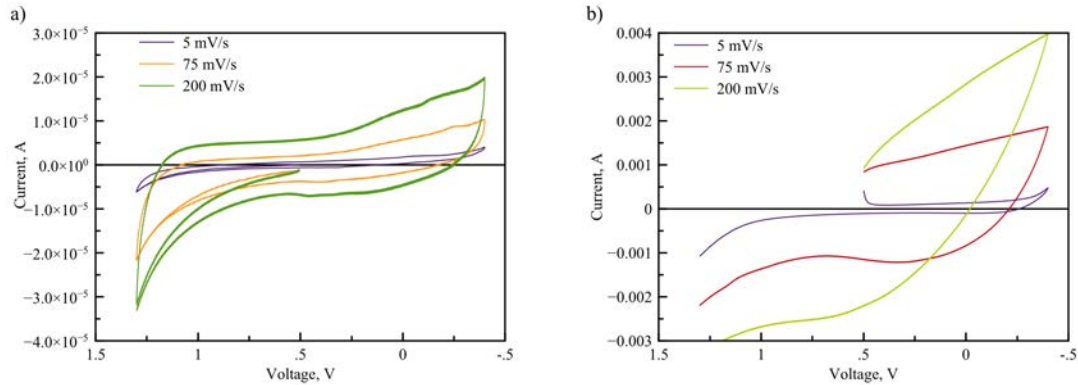with 1% DMPA photoinitiator.

Figure B.6. Voltammograms of (a) isotropic and (b) templated PNIPAM at various scan rates. Note the difference in scale bars on the y-axis.
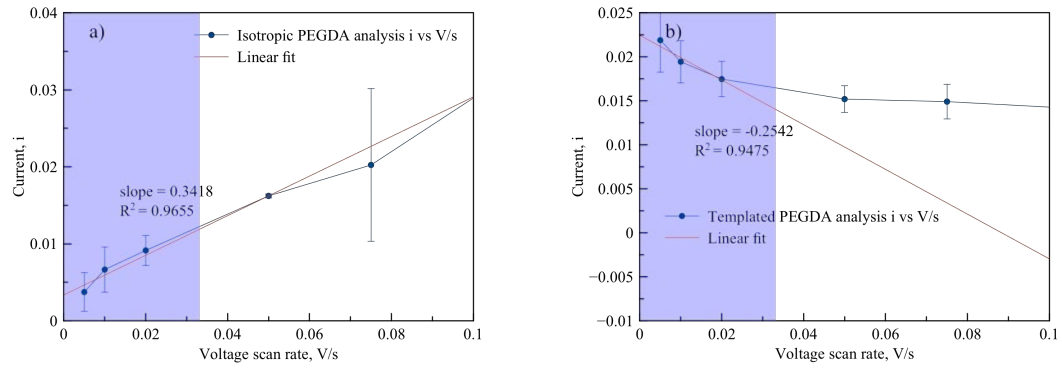

Figure B.7. Analysis of current versus voltage scan rate in silicone films. The slope is equal to capacitance (F). A linear curve was fit to the lower three scan rates of a) isotropic PNIPAM and b) templated PNIPAM.
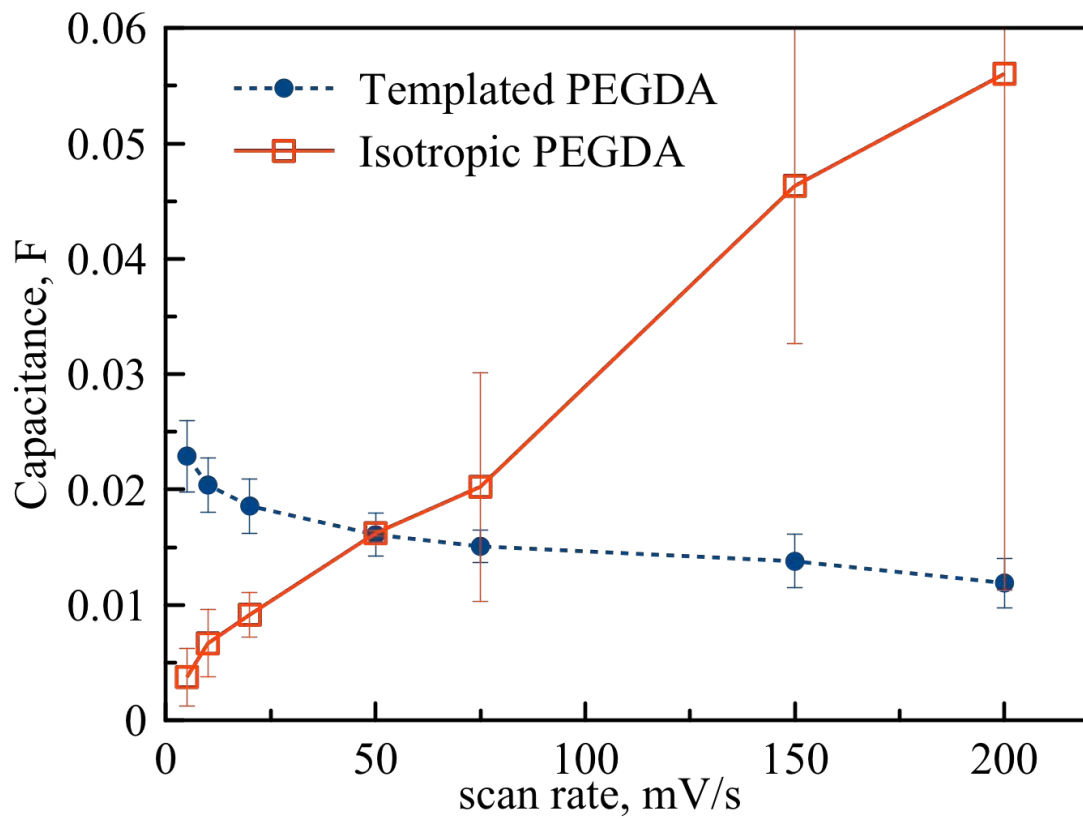
Figure B.8. Capacitance observed as a function of scan rate for (•) templated PNIPAM and (□) isotropic PNIPAM. Samples of 20% PNIPAM were templated with Brij C2, 1% DMPA photoinitiator and 1% MBA as a crosslinker.
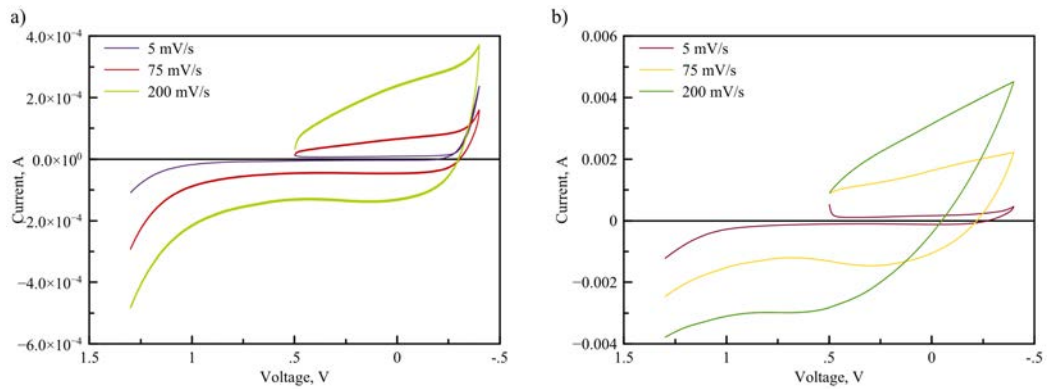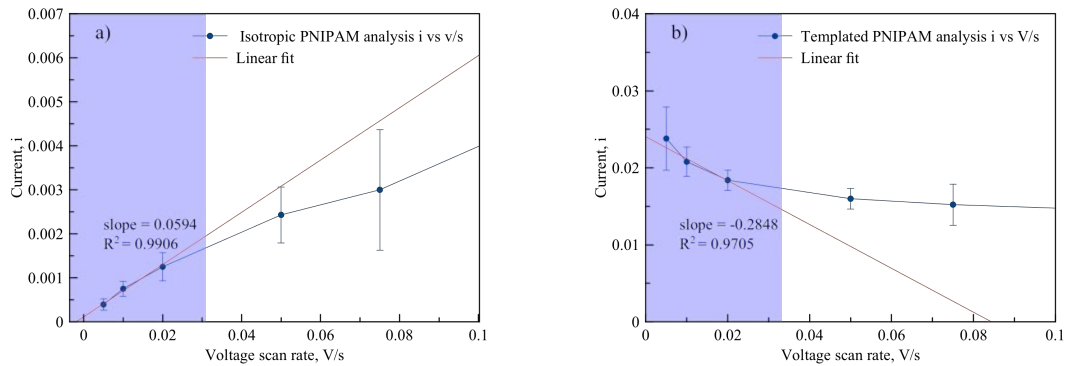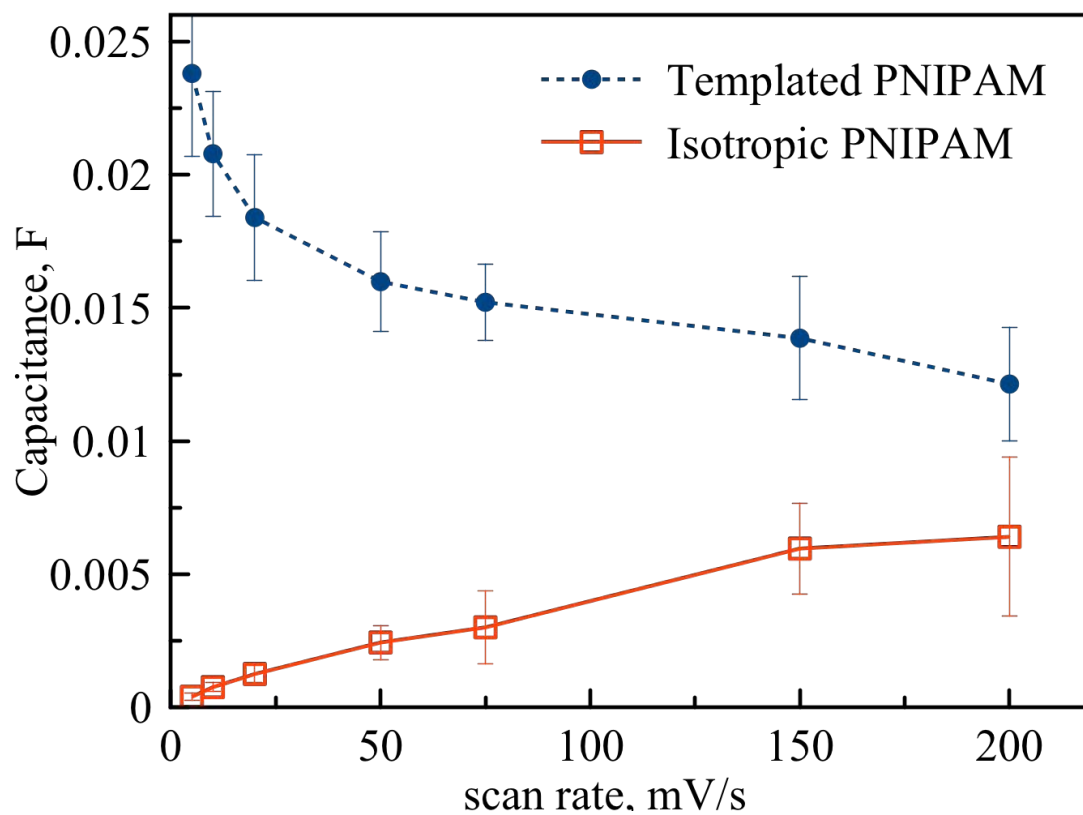
BIBLIOGRAPHY

Ahmed, S., & Jones, F. R. (1990). *Journal of Materials Science, 25*(12), 4933–4942.

Ahn, S., Kasi, R. M., Kim, S.-C., Sharma, N., & Zhou, Y. (2008). *Soft Matter*, *4*(6), 1151–1157.

Amar-yuli, I., Wachtel, E., Shoshan, E. Ben, Danino, D., Aserin, A., & Garti, N. (2007), (12), 3637–3645.

Anseth, K. S., & Bowman, C. N. (1995). *Journal of Polymer Science Part A: Polymer Chemistry*, *33*, 1769–1780.

Anseth, K. S., Bowman, C. N., & Brannon-Peppas, L. (1996). *Biomaterials*, *17*(17), 1647–1657.

Anseth, K. S., Wang, C. M., & Bowman, C. N. (1994), 650–655.

Aoyagi, N., & Endo, T. (2009). *Journal of Polymer Science Part A: Polymer Chemistry*, *47*, 3702–3709.

Bäcker, M., Raue, M., Schusser, S., Jeitner, C., Breuer, L., Wagner, P., Poghossian, A., Förster, A., Mang, T., Schöning, M. J. (2012). *Physica Status Solidi (A) Applications and Materials Science*, *209*(5), 839–845.

Baguenard, C., & Guymon, C. A. (2013). *Angewandte Chemie International Edition*, *52*(34), 8789–8789.

Barón, M. (2001). *Pure and Applied Chemistry*, *73*(5), 845–895.

Bernardo, E., Fiocco, L., Parcianello, G., Storti, E., & Colombo, P. (2014). *Materials*, *7*(3), 1927–1956.

Brannon-Peppas, L., & Harland, R. S. (1990). (L. Brannon-Peppas & R. S. Harland, Eds.) (1st ed.). Amsterdam: Elsevier Inc.

Brazel, C. L., & Rosen, S. L. (2012). Hoboken, New Jersey: John Wiley & Sons, Inc.

Brigo, L., Urciuolo, A., Giulitti, S., Della Giustina, G., Tromayer, M., Liska, R., Elvassore, N., Brusatin, G (2017). *Acta Biomaterialia*, *55*, 373–384.

Buchholz, F. L., & Graham, A. T. (1997). (F. L. Buchholz & A. T. Graham, Eds.) (1st ed.). New York: WILEY-VCH Verlag.

Buck, M. E., & Lynn, D. M. (2012). *Polymer Chemistry*, *3*(1), 66.

Cai, Y., & Hu, X. M. (2016). *Desalination*, *391*, 16–29.

Cai, Y., Shen, W., Loo, S. L., Krantz, W. B., Wang, R., Fane, A. G., & Hu, X. (2013). *Water Research*, *47*(11), 3773–3781.

Cai, Y., Shen, W., Wang, R., Krantz, W. B., Fane, A. G., & Hu, X. (2013). *Chemical Communications (Cambridge, England)*, *49*(75), 8377–8379.

Calvert, P. (1992). *Materials Research Society Bulletin*, (October), 37–40.

Carmignani, G., Sitkiewitz, S., & Webley, J. W. (2012). *US Patent 20120267308 A1*. United States.

Carter, B. M., Wiesenauer, B. R., Noble, R. D., & Gin, D. L. (2014). *Journal of Membrane Science*, *455*, 143–151.

Cath, T. Y., Childress, A. E., & Elimelech, M. (2006), *281*, 70–87.

Chen, Z., Greaves, T. L., Fong, C., Caruso, R. a, & Drummond, C. J. (2012). *Phys. Chem. Chem. Phys.*, *14*(11), 3825–3836.

Christopher Barner-Kowollik. (2008). WILEY-VCH Verlag.

Clapper, J. D., & Guymon, C. A. (2007a). *Macromolecules*, *40*(22), 7951–7959.

Clapper, J. D., & Guymon, C. A. (2007b). *Macromolecules*, *40*(4), 1101–1107.

Clapper, J. D., Iverson, S. L., & Guymon, C. A. (2007). *Biomacromolecules*, *8*(7), 2104–2111.

Clapper, J. D., Sievens-Figueroa, L., & Guymon, C. A. (2008). *Chemistry of Materials*, *20*(3), 768–781.

Coday, B. D., Xu, P., Beaudry, E. G., Herron, J., Lampi, K., Hancock, N. T., & Cath, T. Y. (2014). *Desalination*, *333*(1), 23–35.

Darling, R., Gallagher, K., Xie, W., Su, L., & Brushett, F. (2016). *Journal of The Electrochemical Society*, *163*(1), A5029–A5040.

DePierro, M. A., Baguenard, C., & Guymon, C. A. (2016). *Polymer Chemistry*, *54*, 144–154.

DePierro, M. A., Carpenter, K. G., & Guymon, C. A. (2006). *Chemistry of Materials*, *18*(23), 5609–5617.

Depierro, M. A., & Guymon, C. A. (2014). *Macromolecules*, *47*, 5728–5738.

DePierro, M. a., & Guymon, C. A. (2006). *Macromolecules*, *39*(2), 617–626.

181

Desai, a., Varade, D., Mata, J., Aswal, V., & Bahadur, P. (2005). *Colloids and Surfaces A: Physicochemical and Engineering Aspects*, *259*(1–3), 111–115.

Detcheverry, A., Kang, H., Daoulas, K. C., Müller, M., Nealey, P. F., & Pablo, J. J. De. (2008), 4989–5001.

Dieng, M. a. (2005). *Bautechnik*, *82*(1), 28–32.

Eckel, Z. C., Zhou, C., Martin, J. H., Jacobsen, A. J., Carter, W. B., & Schaedler, T. A. (2015). *Science*, *351*(6268), 58–62.

Eibel, A., Radebner, J., Haas, M.; Fast, D. E., Faschauner, P., Torvisco, A., Lamparth, I., Moszner, N., Stueger, H., Gescheidt, G. (2017). *Polymer Chemistry*, *submitted*.

Eichenbaum, G. M., Kiser, P. F., Simon, S. A., & Needham, D. (1998). *Macromolecules*, *31*, 5084–5093.

Fan, X., Liu, H., Gao, Y., Zou, Z., Craig, V. S. J., & Zhang, G. (2016), 1–6.

Ferrão, P., Fournier, J., Lacarrière, B., & Corre, O. Le. (2017). *Energy Procedia*, *119*, 501–506.

Flory, P. J. (1985). *Polymer Journal*, *17*(1), 1–12.

Flory, P. J., & Rehner, J. (1943). *The Journal of Chemical Physics*, *11*(11), 521–526.

Fontell, K., Hernqvist, L., Larsson, K. R. E., & Sjoblom, J. (1983). *Journal of Colloid And Interface Science*, *93*(2), 453–460.

Forney, B. S., Baguenard, C., & Guymon, C. A. (2013a). *Chemistry of Materials*, *25*(15), 2950–2960.

Forney, B. S., Baguenard, C., & Guymon, C. A. (2013b). *Soft Matter*, *9*(31), 7458–7467.

Forney, B. S., & Guymon, C. A. (2010). *Macromolecules*, *43*(20), 8502–8510.

Forney, B. S., & Guymon, C. A. (2011). *Macromolecular Rapid Communications*, *32*(9–10), 765–769.

Fouassier, Jean-Pierre, Lalevée, J. (2012) Wiley ACH Verlag, Weinheim, Germany.

Frazer, J. C. W., & Myrick, R. T. (1916). *J. Am. Chem. Soc.*, *XXXVIII*(10).

Friberg, S. E., Thundathil, R., & Stoffer, J. O. (1979). *Science*, *205*(4406), 607–608.

Garrey, W. E. (1905). *Biological Bulletin*, *8*(4), 257–270.

Gin, D. L., Bara, J. E., Noble, R. D., & Elliott, B. J. (2008). *Macromolecular Rapid Communications*, *29*(5), 367–389.

Gliveli, D. E., Davis, S. S., & Kayes, J. B. (1983). *Journal of Colloid And Interface Science*, *91*(1), 1–11.

Gody, G., Barbey, R., Danial, M., & Perrier, S. (2015). *Polym. Chem.*, *6*(9), 1502–1511.

Gorsche, C., Griesser, M., Gescheidt, G., Moszner, N., & Liska, R. (2014). *Macromolecules*, *47*(21), 7327–7336.

Gorsche, C., Seidler, K., Knaack, P., Dorfinger, P., Koch, T., Stampfl, J., … Liska, R. (2016). *Polym. Chem.*, *7*(11), 2009–2014.

Graca, M., Bongaerts, J. H. H., Stokes, J. R., & Granick, S. (2009). *Journal of Colloid and Interface Science*, *333*(2), 628–634.

Granik, V. T., Smith, B. R., Lee, S. C., & Ferrari, M. (2002). *Biomedical Microdevices*, *4*(4), 309–321.

Griffin, W. C. (1954). *Journal of the Society of Cosmetic Chemists*, 249–256.

Ha, C.-S., Jung, S., Kim, E.-S., Kim, W., Lee, S., & Cho, W. (1996). *Journal of Applied Polymer Science*, *62*, 1011–1021.

Han, I. S., Han, M.-H. H., Kim, J., Lew, S., Lee, Y. J., Horkay, F., & Magda, J. J. (2002). *Biomacromolecules*, *3*(6), 1271–1275.

Hendrich, M., & Vana, P. (2017), *201700018*, 1–12.

Henkel, R., & Vana, P. (2014). *Macromolecular Chemistry and Physics*, *215*(2), 182–189.

Henkel, R., & Vana, P. (2015). *Macromolecular Materials and Engineering*, *300*(5), 551–561.

Hertle, Y., Zeiser, M., Hasenöhrl, C., Busch, P., & Hellweg, T. (2010). *Colloid and Polymer Science*, *288*(10–11), 1047–1059.

Hinton, T. J., Hudson, A., Pusch, K., Lee, A., & Feinberg, A. W. (2016). *ACS Biomaterials Science and Engineering*, *2*(10), 1781–1786.

Horkay, F., Tasaki, I., & Basser, P. J. (2000). *Biomacromolecules*, *1*(1), 84–90.

Hoyle, C. E., & Bowman, C. N. (2010). *Angewandte Chemie (International Ed. in English)*, *49*(9), 1540–1573.

Hsueh, H., & Ho, R. (2012).

Hu, X., Li, G., & Yu, J. C. (2010). *Langmuir*, *26*(5), 3031–3039.

Huang, H., Zhang, D., Mao, Z., Yu, W., & Yan, H. (2008). *Journal of Applied Polymer*

183

Science, *112*, 123–128.

Huang, K.-L., Sigeta, K., & Kunieda, H. (1998). *Progress in Colloid Polymer Science*, *110*, 171–174.

Hull, C. W. (1973). United States: United States.

Husár, B., Ligon, S. C., Wutzel, H., Hoffmann, H., & Liska, R. (2014). *Progress in Organic Coatings*, *77*(11), 1789–1798.

Hyde, S. T. (2001). In K. Holmberg (Ed.), *Handbook of Applied Surface and Colloid Chemistry* (pp. 299–332). John Wiley & Sons, Inc.

Ii, C. (2015). *Water-Based Chemicals and Technology for Drilling, Completion, and Workover Fluids*.

Ijeri, V. S., Nair, J. R., Gerbaldi, C., Gonnelli, R. S., Bodoardo, S., & Bongiovanni, R. M. (2010). *Soft Matter*, *6*(19), 4666.

Illeperuma, W. R. K., Sun, J.-Y., Suo, Z., & Vlassak, J. J. (2013). *Soft Matter*, *9*(35), 8504–8511.

Inoue, K., & Hoshino, S. (1976). *Journal of Polymer Science*, *14*(8), 1513–1526.

Ishikawa, S., Matsumura, Y., Katoh-Kubo, K., & Tsuchido, T. (2002). *Journal of Applied Microbiology*, *93*(2), 302–309.

Jang, J. H., Kato, A., Machida, K., & Naoi, K. (2006), 321–328.

Janovák, L., Varga, J., Kemény, L., & Dékány, I. (2008). *Colloid and Polymer Science*, *286*(14–15), 1575–1585.

Jiangtao, X., Sivaprakash, S., Nathaniel Alan, C., & Cyrille, B. (2015). *Controlled Radical Polymerization: Mechanisms*, *1187*(1187), 247–267.

Jiao, B., Cassano, A., & Drioli, E. (2004). *Journal of Food Engineering*, *63*, 303–324.

Kaufhold, S., & Dohrmann, R. (2008). *Clays and Clay Minerals*, *56*(6), 686–692.

Kim, S. K., & Guymon, C. A. (2012). *Polymer*, *53*(8), 1640–1650.

Kunieda, H., Uddin, M. H., Horri, M., Furukawa, H., & Harashima, A. (2001). *Journal of Physical Chemistry B*, *105*(23), 5419–5426.

Lalevée, J., Dietlin, C., Morlet-Savary, F., Fouassier, J. P., Dumur, F., Gigmes, D., & Garra, P. (2017). *Polymer Chemistry*.

Landh, T. (1994). *The Journal of Physical Chemistry*, *98*(34), 8453–8467.

Lee, T. Y., Guymon, C. A., Jönsson, E. S., & Hoyle, C. E. (2004). *Polymer*, *45*(18), 6155–6162.

Lee, Y. S. (2008). *Self-Assembly and Nanotechnology: A Force Balance Approach*, 75–101.

Leferink op Reinink, a. B. G. M., Pol, E., Petukhov, a. V., Vroege, G. J., & Lekkerkerker, H. N. W. (2013). *The European Physical Journal Special Topics*, *222*(11), 3053–3069.

Lester, C. L., Colson, C. D., & Guymon, C. A. (2001). *Macromolecules*, *34*(13), 4430–4438.

Lester, C. L., & Guymon, C. A. (2000). *Macromolecules*, *33*(15), 5448–5454.

Lester, C. L., Smith, S. M., Jarrett, W. L., & Guymon, C. A. (2003). *Langmuir*, *19*(22), 9466–9472.

Leung, D., & Bowman, C. N. (2012). *Macromolecular Chemistry and Physics*, *213*(2), 198–204.

Lewis, G. N. (1908). *J. Am. Chem. Soc.*, *30*(5), 668–683.

Li, D., & Wang, H. (2013). *Journal of Materials Chemistry A*, *1*(45), 14049–14060.

Li, D., Zhang, X., Yao, J., Simon, G. P., & Wang, H. (2011, February). *Chemical Communications*.

Li, D., Zhang, X., Yao, J., Zeng, Y., Simon, G. P., & Wang, H. (2011). *Soft Matter*, *7*(21), 10048.

Ligon-Auer, S. C., Schwentenwein, M., Gorsche, C., Stampfl, J., & Liska, R. (2016). *Polym. Chem.*, *7*(2), 257–286.

Liska, R., Schuster, M., Infu, R., Turecek, C., Fritscher, C., Seidl, B., … Stampfl, J. (2007), *4*(4), 505–510.

Liu, F., & Urban, M. W. (2010). *Progress in Polymer Science (Oxford)*, *35*, 3–23.

Liu, H. Y., & Zhu, X. X. (1999), *40*, 6985–6990.

Liu, J., Rad, I. Y., Sun, F., & Stansbury, J. W. (2014). *Polymer Chemistry*, *5*(1), 227–233.

Liu, J., & Stansbury, J. W. (2014). *Dental Materials*, *30*(11), 1252–1262.

Liu, J., Teo, W. K., Chew, C. H., & Gan, L. M. (2000). *Journal of Applied Polymer Science*, *77*(12), 2785–2794.

Lu, L., Yang, N., & Cai, Y. (2005), 5287–5288.

185

Manek, E., Tombácz, E., Geissler, E., & László, K. (2017). *Periodica Polytechnica Chemical Engineering*, *61*(1), 39–50.

Manna, U., Broderick, A. H., & Lynn, D. M. (2012). *Advanced Materials (Deerfield Beach, Fla.)*, *24*(31), 4291–4295.

Martyniak, A., Dilger, H., McKenzie, I., Scheuermann, R., Lagerwall, J., & Roduner, E. (2007). *Colloids and Surfaces A: Physicochemical and Engineering Aspects*, *309*(1–3), 224–230.

McCutcheon, J. R., McGinnis, R. L., & Elimelech, M. (2006). *Journal of Membrane Science*, *278*(1–2), 114–123.

McGinnis, R. L., & Elimelech, M. (2007). *Desalination*, *207*(1–3), 370–382.

Mclaughlin, J. R., Abbott, N. L., & Guymon, C. A. (2018). *Polymer*.

Mendez, S., Andrzejewski, B. P., Canavan, H. E., Keller, D. J., Mccoy, J. D., Lopez, G. P., & Curro, J. G. (2009). *Langmuir*, *25*(18), 10624–10632.

Michel, B. E., & Kaufmann, M. R. (1973). *Plant Physiology*, *51*(5), 914–916.

Mir, S. H., & Ochiai, B. (2018). *Journal of The Electrochemical Society*, *165*(8), B3030–B3034.

Moad, G. (2015). *Acs Symposium Series*, 211–246.

Moehrke, J., & Vana, P. (n.d.), *1600506*, 1–11.

Mohan, Y. M., Premkumar, T., Joseph, D. K., & Geckeler, K. E. (2007), *67*, 844–858.

Mondal, S., & Wickramasinghe, S. R. (2012). *Separation and Purification Technology*, *90*, 231–238.

Money, N. P. (1989). *Plant Physiology*, *91*, 766–769.

Muzzalupo, R., Tavano, L., Rossi, C. O., Cassano, R., Trombino, S., & Picci, N. (2009). *Langmuir : The ACS Journal of Surfaces and Colloids*, *25*(3), 1800–1806.

Nagarajan, R. (2002). *Langmuir*, *18*(1), 31–38.

Nair, D. P., Chatani, S., Berg, G., & Bowman, C. N. (2014).

Nakanishi, E., Hamada, K., Sugiyama, E., Hibi, S., & Hayashi, T. (1991). *Polymer Journal*, *23*(9), 1503–1060.

Nakata, K., Tsuchido, T., & Matsumura, Y. (2011). *Journal of Applied Microbiology*, *110*(2), 568–579.

186

Nandy, D., Mitra, R. K., & Paul, B. K. (2007). *Journal of Colloid and Interface Science*, *310*(1), 229–239.

Ni, C., & Zhu, X.-X. X. (2004). *European Polymer Journal*, *40*(6), 1075–1080.

Odian, G. (2004) (4th ed.). Hoboken, New Jersey: John Wiley & Sons, Inc.

Park, H. Y., Kloxin, C. J., Fordney, M. F., & Bowman, C. N. (2012). *Dental Materials*, *28*(8), 888–893.

Park, H. Y., Kloxin, C. J., Scott, T. F., & Bowman, C. N. (2010). *Macromolecules*, *43*(24), 10188–10190.

Parsegian, V. A., Rand, R. P., Fuller, N. L., & Rau, D. D. (1986). *Methods in Enzymology*, *127*, 400–416.

Pelton, R. (2010). *Journal of Colloid and Interface Science*, *348*(2), 673–674.

Raman, V. I., & Palmese, G. R. (2005). *Langmuir : The ACS Journal of Surfaces and Colloids*, *21*(4), 1539–1546.

Razmjou, A., Barati, M. R., Simon, G. P., Suzuki, K., & Wang, H. (2013). *Environmental Science & Technology*, *47*(12), 6297–6305.

Razmjou, A., Simon, G. P., & Wang, H. (2013). *Chemical Engineering Journal*, *215–216*, 913–920.

Reddy, S. K., Cramer, N. B., O' Brien, A. K., Cross, T., Raj, R., & Bowman, C. N. (2004). *Macromolecular Symposia*, *206*(1), 361–374.

Rodriguez, C., Uddin, M. H., Watanabe, K., Furukawa, H., Harashima, a, & Kunieda, H. (2002). *Journal of Physical Chemistry B*, *106*, 22–29.

Rossi, G., Fuchs, P. F. J., Barnoud, J., & Monticelli, L. (2012). *The Journal of Physical Chemistry. B*, *116*(49), 14353–14362.

Roy, D., Cambre, J. N., & Sumerlin, B. S. (2010). *Progress in Polymer Science*, *35*(1–2), 278–301.

Sasaki, S., Okabe, S., & Miyahara, Y. (2010). *Journal of Physical Chemistry B*, *114*, 14995–15002.

Scherf, R., Müller, L. S., Grosch, D., Hübner, E. G., & Oppermann, W. (2015). *Polymer (United Kingdom)*, *58*, 36–42.

Schnablegger, H., & Singh, Y. (2011) (2nd ed.). Graz, Austria: Anton Paar GmbH.

Scholte, J. P., Ki Kim, S., Lester, C. L., & Guymon, C. A. (2017). *Journal of Polymer Science Part A: Polymer Chemistry*, *55*(1), 144–154.

Schulze, M. W., McIntosh, L. D., Hillmyer, M. A., & Lodge, T. P. (2014). *Nano Letters*, *14*(1), 122–126.

Seisyan, R. P. (2011). *Technical Physics*, *56*(8), 1061–1073.

Shah, P. K., Stasbury, J. W., & Bowman, C. N. (2017). *Polymer Chemistry*, *8*(30), 4339–4351.

Shanmugam, S., Xu, J., & Boyer, C. (2016). *Macromolecules*, acs.macromol.6b02060.

Shi, L., Wu, X., Lu, L., Yang, X., & Wang, X. (2009). *The Journal of Physical Chemistry B*, *113*(9), 2725–2733.

Shiyanovskii, S. V., Lavrentovich, O. D., Schneider, T., Ishikawa, T., Smalyukh, I. I., Woolverton, C. J., … Doane, K. J. (2005). *Molecular Crystals and Liquid Crystals*, *434*, 587–598.

Sievens-Figueroa, L., & Guymon, C. A. (2009). *Chemistry of Materials*, *21*(6), 1060–1068.

Simon, P., & Burke, A. (2008). *Electrochemical Society Interface*, *17*(1), 38–43.

Sorenson, G. P., Coppage, K. L., & Mahanthappa, M. K. (2011). *Journal of the American Chemical Society*, *133*(38), 14928–14931.

Sotiropoulou, S., Sierra-Sastre, Y., Mark, S. S., & Batt, C. A. (2008). *Chemistry of Materials*, *20*(3), 821–834.

Storey, N. (2006) (3rd ed.). Prentice Hall.

Sun, X., Shi, J., Zhang, Z., & Cao, S. (2011). *Journal of Applied Polymer Sciencea*, *122*, 729–737.

Telitel, S., Telitel, S., Bosson, J., Lalevée, J., Clément, J.-L., Godfroy, M., … Soppera, O. (2015). *Langmuir*, *31*(36), 10026–10036.

Thompson, N. A., & Nicoll, P. G. (2011). In *IDA World Congress* (pp. 1–16).

Thorson, T. (2013). University of Iowa.

Tumbleston, J. R., Shirvanyants, D., Ermoshkin, N., Janusziewicz, R., Johnson, a. R., Kelly, D., … DeSimone, J. M. (2015). *Science*, *347*(6228), 1349–1352.

Tumbleston, J. R., Shirvanyants, D., Ermoshkin, N., Johnson, A. R., Kelly, D., Chen, K., … Joseph, M. (2015), (March), 1–7.

Uddin, M. H., Morales, D., & Kunieda, H. (2005). *Journal of Colloid and Interface Science*, *285*(1), 373–381.

Uddin, M. H., Yamashita, Y., Furukawa, H., Harashima, A., & Kunieda, H. (2004). *Trends in Colloid and …*, *123*, 269–274.

UNICEF, & World Health Organization. (2015).

Vink, H. (1971). *European Polymer Journal*, *7*(2), 1411–1419.

Wang, H., Wei, J., & Simon, G. P. (2014). *Environmental Science & Technology*, *48*, 4214–4215.

Wang, R., Luo, Y., Li, B., & Zhu, S. (2009). *Macromolecules*, (42), 85–94.

Wei, J., Low, Z. X., Ou, R., Simon, G. P., & Wang, H. (2016). *Water Research*, *96*, 292–298.

Williams, G., Hunt, M., Boehm, B., May, A., Taverne, M., Ho, D., … Ladak, S. (2017). *Nano Research*, *11*(2), 1–10.

Wood, M. R., Duncalf, D. J., & Rannard, S. P. (2006). *Organic Letters.* (2006). *8*(4), 553-556.

Worthington, K. S., Baguenard, C., Forney, B. S., & Guymon, C. A. (2017). *Journal of Polymer Science Part B: Polymer Physics*, *55*(6), 471–489.

Worthington, K. S., Green, B. J., Rethwisch, M., Wiley, L. A., Tucker, B. A., Guymon, C. A., & Salem, A. K. (2016). *Biomacromolecules*, *17*, 1684–1695.

Worthington, K. S., Wiley, L. A., Kaalberg, E. E., Collins, M. M., Mullins, R. F., Stone, E. M., & Tucker, B. A. (2017). *Acta Biomaterialia*, *55*, 385–395.

Xie, Z., Yu, W., Wang, T., Zhang, H., Fu, Y., Liu, H., … Sun, Q. (2011). *Plasmonics*, *6*(3), 565–580.

Xiong, P., Zhu, J., & Wang, X. (2015). *Journal of Power Sources*, *294*, 31–50.

Xu, Y., Gu, W., & Gin, D. L. (2004). *Journal of the American Chemical Society*, *126*(6), 1616–1617.

Yan, J., Wang, Q., Wei, T., & Fan, Z. (2014). *Advanced Energy Materials*, *4*(4).

Yang, H., Liang, F., Chen, Y., Wang, Q., Qu, X., & Yang, Z. (2015). *NPG Asia Materials*, *7*(4), e176-6.

Yang, S., Park, K., & Rocca, J. G. (2004). *Journal of Bioactive and Compatible Polymers*, *19*(2), 81–100.

Ye, S., Cramer, N. B., & Bowman, C. N. (2011). *Macromolecules*, *44*, 490–494.

Yu, G., Xie, X., Pan, L., Bao, Z., & Cui, Y. (2013). *Nano Energy*, *2*(2), 213–234.

Yu, Q., Zhu, Y., Ding, Y., & Zhu, S. (2008). *Macromolecular Chemistry and Physics*, *209*(5), 551–556.

Zabara, A., Negrini, R., Onaca-Fischer, O., & Mezzenga, R. (2013). *Small (Weinheim an Der Bergstrasse, Germany)*, (21), 3602–3609.

Zeng, F., & Tong, Z. (1997). *Polymer*, *38*(22), 5539–5544.

Zhang, H., & Cooper, A. I. (2007). *Advanced Materials*, *19*(18), 2439–2444.

Zhang, H., Li, J., Cui, H., Li, H., & Yang, F. (2015). *Chemical Engineering Journal*, *259*, 814–819.

Zhang, H., Wang, K., Zhang, X., Lin, H., Sun, X., Li, C., & Ma, Y. (2015). *J. Mater. Chem. A*, *3*, 11277–11286.

Zhang, J., Peng, L., & Han, B. (2014). *Soft Matter*, *10*(32), 5861.

Zhang, X., Pint, C. L., Lee, M. H., Schubert, B. E., Jamshidi, A., Takei, K., … Javey, A. (2011). *Nano Letters*, *11*(8), 3239–3244.

Zhao, S. (2014). *Environmental Science & Technology*, *48*, 4212–4213.

Zhao, S., Zou, L., Tang, C. Y., & Mulcahy, D. (2012). *Journal of Membrane Science*, *396*, 1–21.

Zhou, A., Luo, H., Wang, Q., Chen, L., Zhang, T. C., & Tao, T. (2015). *RSC Adv.*, *5*(20), 15359–15365.

Zhou, M., Kidd, T. J. J., Noble, R. D. D., & Gin, D. L. D. L. (2005). *Advanced Materials*, *17*(15), 1850–1853.

Zhou, Y., Wang, B., Liu, C., Han, N., Xu, X., Zhao, F., … Li, Y. (2015). *Nano Energy*, *15*, 654–661.

Zhu, C. H., Lu, Y., Peng, J., Chen, J. F., & Yu, S. H. (2012). *Advanced Functional Materials*, *22*(19), 4017–4022.

Zohuriaan-mehr, M. J., & Kabiri, K. (2008), *17*(6), 451–477.

 (2014).